AN ABSTRACT OF THE THESIS OF

William Warren Humphreys (Name) for the Master of Science (Degree)

in Mechanical Engineering (Major Department) presented on 5 June 1974 (Date)

Title: AN EXPERIMENTAL INVESTIGATION OF HEAT TRANSFER IN THE TRANSITION AND TURBULENT REGIMES FOR NATURAL CONVECTION IN MERCURY IN A UNIFORMLY HEATED VERTICAL CHANNEL

Abstract approved: Redacted for privacy

James R. Welty

An experimental study was conducted concerning the heat transfer and flow characteristics of natural convection with mercury in a uniformly heated vertical channel. The test apparatus consisted of two 5" x 5" electrically heated stainless steel plates oriented parallel to each other to form a vertical channel. Plastic plates enclosed the two sides of the channel to preclude side flow. Data were taken for three channel spacings at channel width-to-height ratios of 0.25, 0.50 and 0.67. As a separate case the second plate and sideplates were removed, and convection from a single vertical heated plate was studied.

Local and average heat transfer correlations are presented for the three channel spacings and the single plate in terms of Nusselt number and modified Grashof number. The Nusselt number

calculation was based on the heat flux measured in terms of the power dissipated by the plates. The modified Grashof number range for the single plate was $10^5 < Gr_x^* < 10^{11}$ and for the channel was $10^8 < Gr_x^* < 10^{11}$. For each case this extends heat transfer data for mercury two orders of magnitude beyond that previously reported. Although indications from the flow studies were that transition occurred between a modified Grashof number of 2×10^{10} and 6.5×10^{10}, the correlations are in good agreement with previous analytical and experimental results presented for lower Grashof number ranges.

The characteristics of the temperature and velocity boundary layers are also presented in terms of mean velocity and temperature profiles, relative magnitudes of the fluctuating velocity components, and characteristic frequencies of the velocity disturbances. Trends in the mean profiles are in good agreement with analytical predictions and frequency measurements agree very well with linear stability theory predictions. Conclusions concerning instability and the onset of transition are in very good agreement with the most recent studies in this field conducted in water.

The ground work was also laid for the use of a two-sensor "X" configuration probe for turbulence measurements in mercury. While no data from this probe are presented, the theory of operation and problems and recommendations associated with its use are discussed.

An Experimental Investigation of Heat Transfer in the Transition and Turbulent Regimes for Natural Convection in Mercury in a Uniformly Heated Vertical Channel

by

William Warren Humphreys

A THESIS

submitted to

Oregon State University

in partial fulfillment of
the requirements for the
degree of

Master of Science

June 1975

Thesis Submitted June 1974

APPROVED:

Redacted for privacy

Professor of Mechanical Engineering
in charge of major

Redacted for privacy

Head of Mechanical Engineering

Redacted for privacy

Dean of Graduate School

Date thesis is presented 5 June 1974

Typed by Cheryl E. Curb for William Warren Humphreys

ACKNOWLEDGEMENTS

I am indebted to many people for their help, advice, and encouragement during my research and the writing of this thesis. I would like to take this opportunity to express my gratitude to the following persons.

Dr. James Welty, my major professor: The freedom under which he allowed me to operate, accompanied by his helpful guidance and advice and his timely words of encouragement, created a very profitable and enjoyable research experience. His editorial suggestions for this manuscript were also appreciated.

Dr. Don Pierce, my minor professor: His advice on the statistical aspects of this project was very helpful.

Dr. Benjamin Gebhart, visiting professor at O. S. U.: His expertise in fields related to this project and his helpful suggestions were very valuable in the interpretation of my results.

Craig Dutton, Terry Kelley, and Dale Peinecke: Their assistance and suggestions were very much appreciated.

Members of my family and many close friends: While I will not name them individually for fear of missing one, their interest and encouragement have meant a great deal.

I have also relied heavily on Jesus Christ, my Lord, God, and Savior. It has been my desire to place Him first in the priorities

of my time and commitments. I believe that any shortcomings have been a result of my failure to keep these priorities and to appropriate all that He has made available to me, but very definitely He has been my source of strength and purpose in life.

Finally, I wish to acknowledge the Atomic Energy Commission for its financial support of this project.

TABLE OF CONTENTS

Chapter		Page
I	INTRODUCTION	1
II	REVIEW OF LITERATURE	4
	Introduction	4
	General Heat Transfer Results	4
	Instability, Transition, and Turbulence	8
III	EXPERIMENTAL APPARATUS AND PROCEDURE	16
	Introduction	16
	Channel Construction and Location	19
	Temperature Measuring System	23
	Velocity Measuring System	27
	Velocity Calibration Apparatus	35
	The Two-Sensor "X" Configuration Probe	38
IV	HEAT TRANSFER CORRELATIONS	43
	Introduction	43
	Dimensionless Heat Transfer Parameters	44
	Data Taking Procedures	48
	Single Vertical Plate Results	52
	Uniformly Heated Vertical Channel Results	59
V	CHARACTERISTICS OF THE VELOCITY AND TEMPERATURE BOUNDARY LAYERS	68
	Introduction	68
	Mean Velocity and Temperature Profiles	70
	Amplitude of the Instantaneous Velocity Disturbance	78
	Characteristic Frequencies of Velocity Disturbances	86
VI	THE TWO-SENSOR "X" CONFIGURATION PROBE	95
	Introduction	95
	Theoretical Considerations	97
	Operation of the "X" Configuration Probe	104
VII	CONCLUSIONS AND RECOMMENDATIONS	108
	NOMENCLATURE	112

TABLE OF CONTENTS (Cont.)

Chapter		Page
	BIBLIOGRAPHY	115
	APPENDIX A. DATA REDUCTION PROGRAMS	120
	APPENDIX B. DETERMINING THE OPTIMUM LOCATION FOR A BREAKPOINT IN A REGRESSION OF TWO LINEAR FUNCTIONS CONSTRAINED TO MEET AT THE BREAK-POINT	122
	APPENDIX C. DETERMINING THE STATISTICAL SIGNIFICANCE OF PARA-METERS IN A REGRESSION MODEL.	128

LIST OF FIGURES

Figure		Page
II. 1	Schematic representation of a stability plane.	11
III. 1	Schematic of channel configuration.	17
III. 2	Photograph of experimental equipment.	18
III. 3	Photograph of mercury tank and constant temperature bath.	19
III. 4	Schematic of heater element.	21
III. 5	Heat loss through back of plate.	22
III. 6	Schematic of thermocouple junction.	25
III. 7	Schematic of hot film sensor.	25
III. 8	Photographs of single sensor probe with thermocouples attached.	29
III. 9	Photograph of calibration system.	36
III. 10	Photograph showing alignment of laser beam and photocell.	36
III. 11	Schematic of two-sensor "X" configuration probe.	39
III. 12	Photographs of the two-sensor "X" configuration probe.	40
IV. 1	Local heat transfer data for single vertical heated plate.	54
IV. 2	Local heat transfer correlations for single vertical heated plate.	56
IV. 3	Local heat transfer data for uniformly heated vertical channel.	61

LIST OF FIGURES

Figure		Page
IV. 4	Local heat transfer correlations for uniformly heated vertical channel.	62
IV. 5	Channel heat transfer correlations with w/L in correlation.	66
V. 1	Velocity profiles.	71
V. 2	Comparison of the velocity and temperature boundary layers.	73
V. 3	Dimensionless velocity profiles.	76
V. 4	Dimensionless temperature profiles.	77
V. 5	Instantaneous velocity variation with y at constant x.	79
V. 6	Instantaneous velocity variation with x and w/L at constant y.	81
V. 7	Amplitude of the velocity disturbance.	83
V. 8	Hypothesized formation of eddies.	85
V. 9	Stability plane from Hieber (18) showing present results.	88
V. 10	Characteristic frequencies of the velocity disturbance.	91
VI. 1	Velocity component relative to a single sensor.	95
VI. 2	Linearized anemometer output.	98
VI. 3	Parallel and perpendicular velocity components.	98
VI. 4	Coordinate system relative to "X" configuration sensors.	100
VI. 5	Linear calibration curves.	101

AN EXPERIMENTAL INVESTIGATION OF HEAT TRANSFER IN THE TRANSITION AND TURBULENT REGIMES FOR NATURAL CONVECTION IN MERCURY IN A UNIFORMLY HEATED VERTICAL CHANNEL

I. INTRODUCTION

The work conducted for this thesis is part of an ongoing project under the auspices of the U.S. Atomic Energy Commission. The A.E.C. is interested in experimental results for natural convection in liquid metals for safety calculations in the design of the liquid metal fast breeder reactor; in the event of a pump failure, the residual heat in the reactor core would have to be removed by natural convection of the coolant fluid.

The A.E.C. research at Oregon State University began with White (47) who studied natural convection on a single vertical plate. Hurt (20) made some major improvements in the use of a hot film anemometer for measuring the low velocities encountered for natural convection in mercury. This aided the work of Colwell (6), who studied natural convection between two vertical plates, which formed a vertical channel where the channel spacing could be varied. Most recently, Wiles (48) studied natural convection from a single cylinder for three different size cylinders.

All the studies to date have been conducted for laminar flow, where streamlines are well ordered and basically run parallel to the

heat generating surface. At some downstream location, any flow over a surface will become chaotic, or turbulent, where the streamlines are no longer really discernable. The period during which the regime of flow changes from laminar to turbulent is called transition. This phenomena is a common observation to anyone who has ever noticed how the smoke from a cigarette first rises in a well-ordered stream-like fashion, then suddenly seems to break up into little swirls and disappear.

The objective of the present work was to extend the study of the uniformly heated channel, started by Colwell (6), into the turbulent regime. The study of turbulent natural convection where the velocity and temperature readings were fluctuating rapidly required the development of new data taking procedures and the procurement of additional equipment, in particular, the two-sensor "X" configuration probe. The basic results to be presented are as follows.

1. Heat transfer results are presented in terms of the Nusselt number, based on the wall heat flux, and the modified Grashof number. For a single vertical plate, results cover the range of $10^5 < Gr_x^* < 10^{11}$. For the uniformly heated channel, three channel spacings were studied. For channel width to height ratios, w/L, of 0.67, 0.50, and 0.25 results are presented for a range of $10^8 < Gr_x^* < 10^{11}$. These results are compared to analytical and experimental results, where applicable.

2. The basic characteristics of the boundary layer are studied in terms of the mean temperature and velocity profiles, the relative magnitudes of the velocity disturbances, and the characteristic frequencies of the disturbances. Profiles are compared to both analytical and other experimental work. Characteristic frequencies are compared with linear stability theory. The level of development of the turbulent flow is indicated, and a model is postulated to describe the flow mechanisms within the channel.
3. Use of the two-sensor "X" configuration probe is considered. No data from the probe are presented, but the theory of operation, problems, and recommendations associated with its use are discussed.

II. REVIEW OF LITERATURE

Introduction

The study of natural convection began in 1881 with the analytical work of Lorenz (28) followed by the experimental studies of Griffiths and Davis (17) in 1922, and of Schmidt and Beckman (34) in 1930. From there it has branched into the many subjects of various test fluids and test conditions available in the literature today. The reader who is interested in a more complete historical development of the study of natural convection from its beginning in 1881 to the present work in liquid metals is referred to references (4) and (5). Since the present work in many ways continues the work started by White (47) and most recently by Colwell (5), a recapitulation of their literature reviews will not be attempted. Rather, those papers most directly related to this work will be discussed briefly, followed by a more detailed discussion of new material relating to natural convection instability, transition, and turbulence.

General Heat Transfer Results

In 1950, Eckert and Jackson (10) reported heat transfer correlations for natural convection from isothermal vertical surfaces in air. While their study pertained to a different test fluid and boundary condition, their results are of interest because they found a significant

increase in the slope of the heat transfer correlation curve when transition occurred at a Rayleigh number of about 10^9. They recommended the following correlation

$$Nu_L = 0.555(Gr_L Pr)^{.25} \qquad Gr_L Pr < 10^9 \qquad (II.1)$$

$$Nu_L = 0.021(Gr_L Pr)^{.40} \qquad Gr_L Pr > 10^9 \qquad (II.2)$$

For mercury (Pr = 0.023), in terms of the local modified Grashof number this correlation becomes

$$Nu_x = 0.235(Gr_x^*)^{.2} \qquad Gr_x^* < 2.34 \times 10^{11} \qquad (II.3)$$

$$Nu_x = 0.0247(Gr_x^*)^{.286} \qquad Gr_x^* > 2.34 \times 10^{11} \qquad (II.4)$$

In 1956, Sparrow and Gregg (36) presented a similarity solution for the uniform flux surface, for Prandtl numbers of 0.1, 1, 10, and 100. In 1959, they presented results for lower Prandtl numbers for the isothermal surface (38) but not the uniform flux condition. Their heat transfer results for the uniform flux condition, extrapolated to a Prandtl number of 0.023 are

$$Nu_x = 0.16(Gr_x^*)^{.2} \qquad (II.5)$$

In 1964, Chang, Akins, Burris and Bankoff (4) used a first order perturbation analysis to extend the results of Sparrow and Gregg for the uniformly heated vertical plate at low Prandtl numbers. Their heat transfer results were

$$Nu_x = 0.632(Pr)^{.37}(Gr_x^*)^{.2} \qquad \text{(II. 6)}$$

When expressed for Pr = 0.023, this becomes

$$Nu_x = 0.154(Gr_x^*)^{.2} \qquad \text{(II. 7)}$$

Cygan and Richardson (8) in 1968 approximated the velocity profile as two exponentials, one represented a viscous region near the wall and one represented an inviscid region. This method allowed incorporation of Pr in the velocity profile for determination of the wall shear stress. They recommended the heat transfer correlation

$$Nu_x = 0.52976(Gr_x Pr^2)^{.25} \qquad \text{(II. 8)}$$

for Pr = 0.03, which in terms of the local modified Grashof number is

$$Nu_x = 0.148(Gr_x^*)^{.2} \qquad \text{(II. 9)}$$

Kuiken (24), in 1969, resolved the coupled boundary layer equations for an isothermal plate using the method of matched asymptotic expansions. His results for Pr = 0.03 were

$$Nu_x = 0.5443(Gr_x Pr)^{.25} \qquad \text{(II. 10)}$$

In terms of the local modified Grashof number this becomes

$$Nu_x = 0.152(Gr_x^*)^{.2} \qquad \text{(II. 11)}$$

Also in 1969, Julian and Akins (22) experimentally studied natural convection from an electrically heated vertical plate in mercury. Their velocity and temperature profiles were in good agreement with similarity and perturbation solutions. Their heat transfer correlation was

$$Nu_x = 0.196(Gr_x^*)^{.188} \qquad 10^4 < Gr_x^* < 10^9 \qquad \text{(II. 12)}$$

Finally, in 1973, Colwell and Welty (5, 6) studied natural convection from both a single vertical plate and a uniformly heated channel. They also found good agreement between their results and the similarity and perturbation solutions. Their heat transfer correlation for a single vertical plate was

$$Nu_x = 0.23(Gr_x^*)^{.18} \qquad 10^4 < Gr_x^* < 10^9 \qquad \text{(II. 13)}$$

In regard to channel flow, Colwell made a remarkable discovery, unique to low Prandtl number fluids. He found that the average plate temperature decreased, causing the Nusselt number to increase as the channel spacing decreased until the ratio of the channel width, w, to the channel height, L, was less than 0.10. Thus he found an optimum plate spacing where the channel was most efficient in transferring heat to the fluid. That is, for a given heat flux a minimum plate temperature will occur, or for a given average plate temperature a maximum average heat flux will occur.

For heat transfer in a vertical channel, Colwell included the channel spacing, w/L, in the correlation and recommended

$$Nu_x(w/L) = 0.194[Gr_x^*(w/L)^5]^{.18}$$
$$10^3 < Gr_x^*(w/L)^5 < 10^9 \qquad \text{(II. 14)}$$

The majority of Colwell's work was conducted in a channel with no side plates. When he checked for the possible effect of side flow by adding side plates, he found that the Nusselt number increased, with this effect being most noticeable for the narrower channel spacings and higher Grashof numbers. His heat transfer correlation, based on the data using side plates, was

$$Nu_x(w/L) = 0.268[Gr_x^*(w/L)^5]^{.165}$$
$$10^3 < Gr_x^*(w/L)^5 < 10^9 \qquad \text{(II. 15)}$$

Instability, Transition, and Turbulence

In 1962 Szewczyk (40) studied the stability of a free convection layer along a vertical plate in water. While his stability calculations are rather crude in comparison to more recent literature, his experimental observations are of particular interest. By introducing a layer of die at the leading edge, he observed the formation of a double row vortex system. A row of vortices inside the velocity peak rolled toward the plate while a row of vortices outside of the velocity peak

rolled in the opposite direction away from the plate. He further noted that the outside vortices appeared sooner and appeared to be much less stable than the inner vortices, impressing their effect on the more stable inner layer.

In 1968 Coutanceau (7) conducted an analytical and experimental study of turbulent natural convection from an isothermal flat plate. His only test fluid was water. He suggested that the quantity $[(T_s-T_a)/T_a]^n$ should be included in the heat transfer correlation

$$Nu_x = K[(T_s-T_a)/T_a]^n(Gr_x)^m \qquad \text{(II. 16)}$$

He found, however, that n and m were of nearly the same magnitude, so that his heat transfer correlation for air was

$$Nu_x = 0.00811(gx^3/\nu^2)^{.41} \qquad \text{(II. 17)}$$

He suggested that gx^3/ν^2 was a better heat transfer parameter than the conventional Grashof number for turbulent flow. This result was for an isothermal plate, but implies that the convective heat transfer coefficient, $h = Nu_x k/x$, for turbulent flow is dependent only on x and not on the relative magnitude of temperature difference or heat flux. Coutanceau also reported the onset of transition at a relative Grashof number of $Gr_x = 1.462 \times 10^9(T_s/T_a)^{-8.352}$.

The beginning of the present understanding of natural convection instability began several years earlier, however, with Plapp (32) in

1957. He applied linear stability theory to the governing equations of natural convection, which lead to the formation and eventual solution of the Orr-Sommerfeld equations. While a brief description of linear stability theory applied to natural convection will be presented in the following paragraph, references (12) and (13) are recommended for a more complete introduction to the subject.

For linear stability theory, a temperature and velocity similarity function are selected which can represent a steady value with a superimposed fluctuating component that can vary in both frequency and amplitude with downstream position, x, and time, t. When these functions are introduced into the governing equations for natural convection the Orr-Sommerfeld equations result. The solution of these equations, an eigenvalue problem, indicates that a disturbance will be amplified (extract energy from the mean flow and grow) or be damped (lose its energy to the mean flow) depending on its frequency, f, and its value of local vigor, $G^* = 5(Gr_x^*/5)^{\cdot 2}$. These results are best expressed in terms of a stability plane where the dimensionless frequency, β^*, is presented against G^*, with lines of constant physical frequency and amplification rate as shown in Figure II. 1. The indication from linear stability theory is that only a narrow range of frequencies around f_1 will be amplified, and that f_1 will appear as the characteristic frequency of the disturbance.

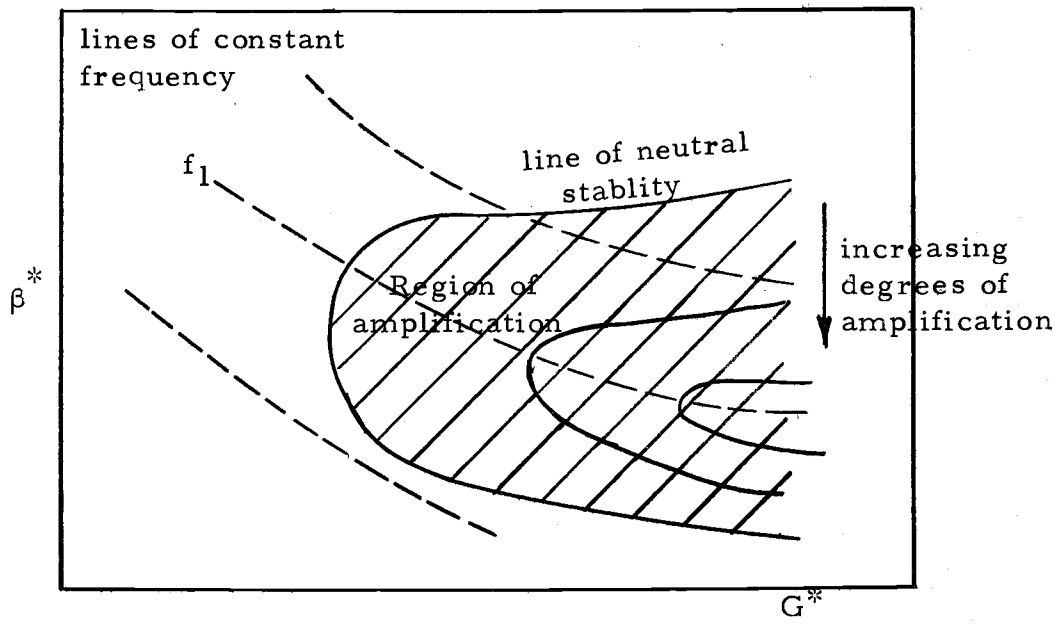

Figure II. 1. Schematic representation of a stability plane.

In 1968 Knowles and Gebhart (23) studied the effect of the heat generating surface on the linear stability theory predictions. Defining the relative thermal capacity of the surface as

$$Q^* = \left(\frac{Pr}{5}\right) \frac{(\rho lc)surface}{(\rho lc)fluid} \qquad (II.18)$$

they found for Pr = .733 and Pr = 6.9 that a low value of thermal capacity, where the surface could follow the fluid temperature fluctuations, significantly changed the stability predictions, but that this effect decreased as the Prandtl number decreased. They also studied the effect of thermal capacity on the location of maximum temperature and velocity disturbance amplitudes. For a low value of Q^*, as

occurred with the present work, they found that the maximum velocity disturbance amplitude occurred approximately at the inflection point of the mean velocity curve. The maximum temperature fluctuation occurred slightly closer to the velocity peak and temperature fluctuations at the wall only decreased to 80% of their maximum values.

Dring and Gebhart (9) used an improved numerical technique to solve the coupled Orr-Sommerfeld equations for Pr = 6.7 for a heat generating surface with no relative thermal capacity ($Q^* = 0$). It was noted that the lower frequency disturbances which appear first are not the ones that are amplified the most and are soon dominated by higher frequency disturbances which are amplified more. Dring also introduced the technique of studying the growth of a disturbance as it is convected downstream from G_1^* with amplitude A_1 to G_2^* with amplitude A_2, by integrating

$$A_2/A_1 = \exp\left\{-\frac{1}{4}\int_{G_1^*}^{G_2^*} a^* dG^*\right\} \qquad \text{(II-19)}$$

This allows expressing amplitude ratios on the stability plane, which have more physical significance than the amplification rates, a^*.

In 1971, Hieber and Gebhart (18) continued the analysis of instability with another improved numerical method that allowed the solution of the Orr-Sommerfeld equations for a wide range of Prandtl numbers. Dring's results for Pr = 0.025 were determined for the case of a plate with high thermal capacity. The stability plane from

his work is presented in Figure V. 9. He found that the uncoupled Orr-Sommerfeld equations were in close agreement with his results using the coupled equations for a plate with high thermal capacity, but that for a plate with low thermal capacity the coupling between the fluid and plate temperature fluctuations had a destabilizing effect on the solution. Since the present work used a plate with low thermal capacity, this indicates that Hieber's results should be used with caution.

In 1973 Godaux and Gebhart (15) conducted an experimental study in water of transition mechanisms from a vertical heated surface. Godaux defined the onset of transition as occurring when the mean temperature profile first deviated from the $x^{1/5}$ dependence of laminar flow, and attempted to correlate his results with a dependence on $G^*/x^{.6}$, which is proportional to $(qx)^{.2}$. Jaluria and Gebhart (21) continued the same study, but chose to define the onset of transition from the instantaneous readings from a hot wire anemometer. They defined the onset of transition as occurring when the first turbulent bursts appeared. A burst is a higher frequency disturbance which superimposes itself on the laminar characteristic frequency for a period of time, causing a distortion of the sinusoidal behavior characteristic of laminar flow. They defined the intermittency as the average proportion of time that these bursts were seen. Finally, they defined as the end of transition when the intermittency reached a value of 1, so that only the higher frequency disturbances were apparent.

Jaluria had more success than Godaux in predicting transition by using G^*/x^n, a more general case of $G^*/x^{.6}$, where he found a value of n = 0.40 predicted the onset of transition and n = 0.54 the end of transition. The dependence of the onset of transition on $x^{.4}$ he incorporated into an E factor, defined as

$$E = G^*(\nu^2/gx^3)^{2/15} \qquad \text{(II-20)}$$

He reports that his values of E = 13.6 for velocity transition and E = 15.2 for thermal transition are in good agreement with similar calculations based on other data available in the literature. Finally, Jaluria noted that there was basically one characteristic frequency for laminar flow and another considerably higher frequency for turbulent flow, and that the characteristic frequency as transition continued increased rapidly. Also, he observed that as disturbances proceeded downstream their amplitude decreased, which he attributed to the breaking down of eddy size and filling out of the frequency spectrum.

Colwell (5) also studied the onset of transition for his channel configuration in mercury. His data were taken at relatively low G^* values and, when plotted on the stability plane from Hieber (18), lie within the amplified region but below the most amplified frequency. He observed frequencies in the range from 0.065 Hz to 0.106 Hz. From the figures he has included showing the instantaneous anemometer plots, the disturbances which he refers to as early transition

waves are quite regular and sinusoidal in appearance, with no higher frequency bursts appearing. With the transition criteria proposed by Jaluria (21), these waves appear to be more characteristic of unstable laminar flow than of the onset of transition. Colwell did observe, however, the appearance of a higher characteristic frequency further downstream. He also found that the maximum velocity disturbance amplitude increased as the channel spacing was decreased until a channel width to height ratio of about $w/L = .4$, and then the disturbance amplitude decreased as the channel spacing decreased further. Apparently the effect of the two walls increases the turbulence level until the dissipating effect of the plates is felt.

III. EXPERIMENTAL APPARATUS AND PROCEDURE

Introduction

Data for this thesis were taken in a symmetrically heated vertical channel. This configuration is shown schematically in Figure III. 1. The channel had a vertical length, L, of 5 inches and the width, w, was varied from 1.25 inches to 3.33 inches. The channel was open at the top and bottom but was enclosed on each side by 1/8 inch thick plastic side plates. As a separate situation, plate number 2 and the side plates were removed and data taken for a single vertical plate. The coordinate system indicated in Figure III. 1 will be used consistently throughout this thesis. The construction of the channel will be discussed in more detail in "Channel Construction and Location".

This chapter will treat in succession the temperature measuring system, the velocity measuring system, the calibration apparatus, and the two-sensor "X" configuration probe. Figures III. 2, III. 3, III. 9, and III. 10 show photographs of the layout of different aspects of these systems. As different components of these systems are discussed, the reader will be referred to a figure and a number in brackets which will identify that component. To avoid confusion, these numbers are consecutive throughout the chapter.

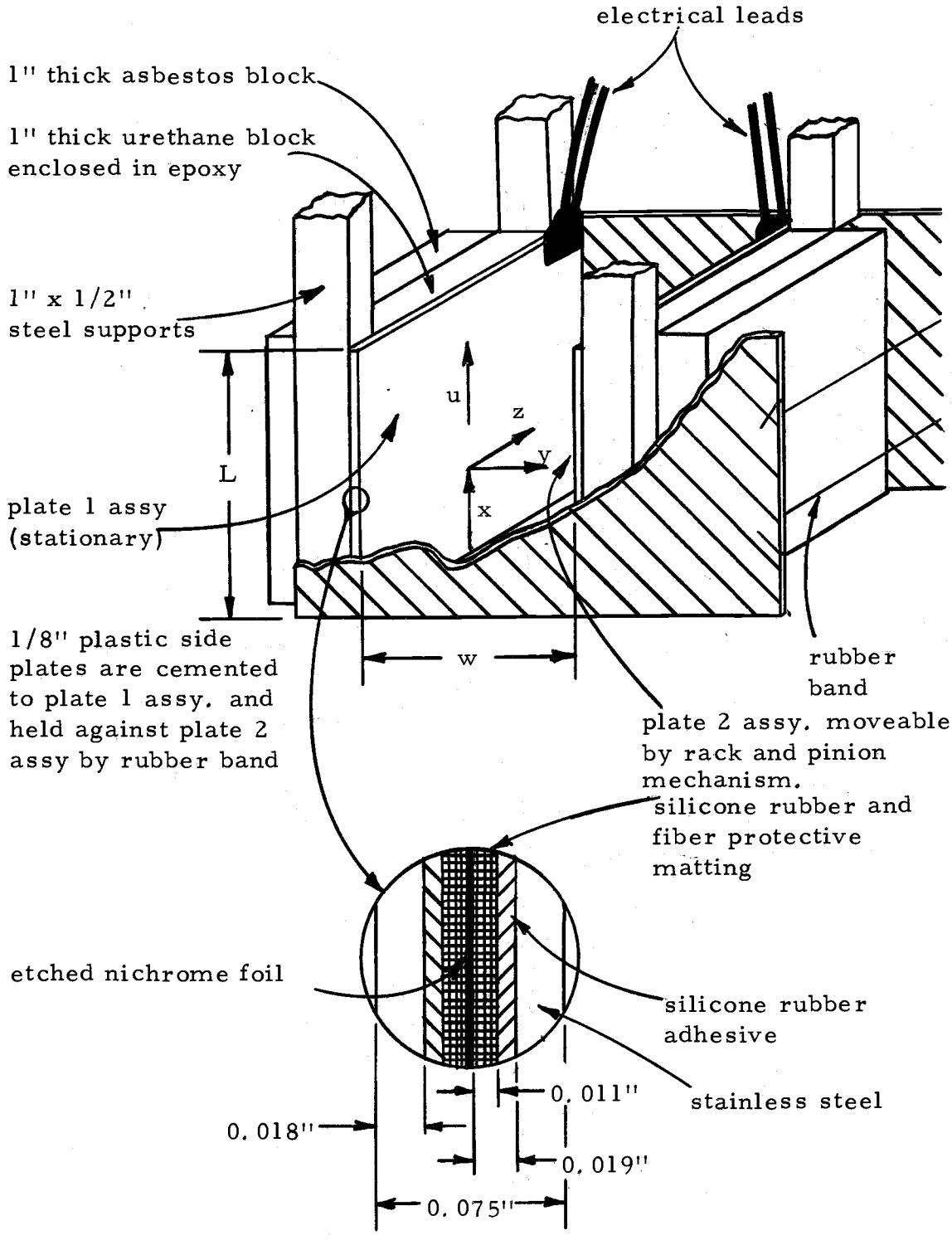

Figure III. 1. Schematic of channel configuration.

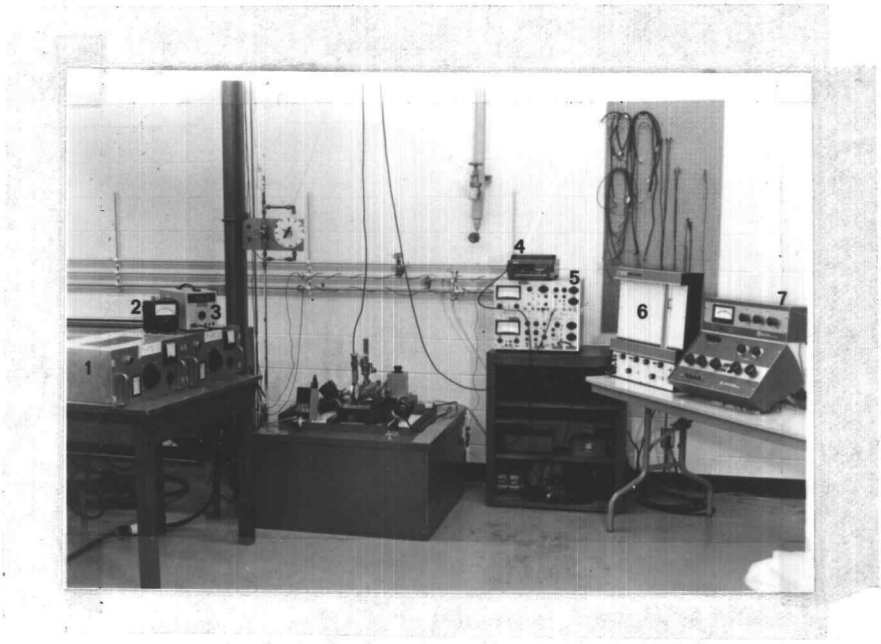

Figure III. 2. Photograph of experimental equipment.

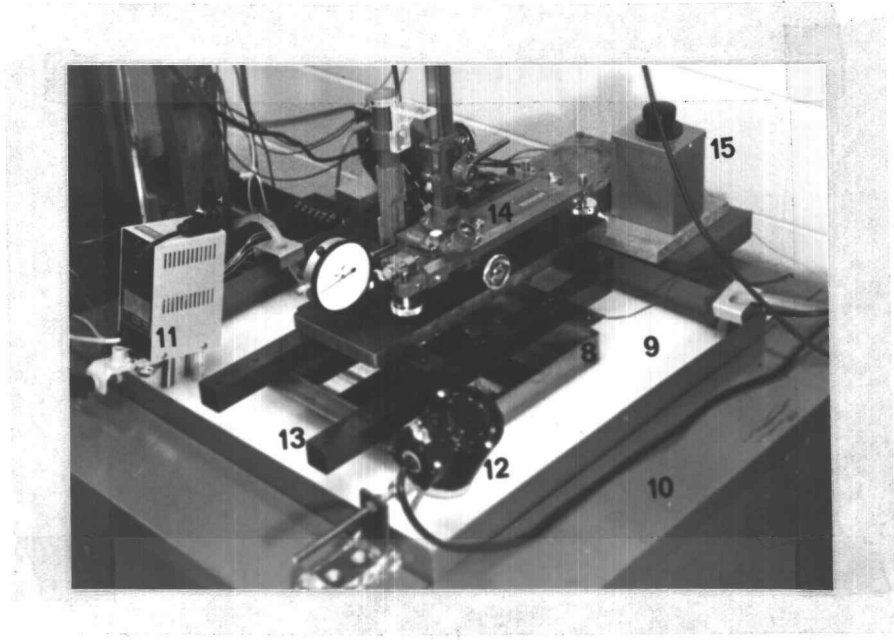

Figure III. 3. Photograph of mercury tank and constant temperature bath.

Channel Construction and Location

The basic channel configuration was already introduced. The channel was placed in a 12-inch square by 16-inch deep stainless steel tank of mercury [8], shown in Figure III. 3. The mercury tank was surrounded by a 35 gallon constant temperature water bath [9] and 6 inches of vermiculite insulation housed in a plywood cabinet [10]. The constant temperature bath appears white due to rust inhibitor which was added to the water. The bath was maintained constant by balancing the heat from the heaters and cooling from tap water running through copper coils with a Haake model E 51 one kilowatt heater [11]. With the aid of two stirrers [12] the ambient temperature was maintained within $\pm$ 0. 5°F over a several hour run, which was quite acceptable. The channel was held in the mercury by a steel frame [13] which was bolted securely to the stainless steel tank. Plate 1 was mounted stationary while plate 2 was mounted moveable on a rack and pinion assembly. The velocity and temperature probes were located in the x and y directions by a x-y positioner [14] Positions could be located in the x direction to within 0. 001 inch, and in the y direction to within 0. 0001 inch by use of the dial indicator shown.

Referring again to Figure III. 1, the heated plates were a sandwich construction of an electrical resistance heater manufactured by

Electrofilm, Inc., inserted between two 0.018 inch stainless steel plates. The heating element itself consisted of a chemically etched 0.001 inch sheet of nichrome foil, shown schematically in Figure III-4, protected by a matting of fiber and silicone rubber. The stainless steel plates were 6 inches wide while the heater was 5 inches high so that the 1/2 inch on each side of the plate that was attached to the steel supports was not heated. Rubber shims the same thickness as the heating element were placed along these 1/2 inch side strips. A plate, the heater and shims, then the other plate were placed in a holding fixture to assure proper alignment, with silicone rubber cement between each layer, then the entire assembly placed under a hydraulic press to maintain uniform thickness during curing. The resulting heated plate was 0.075 ± 0.002 inches thick.

In order to eliminate asymmetrical effects from the back sides of the plates and to keep the power input as low as possible, the back side of each plate was insulated. The insulation consisted of a 1 inch thick block of asbestos for good heat resistance next to the hot plate, with a 1 inch thick block of urethane encased in epoxy (which has a much higher thermal resistance) cemented to it. It is of vital concern for the heat transfer data that the heat loss through the back side of the plates be very small so that the entire power input can be considered as contributing to the heat flux in the channel. The maximum temperature that the heater foil can withstand is $400^{\circ}F$, the

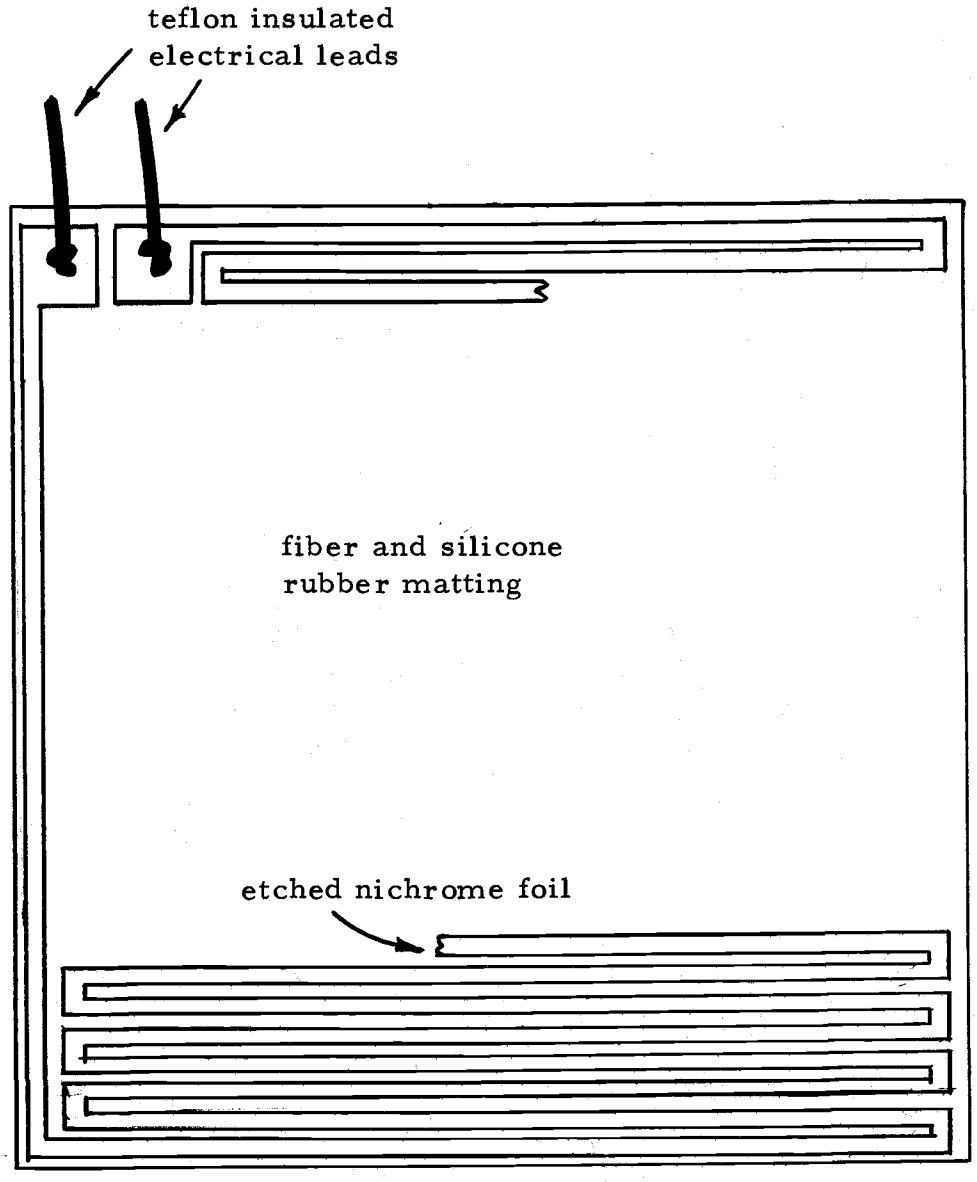

Figure III. 4. Schematic of heater element (actual size).

temperature it reaches being controlled by the thermal resistance between the foil and the fluid in the channel. Using this maximum condition and a typical plate surface temperature of 100°F and ambient of 80°F, it will now be shown that the maximum loss through the back side of each plate is less than 0.2% of the total power input.

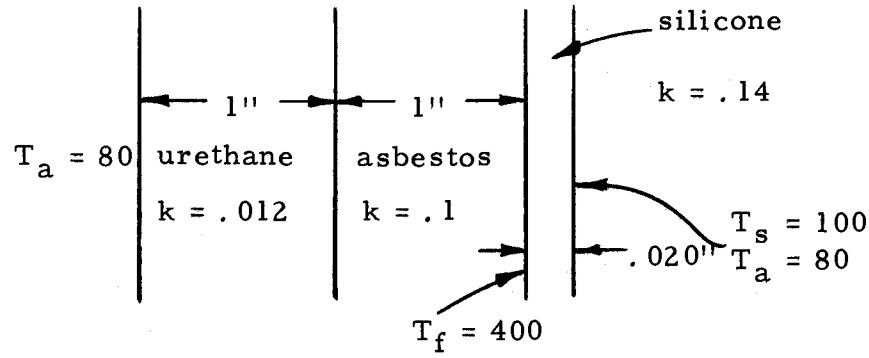

Figure III. 5. Heat loss through back of plate.

Let q_1 and q_2, R_1 and R_2 be the heat fluxes and thermal resistances from the front and back sides of the plates, respectively. Then

$$q_1 = (T_f - T_s)/R_1$$

$$q_2 = (T_f - T_a)/R_2$$

$$R_1 = (.020/12)/(.14) = .012$$

$$R_2 = (1/12)/(.012) + (1/12)/(.1) = 6.95 + .83 = 7.78$$

$$q_1 = (400-100)/(.012) = 25,000 \text{ BTU/hr ft}^2$$

$$q_2 = (400-80)/(7.78) = 41 \text{ BTU/hr ft}^2$$

$$q_2/(q_1 + q_2) = (41)/(25041) = 0.00164 = 0.164\%$$

It appears that the heat loss from the back side of the plates was always less than 0. 2% and therefore could be ignored.

The plates were powered by two unregulated power supplies from Manson Laboratories [1] shown in Figure III. 2. These accounted for the largest source of error in the data as they were monitored and sometimes found to vary as much as 2. 5% from their original settings. The power was measured using a Honeywell Digitest voltmeter [3] and a Weston model 931 analog ammeter [2]. The most accurate readings were taken here by setting the current to read on an exact line on the ammeter.

Temperature Measuring System

Temperatures were measured with iron-constantan sub-miniature grounded thermocouples manufactured by Omega Engineering, Inc. The active junction was referenced against a distilled water ice junction contained in a small thermos bottle. Voltage differences from the two junctions were measured under steady conditions with a Leeds and Northrup model K4 potentiometer [7] shown in Figure III. 2 and under fluctuating conditions with the millivolt option on a Fluke model 8200A digital voltmeter [4]. Each probe was individually calibrated for a range of 25°C to 50°C using a Hewlett-Packard model 2800A quartz thermometer and the K4 potentiometer.

The subminiature thermocouple consists of the two dissimilar wires, each 0.001 inch in diameter, housed and insulated within a 0.010 inch OD stainless steel sheath, and brought together into a flat weld bead as shown in Figure III.6. The bead was sufficiently small and the true junction location easy enough to determine that the probe could be considered to be taking point temperature measurements. Wall temperature readings were taken by slowly moving the probe toward the wall until the temperature ceased to increase, indicating the probe was butted up against the wall. The question should be asked if this was really a representative wall temperature since the thermocouple junction would actually be several thousands of an inch away from the plate. Previous work done by Colwell (5) indicated that attempting to correct for this effect by estimating the temperature gradient and extrapolating to the wall increases the uncertainty of the results considerably while not changing the overall correlation significantly. Therefore, the thermocouple reading was considered as a representative reading of the wall temperature.

For temperature measurements in a fluctuating temperature or velocity field, the time response of the thermocouple is also important. The time constant of the sub-miniature probe was experimentally determined to be 20 milliseconds in water and less than 1 millisecond in mercury. This was determined by subjecting the probe to a step change in temperature and monitoring the thermocouple output on a

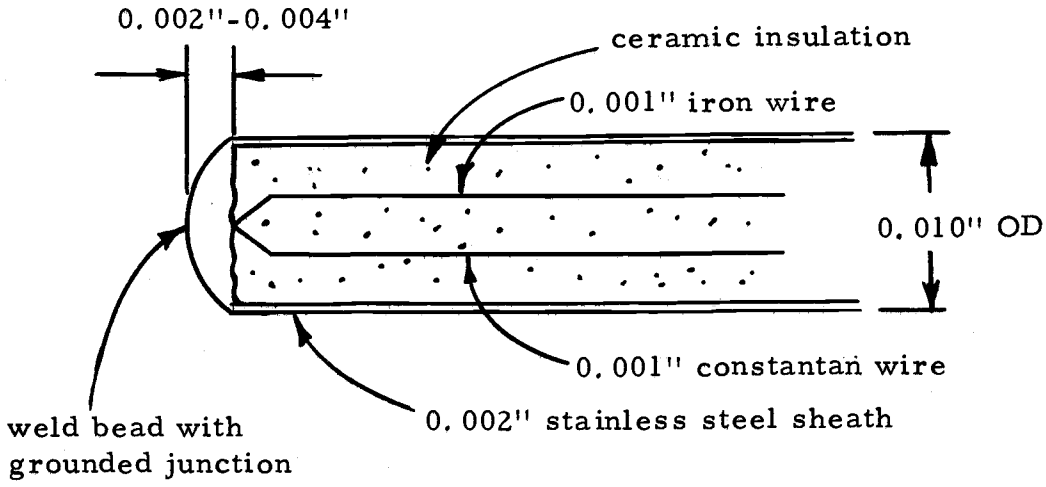

Figure III. 6. Schematic of thermocouple junction.

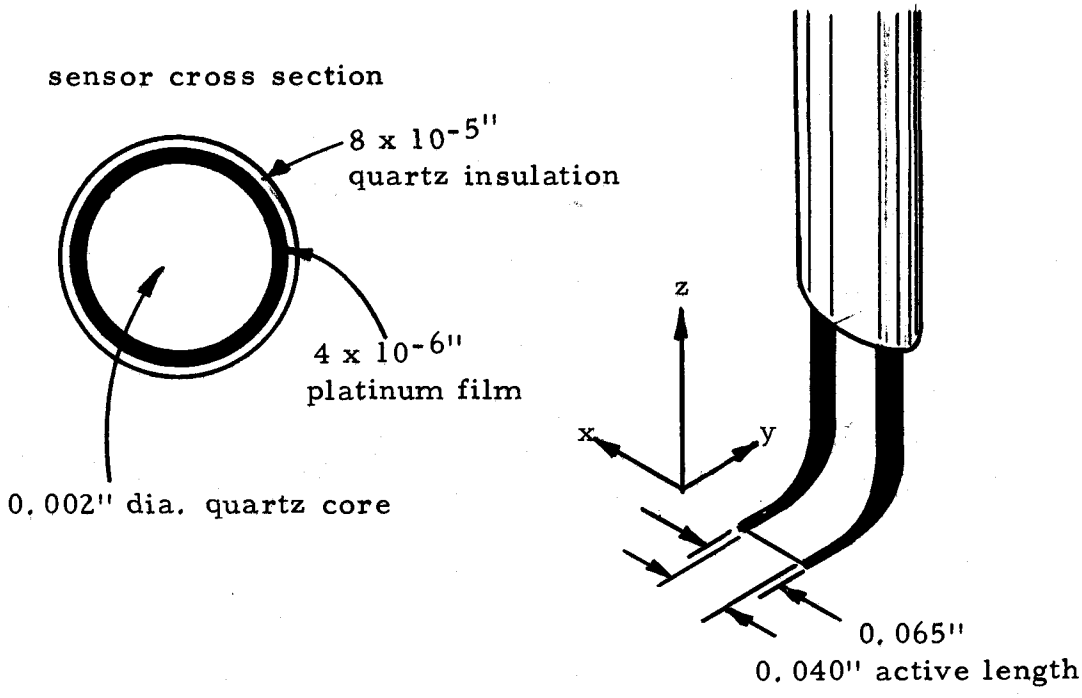

Figure III. 7. Schematic of hot film sensor.

storage oscilloscope. Since the characteristic frequencies encountered in natural convection are on the order of 1 Hz or less, it appears that the thermocouple was able to follow all temperature fluctuations.

Stable temperature readings were taken with the Leeds and Northrup K4 potentiometer used with a model 9828 null detector, model 9879 guarded voltage supply, and an Eppley unsaturated standard cell. The K4 system can read accurately to 0.0001 mV, which corresponds to about 0.003°F. The temperature for most of the data was sufficiently unsteady, however, that it was impossible to zero the null meter to take a reading. The K4 was only used, therefore, for calibrating the thermocouples and for taking ambient readings, where it was used as a standard to zero the millivolt scale of the Fluke digital voltmeter. Mean temperature readings were determined by taking readings from the digital voltmeter at intervals of five seconds for a period of two or three minutes, depending on the intensity of the fluctuations. The readings were recorded on an HP-35 hand calculator and then averaged. This method did not provide a means of recording the intensities or frequencies of the temperature fluctuations, but the scope of this project did not require that information.

It was originally desired to use an analog time-averaging circuit to determine the mean temperatures. The state of the art in analog equipment is not such, however, that it can average a signal on the order of 1 millivolt for several minutes, because of the very slow

frequencies, without completely losing the signal in its own noise level. It appears that the most elegant way to handle this type of data is to use a digital recorder and then use a digital computer to statistically analyze the data. If the interval between readings is small enough, in addition to mean quantities, this will provide intensity measurements and a spectral analysis. A similar procedure is to make strip charts and have them digitized. In either case, the digital method is expensive both in terms of equipment acquisition and computer analysis; therefore, consideration should be given to see if the additional information gained justifies the expense. For this project, the digital recording equipment was not available and satisfactory results were obtained without it.

Velocity Measuring System

Velocities were measured with a hot-film constant temperature anemometer system manufactured by Thermo-Systems, Inc. Figure III. 7 shows a schematic diagram of the hot film sensor itself. It consists of a 0. 002 inch diameter quartz rod, a 0. 000004 inch layer of platinum, and two layers of quartz insulation of total thickness 0. 00008 inch. A small current is passed through the platinum causing a voltage drop proportional to the velocity. The operation of a constant temperature anemometer system will be discussed in more detail at the end of this section. The outer double quartz layer is unique to

measurements in mercury and other conducting fluids and acts as an insulator between the platinum and the fluid.

The velocity probe assembly consisted of a hot-film anemometer with two thermocouples epoxied to the sensor supports as can be seen in the close-up photograph in Figure III. 8. Both thermocouples were located in the horizontal plane of the hot film sensor. The one thermocouple was mounted so that the center of its junction was also the same distance from the plate as the hot-film sensor. Since this thermocouple was at the same x and y positions as the sensor, it measured the temperature for use in setting the proper overheat ratio and provided information for temperature profiles. The second thermocouple was used to locate the plate without damaging the hot film sensor, and to measure the wall temperature.

The hot film sensor was connected through the probe support by way of a 15 foot guarded triaxial cable to a TSI model 1050 constant temperature anemometer with a monitor and power supply, temperature and switching circuit, and signal conditioner. Figure III. 2 shows the entire anemometer system which is housed in one cabinet [5]. The equipment named above is contained on the upper of two rows of equipment. The lower row contains the model 1060 true RMS voltmeter which will be discussed later in this section, and the model 1054 anemometer used with the model 1056 variable decade, and the model 1015C correlator, which were used with the two-sensor "X"

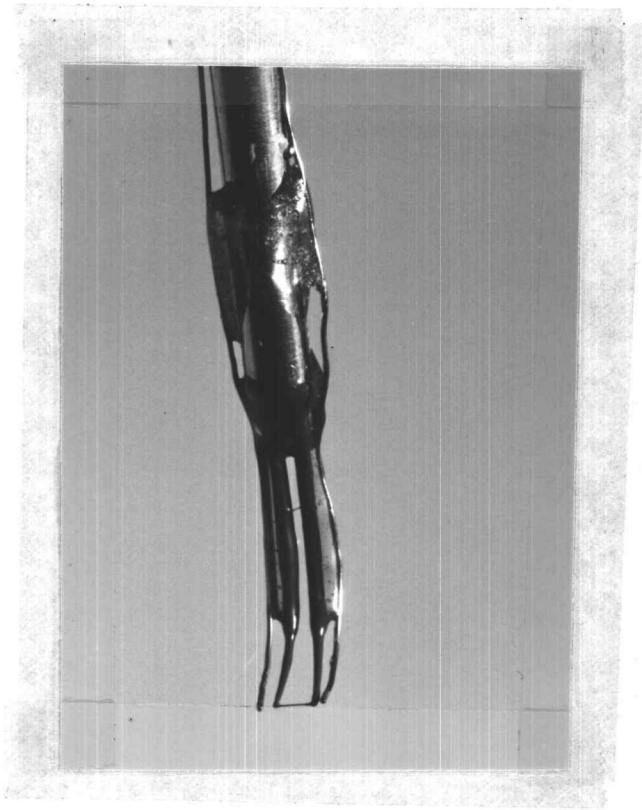

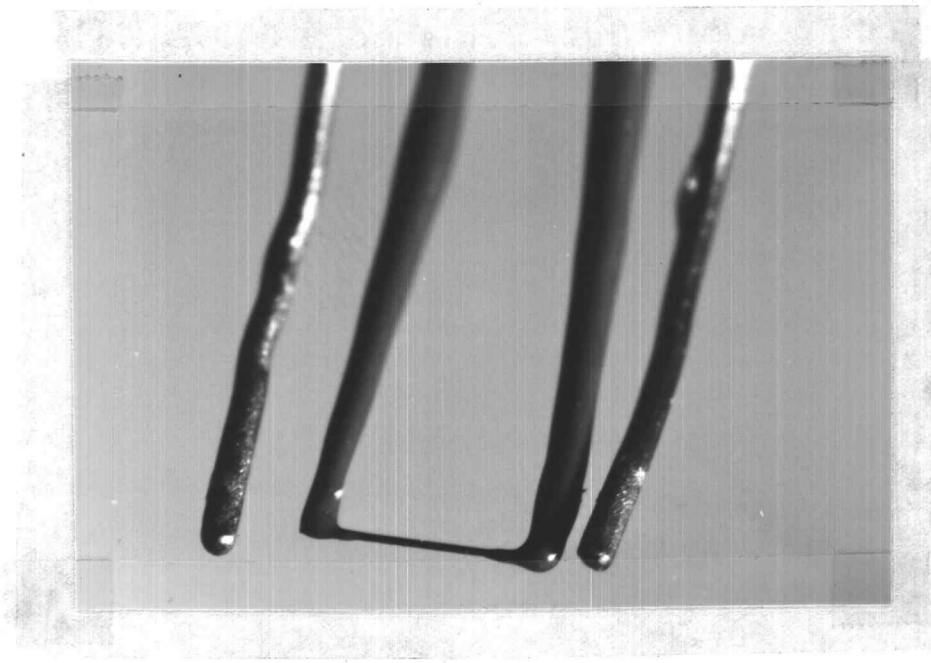

Figure III. 8. Photographs of single sensor probe with thermocouples attached.

configuration probe.

The output signal from the anemometer was channeled into an EAI (Electronic Associates, Inc.) model 1130 Variplotter [6], also shown in Figure III. 2. This x-y plotter with moving stylus has a range in vertical sensitivities from 0.25 mV/cm to 10 volts/cm, and a horizontal time sweep range of 0.25 sec/cm to 10 sec/cm. While the plotter does not have as good a frequency response as the anemometer (250 KHz), it responds to frequencies much higher than those encountered in this experiment. The anemometer output-versus-time plots were used to determine the mean velocity, and provided a permanent record for analyzing characteristic frequencies and relative intensities, and for demonstrating general trends in the velocity as the x and y positions and channel spacing were varied.

The anemometer output was also simultaneously channeled into the true RMS voltmeter. The RMS voltmeter presented one basic difficulty which was never really overcome, hence it did not provide much useful information. The largest peak to peak fluctuations observed were on the order of one volt; however, most of the fluctuations were much smaller. As was mentioned previously, the characteristic frequency of the flow was in the range from 0.1 to 1 Hz. For these slow frequencies, an averaging time period for the RMS voltmeter of either 30 or 100 seconds was required. While TSI suggests about five time periods to be required for the meter to provide a stable

reading, it was found that a much longer time was required so that often even after 15 minutes the RMS reading was still very slowly decreasing as if it were a very slow exponential decay. This problem will be discussed again in Chapter VI in relation to the "X" configuration probe. Since for the single sensor results, similar information to the intensities from the RMS meter can be obtained from the anemometer versus time plots using average peak to peak values, this problem was more bypassed than solved.

The constant temperature anemometer operates using a feedback circuit to vary the current passing through the sensor such that the sensor remains at a constant temperature difference above the fluid temperature. This temperature difference is controlled by effectively increasing the probe resistance a given ratio above its value at the fluid temperature. For this project an overheat ratio of 1.1 was used. Because the resistance changes with temperature, three matters must be considered: (1) the effect of temperature on over-heat ratio, (2) the effect of temperature level on probe calibration, and (3) the effect of temperature fluctuations on the apparent velocity fluctuations. The operation of the anemometer and these effects will now be discussed.

For most materials, the electrical resistance for the temperature range of interest can be expressed as

$$R = R_e + a_1(T-T_e) \tag{III. 1}$$

where R_e is the resistance at some reference temperature, T_e. Letting R be the sensor resistance and T be the sensor temperature during operation, and letting R_e be the normal sensor resistance at the fluid temperature T_e, then dividing by R_e, the overheat ratio is

$$OHR = R/R_e = 1 + b_1(T-T_e),\ b_1 = a_1/R_e \tag{III. 2}$$

The constant temperature difference is therefore

$$T-T_e = (OHR-1)/b_1. \tag{III. 3}$$

The heat generated within the sensor ($volt^2/R$) must be carried away by convection due to the flow velocity. The voltage drop across the sensor is thus equal to some function of the velocity times the temperature difference,

$$volt^2/R = F(velocity)(T-T_e). \tag{III. 4}$$

or using the information above,

$$\begin{aligned} volt^2 &= F(velocity)(R)(OHR-1)/b_1 \\ &= F(velocity)(OHR)(R_e)(OHR-1)/b_1. \end{aligned} \tag{III. 5}$$

The anemometer signal is therefore proportional to the function F which is the desired probe calibration, and is also proportional to

the probe resistance and actual over-heat ratio.

For a steady temperature field, the over-heat ratio can always be set at the desired value by setting the correct probe resistance on the variable decade resistance. This effectively changes the probe resistance by changing the resistance in the leg opposite the probe in the anemometer bridge circuit. This proper resistance is determined by making a probe resistance versus temperature curve and then multiplying this resistance by the desired overheat ratio. The decade resistance provides the capability to set the desired resistance to the nearest 0.01 ohm. Since the desired resistance was never "right on" the nearest 0.01 ohm, a correction factor was incorporated in the data reduction program using the resistance versus temperature relation and a measurement of the effect of probe resistance on anemometer output (9.5 volts/ohm) to calculate what the anemometer output would have been if the overheat ratio had been set exactly.

The effect of temperature level on the velocity measurement can be seen by examining equation III. 5. Since the overheat ratio can be properly set once the temperature is measured, and since b_1 is effectively a constant, the only effect on the voltage other than the velocity will be the temperature variation of R. For the sensor used, $b_1 = 0.0026/^{o}C$ and $R_e = 6$ ohms. For the total range of operation of about $30^{o}F$, from equations III. 1 and III. 2 this corresponds to a variation in resistance of about 0.025 ohm. This corresponds to about a

0.4% variation in the velocity calibration due to temperature, which is not significant enough to worry about.

Finally, the effect of temperature fluctuations on the apparent velocity fluctuations can never be eliminated with the use of a single sensor. It can be shown, however, that the maximum effect of the observed temperature fluctuations on the anemometer output were much less than the observed velocity fluctuations. From equation III.3, the actual temperature difference between the hot sensor and the local fluid was calculated to be 69°F. The maximum temperature fluctuations observed were on the order of 3°F to 4°F, with a more representative fluctuation about 1.5°F. Observing equation III.4 and recalling from the previous paragraph that a 30°F difference only changed R by .4%, it can be seen that the only noticeable effect that temperature fluctuations will have on the anemometer output is in changing the actual operating temperature difference. A 4°F fluctuation will cause a deviation from the mean temperature difference of 2°F, which will cause a variation of about 2.9% in the square of the voltage, or a variation in the anemometer output of about 1.7%. This is the maximum estimated effect, but should be kept in mind when interpreting the anemometer output.

Velocity Calibration Apparatus

In "Velocity Measuring System" the functional relationship between the fluid velocity and the square of the anemometer voltage was demonstrated. The only accurate way to determine this functional relationship is to find it empirically using a calibration apparatus where the voltage and actual fluid velocity can be measured simultaneously. The apparatus and techniques used for this thesis to calibrate the hot film anemometer were developed and used by White (47), Hurt (20), and Colwell (5). Figures III. 9 and III. 10 show photographs of the calibration set up. This apparatus allows calibrating the anemometer as it descends vertically in a quiet tank of mercury, producing the exact same flow over the sensor as occurs when the probe is stationary and the mercury is flowing upward due to natural convection. Hurt demonstrated that these calibrations were repeatable with reinsertion of the probe as long as the probe was inserted through a clean water or mercury interface. For this work the probe was calibrated before taking data, removed from the mercury and set up in the channel configuration and reinserted, but then it was recalibrated after data taking, without removing the probe from the mercury to set up the calibration apparatus. The calibration curves were repeatable.

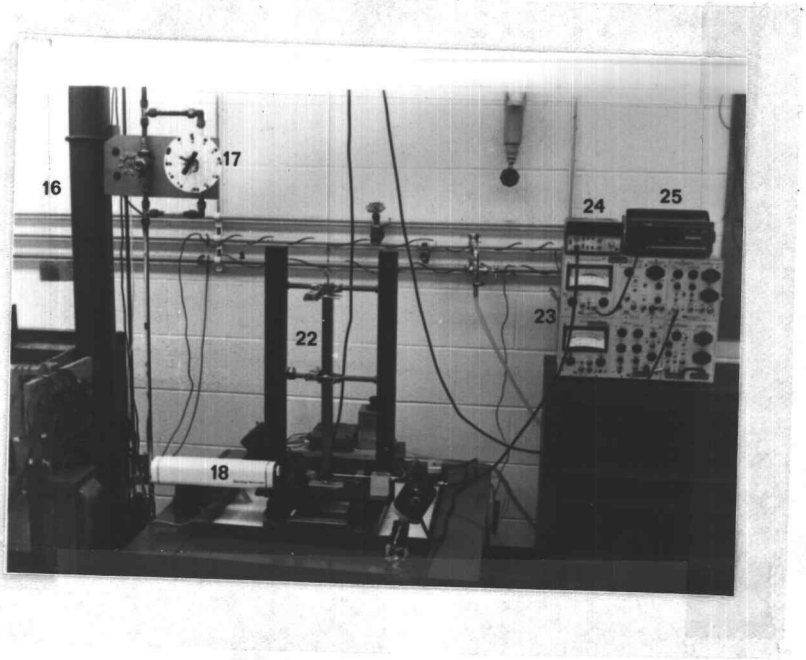

Figure III. 9. Photograph of calibration system.

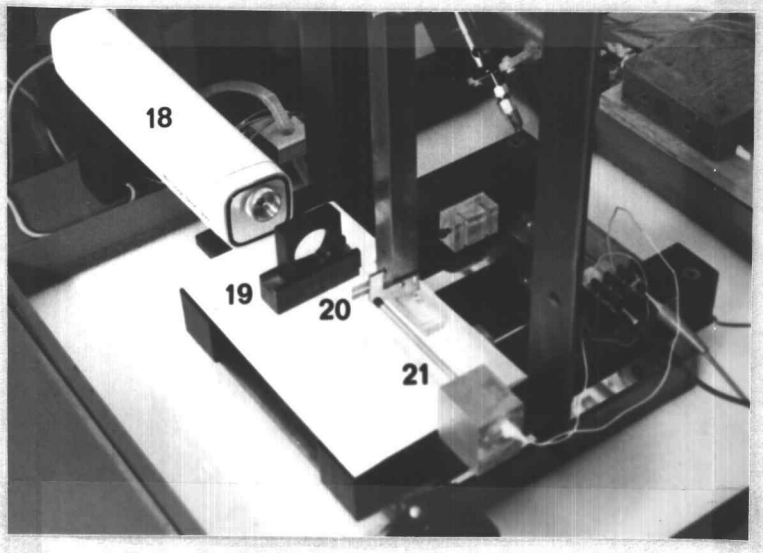

Figure III. 10. Photograph showing alignment of laser beam and photocell.

The velocity probe was attached at the bottom end of the 1 inch square steel bar with ground surfaces [22]. The bar was constrained to move in a vertical direction by eight precision roller bearings attached to the rigid frame. As the steel bar descended, by means of a steel wire and two pulleys it drew a piston through a 3 inch inner diameter pipe [16] with lapped inner surface. The rate at which the steel bar dropped was controlled by the selection of three different size pistons which allowed more or less leakage, and by opening or closing the 13 turn needle valve [17] through which the water had to circulate as the piston moved. The viscous drag of the piston was such that a terminal constant velocity was reached before the voltage and velocity were measured.

The velocity of the steel bar was determined by measuring the time interval between when the leading edges of two razor blades [20] crossed the beam from a laser manufactured by Metrologic [18], which was focused to a pinpoint with a single lens [19]. The two razor blades were parallel with the distance between leading edges measured to be 0.2235 inch, using a Nikon model 6C shadowgraph. The break in the light beam was detected by a photocell located at the end of the columnator [21] which, in conjunction with a shunting circuit, produced two square wave pulses that were sent to a Hewlett-Packard model 5300A counter [24].

The counter gate opened on the positive slope of the first square wave (corresponding to the leading edge of the first razor blade) and shut on the positive slope of the second square wave (corresponding to the leading edge of the second razor blade). The anemometer output was monitored as the steel bar descended using the Fluke digital voltmeter [25] and a voltage reading was taken as the timer gate opened. This procedure was repeated over the range of anticipated velocities (about 5 in/min to 200 in/min). The timer measurements were then converted to velocities using the known distance between the two razor blades, and a functional relation obtained for velocity as a function of voltage using SIPS, a statistical linear regression program available on the CDC3300 computer at Oregon State University.

The Two-Sensor "X" Configuration Probe

The final phase of the work for this thesis utilized a two-sensor "X" configuration probe. The entire probe is shown schematically in Figure III. 11 and close-up photographs of the sensing portion of the probe are shown in Figure III. 12. The theory and problems associated with the use of this probe will be considered in more detail in Chapter VI, but the probe itself will be discussed briefly here. This probe has two hot film sensors which are identical in construction to that of the single sensor probe described in "Velocity

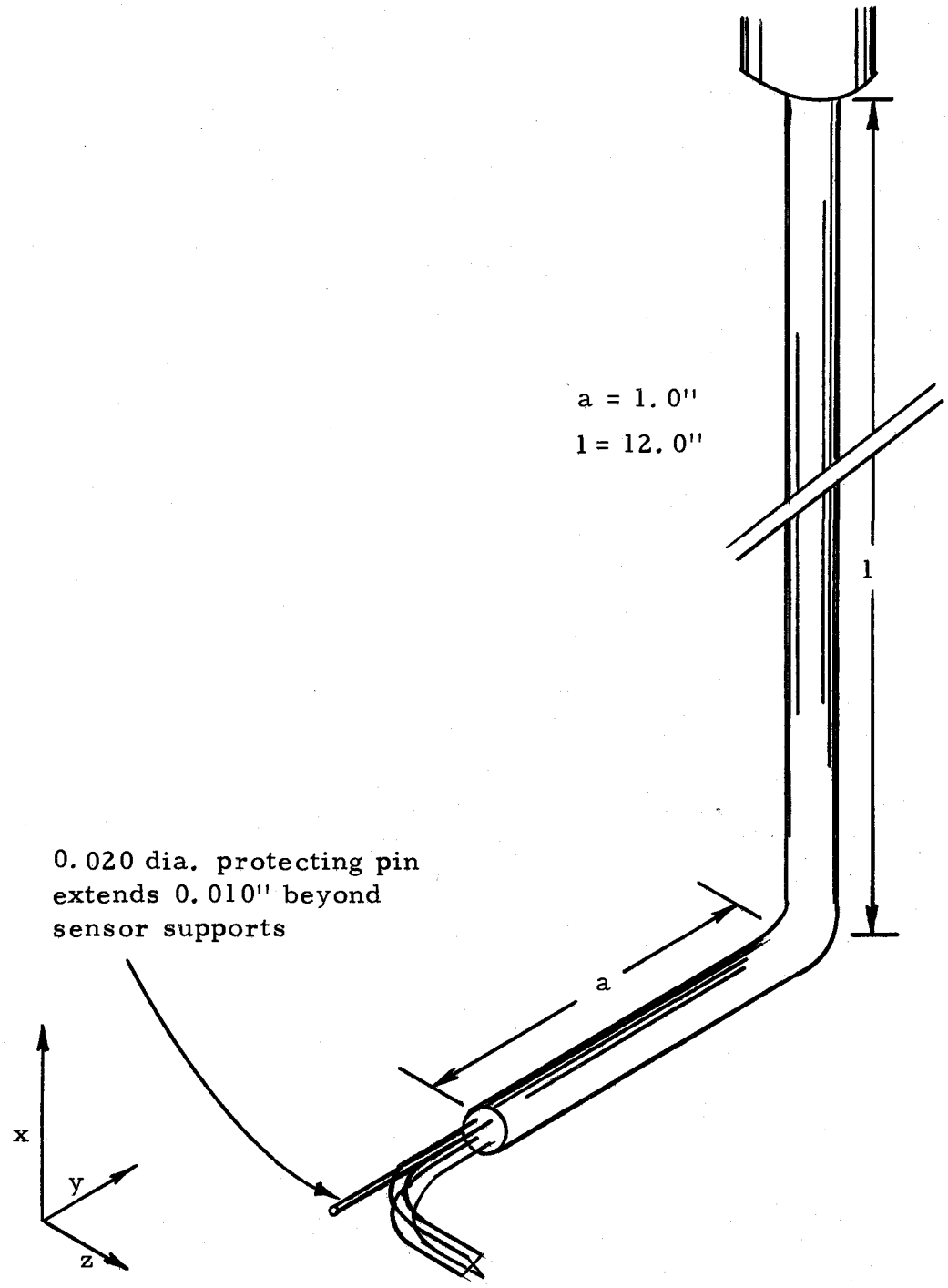

Figure III.11. Schematic of two-sensor "X" configuration probe.

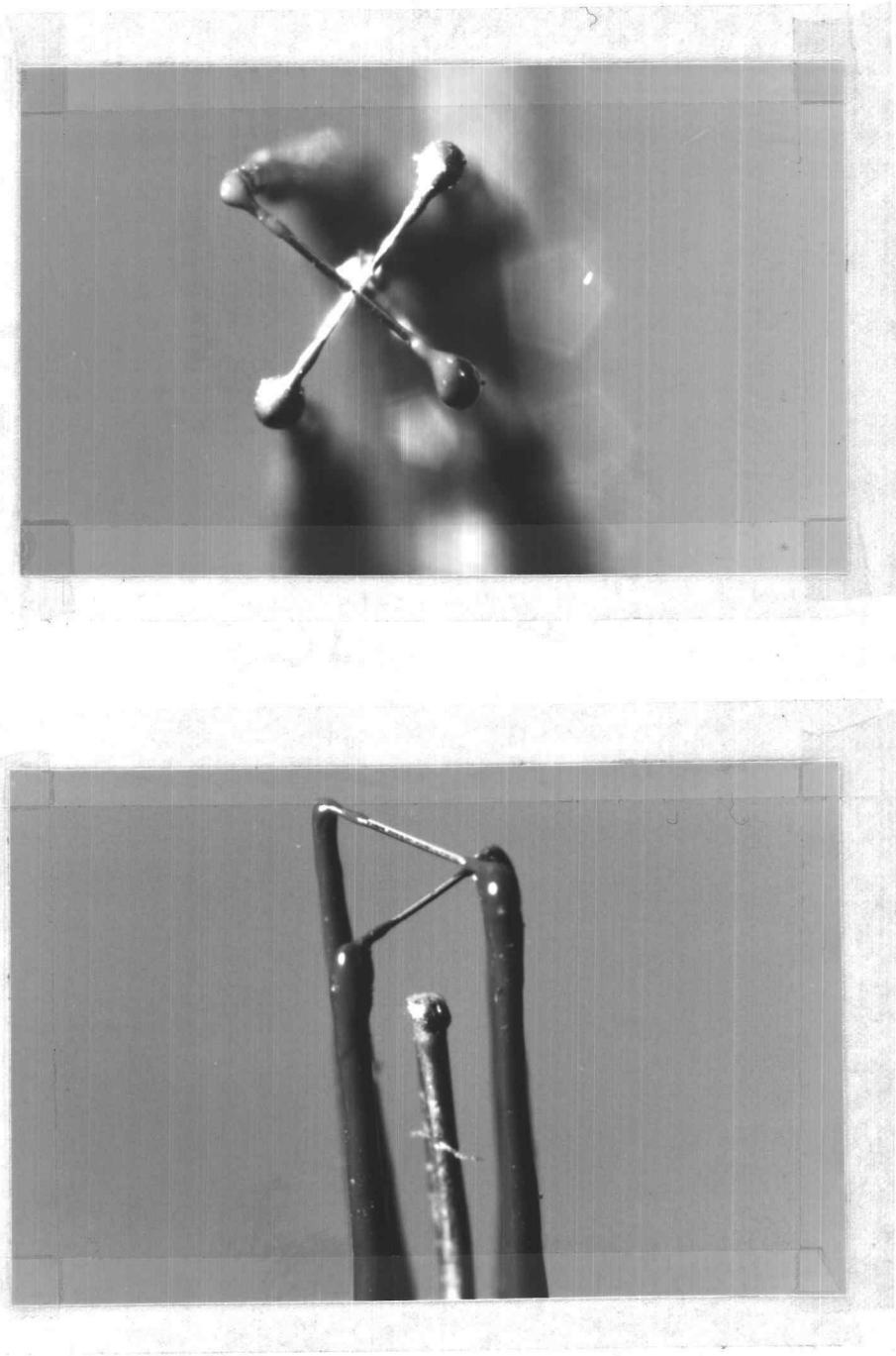

Figure III. 12. Photographs of the two-sensor "X" configuration probe.

Measurement System". The sensors are now located in the x-y plane, each at an angle of 45° to the vertical plate and at a nominal angle of 90° to each other.

Just as with the single sensor probe, two thermocouples were epoxied to the "X" configuration probe. One thermocouple was located at the same horizontal and vertical positions as the intersection of the two hot film sensors (note that the two sensors do not really intersect as they are both separated from each other and the thermocouple in the z direction). This thermocouple was used to determine the average temperature for setting the proper probe resistances. Since the temperature varied across the two sensors in the x and y directions and was varying with respect to time, this reading was an average temperature over x, y and time. The second thermocouple was located on a protecting pin, 0.020 inch in diameter, such that the bead of the thermocouple was 0.010 inch to 0.015 inch closer to the plate than the sensor supports. This thermocouple was used to locate the plate without damaging the sensors by allowing them to make contact with the plate.

The resistance of each probe was set individually in the same way as for the single sensor except, as will be noted in Chapter VI, each probe resistance should be measured while the other probe is operating at the desired overheat ratio. The output from each sensor was connected by way of a 15-foot guarded triaxial cable to a series

1050 anemometer. The one anemometer used was the TSI model 1050 general purpose anemometer already discussed for use with the single sensor probe. The second anemometer was a model 1054A which, when used on the unlinearized bridge output with a model 1056 variable decade resistance, functioned identically to the model 1050. The outputs from the two anemometers were then channeled into the model 1015C correlator. The correlator provides the option of reading either signal individually, taking the sum, difference, or finding the correlation coefficient between the two signals. The output from the correlator was then sent to the x-y plotter, the true RMS voltmeter, or the digital voltmeter.

IV. HEAT TRANSFER CORRELATIONS

Introduction

In the study of natural convection, the information that has probably the most direct application to the engineer is that information pertaining to heat transfer. The engineer wants to know how the surface and bulk fluid temperatures relate to the amount of heat being transferred. When heat transfer data is collected, analyzed, and an empirical functional relationship for it expressed, the results can be used in two ways. On the one hand, the empirical relations obtained can be used to demonstrate trends in heat transfer as different parameters are varied. For this thesis, information was desired concerning how vertical position on the plate and spacing of the channel affected the heat transfer. From this point of view, statistical analysis is of great value. Trends might be very slight, but if the data indicate these trends to be statistically significant, conclusions can be made.

The second use of the heat transfer results is in predicting a maximum surface temperature or heat transfer rate in a design situation. In this situation, the significance of results should be regarded from a practical, not statistical, point of view. If the engineer knows that the uncertainty of a parameter in his calculations is plus or minus ten percent, he is not really interested in using a more elegant equation which includes additional parameters which change the results by plus or minus two percent, even though these

other parameters might be very significant statistically. For this situation, the engineer wants as simple a relationship as possible that still allows him to make use of all the significant information he has. In the following discussion of heat transfer results, both the statistical and practical significance will be discussed.

Dimensionless Heat Transfer Parameters

In the dimensional analysis and empirical correlation of natural convection heat transfer data, three dimensionless parameters are significant -- the Nusselt number (Nu), the Prandtl number (Pr), and the Grashof number (Gr). The Nusselt number, defined as

$$Nu_L = \frac{hL}{k} \quad \text{or} \quad Nu_L = \frac{h}{k/L}, \tag{IV. 1}$$

is equal to the convective heat transfer coefficient, h, times a significant length, L, divided by the thermal conductivity of the fluid, k. The Nusselt number can also be thought of as the ratio of the conductive resistance L/k to the convective resistance 1/h, as is indicated by the second expression. Also, for a fluid in a temperature range where k does not vary greatly, the Nusselt number is directly indicative of the value of h. This in turn is indicative of the amount of heat that can be transferred to the fluid at ambient temperature T_a from the heated wall at temperature T_s, since the definition of h is

$$q = Q/A = h\,(T_s - T_a) \qquad \text{(IV. 2)}$$

In design situations, the expression for the Nusselt number is used to calculate the convective coefficient, h, since k is a property of the fluid and T_s and T_a are either known or are the desired unknowns. In measuring the Nusselt number, however, h cannot be measured, so it must be expressed in terms of the heat flux, q, and the temperature difference, $T_s - T_a$. At the wall, due to shear forces and the "no-slip" condition, the fluid velocity is zero and hence all the heat transfer is due to conduction. The heat flux, therefore, can also be expressed as

$$q = -k\, dT/dx\Big|_{wall} \qquad \text{(IV. 3)}$$

The convective coefficient can be expressed as

$$h = q/(T_s - T_a) = \frac{-k\, dT/dx\Big|_{wall}}{T_s - T_a} \qquad \text{(IV. 4)}$$

The temperatures and property values to be used in calculating the Nusselt number vary as a function of the vertical and horizontal positions in the channel. For this study, the length of the plate (distance in the vertical direction) is used as the significant length, L. For natural convection from a vertical plate, Sparrow and Gregg (37) showed that the variation of properties in the horizontal direction can be accounted for by calculating fluid properties at a reference

temperature $T_r = 0.7\ T_s(x) + 0.3\ T_a$. A local Nusselt number, Nu_x, can therefore be defined which is only a function of the vertical position, x:

$$Nu_x = \frac{q\ \ x}{k(T_s - T_a)} = -\frac{x\ dT/dx\Big|_{wall}}{T_s - T_a} \qquad \text{(IV. 5)}$$

For some purposes this local Nusselt number is more useful than the average Nusselt number; however, the average Nusselt number (more useful in actual engineering application) is often defined as

$$Nu_L = \frac{1}{L}\int_o^L Nu_x dx \qquad \text{(IV. 6)}$$

The second significant parameter in convection is the Prandtl number, defined as

$$Pr = \frac{\nu}{\alpha} = \frac{\mu c}{k} \qquad \text{(IV. 7)}$$

The Prandtl number is a ratio of the molecular diffusivity of momentum, ν, which is the viscosity, μ, divided by the density, ρ, and the molecular diffusivity of heat, α, which is the thermal conductivity, k, divided by the density times the specific heat, c.

$$\nu = \frac{\mu}{\rho}\ ,\ \alpha = \frac{k}{\rho c} \qquad \text{(IV. 8)}$$

This thesis is concerned with a low Prandtl number fluid, mercury, whose thermal diffusivity is much greater than its momentum diffusivity. Only one fluid was studied in this work, and since the Prandtl number only varied about 3% from 0.022 to 0.0235, the Prandtl number was not included in the correlation.

The third dimensionless parameter of interest in natural convection flows is the Grashof number

$$Gr_L = \frac{\beta g \rho^2 L^3 (T_s - T_a)}{\mu^2} \qquad \text{(IV. 9)}$$

The only property included in the Grashof number not included before is β, the coefficient of thermal expansion. The Grashof number is basically a ratio between the thermal driving force which accelerates the vertical flow, β T, and the viscous effects which decelerate the flow. The larger the Grashof number, the more intense one would expect the flow to be, hence the Grashof number serves the role in natural convection that the Reynolds number serves for forced convection.

For a constant heat flux plate, one generally knows q but does not know ΔT, though the two are related through the Nusselt number. Since it seems logical to use a parameter that makes use of the information available, a modified Grashof number is defined, which is simply the Grashof number multiplied by the Nusselt number based on the heat flux, q. As with the Nusselt number, only local conditions

can be measured, therefore the Sparrow and Gregg reference temperature is used and the local modified Grashof number is defined as

$$Gr_x^* = Gr_x Nu_x = \frac{\beta g \rho^2 x^3 \Delta T}{\mu^2} \cdot \frac{qx}{k \Delta T} = \frac{\beta g \rho^2 x^4 q}{k \mu^2} \qquad \text{(IV. 10)}$$

and the average modified Grashof number is

$$Gr_L^* = \frac{1}{L} \int_o^L Gr_x^* \, dx. \qquad \text{(IV. 11)}$$

One final parameter is the dimensionless ratio, w/L. L is the height of the channel which was a constant 5 inches, and w is the width of the channel which was varied from 1.25 to 3.33 inches.

Data Taking Procedures

In "Dimensionless Heat Transfer Parameters", two different expressions were presented for calculating the Nusselt number, one using the measured heat flux, q, the other using the temperature gradient at the wall. As was previously mentioned, because the power supplies were not regulated there is a potential 5% error introduced in the data because of the uncertainty in Q, the total heat input. Colwell (5) demonstrated the potential error in evaluating the temperature gradient to be much greater than this, however, possibly as large as 30%. This is because the gradient must be evaluated by measuring the temperature at several distances from the plate. Colwell tried

both graphical techniques and polynomial regressions, but found that small errors in absolute temperature readings created large errors in the estimate of the gradient. This was because the overall temperature difference for the region where the temperature measurements were taken was small. Since small temperature differences would be even more difficult to measure in this present work due to the instability of the flow than for Colwell's case of laminar flow, the Nusselt number was calculated using q rather than the temperature gradient.

From "Dimensionless Heat Transfer Parameters", the quantities needed to calculate local Nusselt and modified Grashof numbers, Prandtl number, and channel spacing parameter are c, β, g, ρ, x, k, μ, Q, L, A_s, w, T_s, and T_a. Of these, β and g are, for all practical purposes, constants with values

$$\beta = 0.000101 \text{ (deg F)}^{-1}$$

$$g = 32.174 \text{ ft/sec}^2.$$

c, ρ, k, and μ are all fluid properties which can be expressed as functions of the reference temperature $T_r = 0.7T_s + 0.3T_a$. Property values for the temperature range of concern were taken from the Liquid Metals Handbook (29), and were checked against the polynomial representations used by Sparrow and Gregg (37). These were found to be in very good agreement; thus for consistency in comparing results, these same expressions were used and are presented below:

$$k = 4.47924 + 8.30958 \times 10^{-3} T_r - 3.80163 \times 10^{-6} T_r^2$$

$$\mu = 4.34620 - 9.91162 \times 10^{-3} T_r + 1.79060 \times 10^{-5} T_r^2 - 1.27524 \times 10^{-8} T_r^3 \qquad \text{(IV.12)}$$

$$c = 3.34620 \times 10^{-2} - 3.93353 \times 10^{-5} T_r + 3.44649 \times 10^{-9} T_r^2$$

$$\rho = 851.514 - 8.64880 \times 10^{-2} T_r + 9.86194 \times 10^{-6} T_r^2 - 5.92566 \times 10^{-9} T_r^3$$

The units of each are:

k = Btu/hr ft deg F

μ = lbm/ft-hr

c = Btu/lbm-deg F

ρ = lbm/ft^3

As was described in "Channel Construction and Location", temperatures were measured with a single iron-constantan thermocouple calibrated against a quartz thermometer. Since time-averaged readings were taken, reading errors should have been random. The major source of error for $T_s - T_a$ was a possible systematic error due to a poor calibration. This error would, at most, be 3%.

The quantities remaining to be measured are x, Q, A, L, and w. The vertical position along the plate, x, was determined using the x-y vernier positioner already described, accurate to 0.001 inch. Wall temperature readings were taken at one-eighth inch intervals from one

inch to four and one half inches above the leading edge. There were three sources of error in the determination of x: a degree of ambiguity in finding the leading edge, misplacement of the vernier when setting a plate position, and buoyancy effects on the probe. The temperature probe construction was such that buoyancy effects should have been negligible, and an occasional misplacement of the probe would be unlikely but random; therefore, the dominant uncertainty exists due to the curvature of the leading edge of the steel plate. This uncertainty in defining the leading edge was less than 0.005 inch, which means the maximum percentage error in x occurring at the smallest x, 1 inch, was 0.5%. A more representative value for this uncertainty would be 0.25% to 0.125%.

The heat output from the plate was measured from the current and voltage drop across the plate. The uncertainty of these measurements were, respectively, $\pm$ 0.05 ampere and $\pm$ 0.8 volt. These uncertainties and the fact that about 0.1% of the heat was lost to the back side of the plates, however, were overshadowed by drift in the power output of the power supplies, already mentioned, which was at worst 5%.

The heat flux area, A_s, was measured in two different ways. There was potential error in measuring the heater element area and in the variation from one element to the next. Referring back to Figure III.4, the area was defined as the foil area where one half the

distance between etched rows was added to each edge, minus the tab area where the leads were connected. Colwell took these dimensions from an x-ray photograph and estimated the potential error to be 2%. This value was checked using a light table and direct measurement with caliper gauges on a different heating element and found to agree within about 0.6%, so an estimated uncertainty of 2% seems very safe.

The values of L and w were only used in the average correlations, but were measured using caliper and expanding gauges. Here, L was not used as the heating element height but as the actual physical channel height which was 5.00". The width of the channel, w, varied by as much as 0.010 inch, but for the smallest value of w, 1.25 inches, this was still less than 0.5% deviation.

Single Vertical Plate Results

Before heat transfer data were taken for the vertical channel with side plates, data were taken using a single heated vertical plate without side plates at four heat fluxes ranging from 7,900 to 12,300 $BTu/hr\text{-}ft^2$. This range was selected because preliminary work indicated that it would produce turbulent convection without exceeding the limits of the present equipment. The single plate represents a limiting case as the ratio, w/L goes to infinity. This case lends itself more easily to analysis and has been studied more experimentally, hence offers the opportunity for comparing the validity of results and techniques.

The local Nusselt and modified Grashof numbers have been calculated for the single vertical plate data using the computer program TURBHTX2 listed in the Appendix, and have been plotted in Figure IV. 1. The linear form of these data on log-log coordinates, $\log Nu_x = a + b \log GR_x^*$, indicates that the data can be expressed well as a power function by exponentiating each side:

$$Nu_x = K(Gr_x^*)^n \qquad \text{(IV. 13)}$$

Using the OS3 computer system Statistical Interactive Programming System (SIPS), the data were regressed and the local correlation found to be

$$Nu_x = 0.196(Gr_x^*)^{.188} \qquad \text{(IV. 14)}$$

Though the trend is very slight and difficult to see without using a straight edge, the slope of the line formed by the data increases as the Grashof number increases. This is demonstrated in Figure IV. 1. Since a marked increase in the slope was expected as fully turbulent flow occurred, a statistical computer program, LIKLEHUD, was developed which allowed the fitting of two regression lines of different slopes which were constrained to intersect at their breakpoint. The breakpoint was selected so as to minimize the residual sum of squares between the regression lines and the data. The statistical development and use of this program is included in the Appendix.

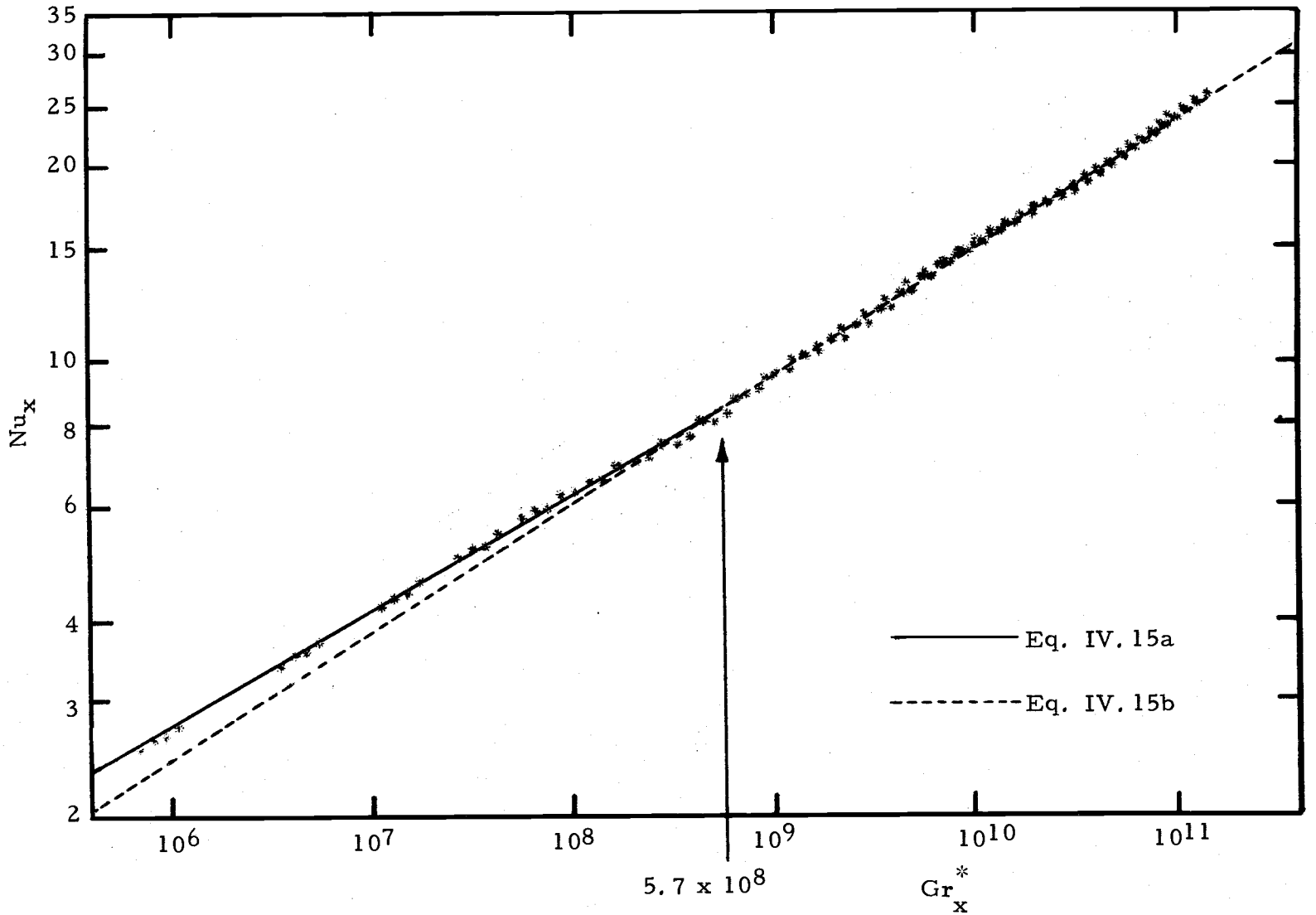

Figure IV. 1. Local heat transfer data for single vertical heated plate.

Figure IV. 1 shows the results when the data were fitted with two lines as described above. The optimum breakpoint was found to be $Gr_x^* = 5.7 \times 10^8$ and the two regression lines were:

$$Nu_x = .227\,(Gr_x^*)^{.179} \quad \text{for } 10^6 < Gr_x^* < 5.7 \times 10^8 \qquad \text{(IV. 15a)}$$

$$Nu_x = .156\,(Gr_x^*)^{.197} \quad \text{for } 5.7 \times 10^8 < Gr_x^* < 2 \times 10^{11} \qquad \text{(IV.15b)}$$

These results are first compared to the results of Colwell (5), who used basically the same test configuration at lower Grashof numbers, in order to stay in stable laminar flow. His regression equation for the single vertical plate was:

$$Nu_x = .230\,(Gr_x^*)^{.180} \quad \text{for } 10^4 < Gr_x^* < 10^9 \qquad \text{(IV. 16)}$$

This result is in very good agreement with the present results, using equation (IV. 15a) which covers approximately the same region as Colwell's work. These results are also compared to the experimental results of Julian and Akins (22) and the analytical results of Chang, Akins, Burris, and Bankoff (4). Their results are, respectively:

$$\text{Julian: } Nu_x = .196(Gr_x^*)^{.188} \quad \text{for } 10^5 < Gr_x^* < 10^9 \qquad \text{(IV. 17)}$$

$$\text{Chang: } Nu_x = .154(Gr_x^*)^{.2}. \qquad \text{(IV. 18)}$$

Equations (IV. 14) through (IV. 18) have been graphed in Figure IV. 2 for comparison. All equations are shown for the entire range of the present work for purposes of comparison even though most of these

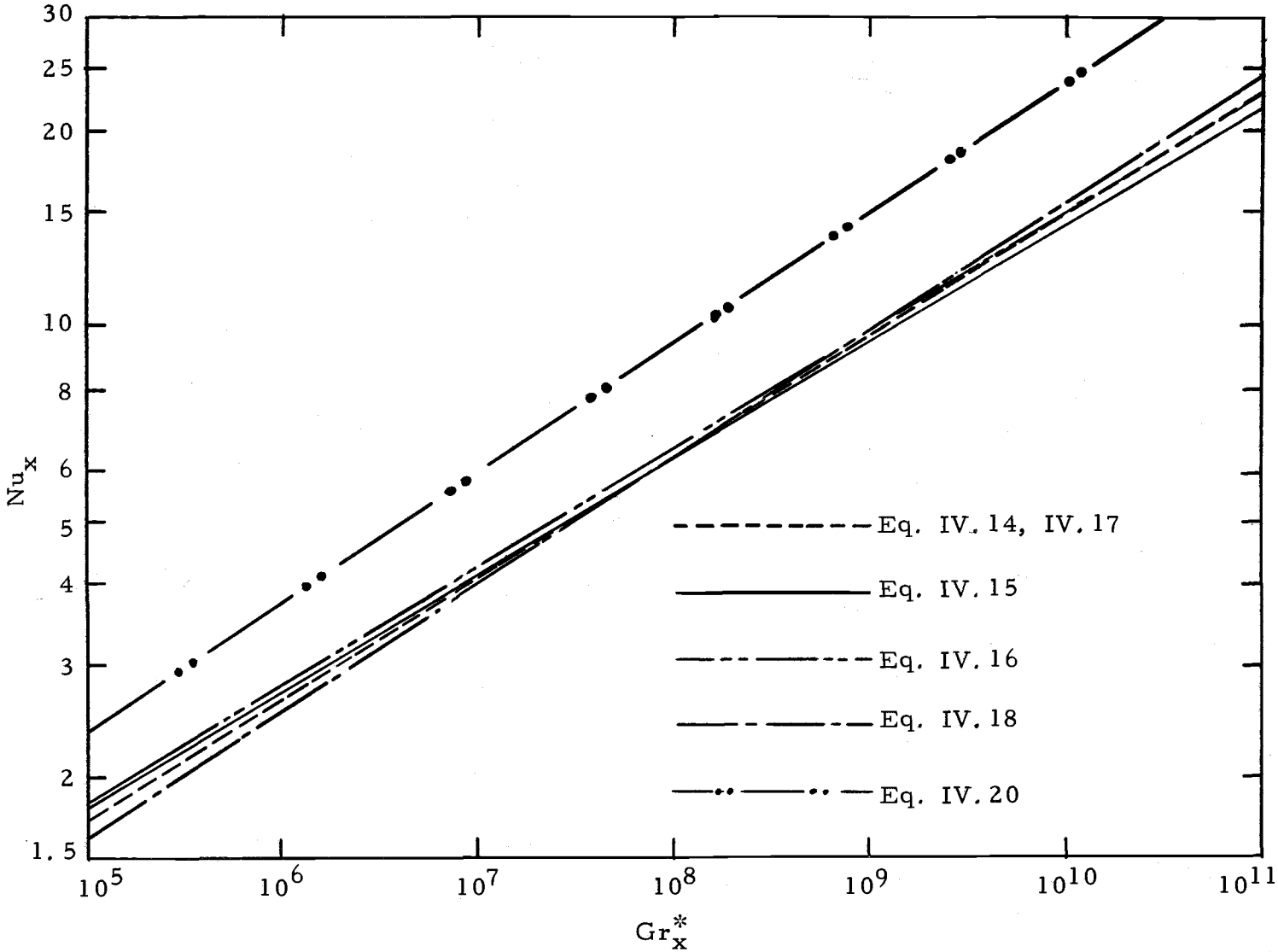

Figure IV. 2. Local heat transfer correlations for single vertical heated plate.

lines do not apply for this entire range.

Note that Julian's regression line, equation (IV. 17) is identical to the single regression line from the present work, equation (IV. 14). Also note that the perturbation solution result, equation (IV. 18) is nearly identical to equation (IV. 15b). This is somewhat surprising since these results are for laminar flow at lower Grashof numbers. With the exception of the lower boundary, percentage differences between results are very small and it appears that results of the different studies are in good agreement. This verifies Colwell's conjecture that his regression line would be valid into transition up to $Gr_x^* = 10^{11}$. This agreement also indicates the data taking and regression techniques to be valid.

Finally, Figure IV. 2 shows the results of Eckert and Jackson (10) for natural convection from isothermal vertical surfaces in air. They found that transition occurred in the region from $10^8 < GrPr < 10^{10}$ and suggest the following heat transfer correlations

$$Nu_L = 0.555(Gr_L Pr)^{.25} \text{ for } Gr_L Pr < 10^9 \qquad \text{(IV. 19a)}$$

$$Nu_L = 0.021(Gr_L Pr)^{.4} \text{ for } Gr_L Pr > 10^9 \qquad \text{(IV. 19b)}$$

Using a Prandtl number of 0. 023, equation (IV. 19), when expressed in terms of the modified local Grashof number, becomes:

$$Nu_x = .235\,(Gr_x^*)^{.2} \quad \text{for } Gr_x^* < 3 \times 10^{11} \qquad \text{(IV. 20a)}$$

$$Nu_x = .0246(Gr_x^*)^{.286} \quad \text{for } Gr_x^* > 3 \times 10^{11} \qquad \text{(IV. 20b)}$$

These results are presented to indicate a trend which was not observed in the present work. Eckert and Jackson found that when the flow became fully turbulent there was a very significant increase in slope of the regression line, as indicated by the exponent of .286 in equation (IV.20b). They did not work in liquid metals and their boundary condition was different, so it is not surprising that their results do not agree even in the lower regime. This comparison simply brings up a point which will be discussed in further detail both in this chapter and in Chapter V. The effect of turbulent flow was not observed in the heat transfer data because the large temperature and velocity fluctuations only occurred at the upper end of the data and it appears that these fluctuations are characteristic of transition and not fully turbulent convection.

In the previous comparisons, correlations were converted from average to local and from normal Grashof number to modified Grashof number. The relationship between local and average parameters was already defined in equation (IV.11). For the case of local Nusselt number as a function of the local modified Grashof number,

$$Nu_x = K(Gr_x^*)^n, \tag{IV.13}$$

by performing the necessary integration with respect to x, the average Nusselt number becomes

$$Nu_L = K/4n\,(Gr_L^*)^n. \qquad \text{(IV. 21)}$$

Converting from average to local correlations is simply the inverse of equation (IV. 21). To conclude this section, equations (IV. 14) and (IV. 15) in terms of average Nusselt and Grashof numbers are as follows:

$$Nu_L = .252(Gr_L^*)^{.188} \qquad 10^5 < Gr_L^* < 10^{11} \qquad \text{(IV. 22a)}$$

$$Nu_L = .317(Gr_L^*)^{.179} \qquad 10^5 < Gr_L^* < 5.7 \times 10^8 \qquad \text{(IV. 22b)}$$

$$Nu_L = .198(Gr_L^*)^{.197} \qquad 5.7 \times 10^8 < Gr_L^* < 10^{11} \qquad \text{(IV. 22c)}$$

Uniformly Heated Vertical Channel Results

Heat transfer data were taken for three relatively wide channel spacings, w/L = 0.25, 0.50, and 0.67. With a channel height, L, of 5 inches, this corresponded to channel widths of 1.25, 2.50 and 3.33 inches. No narrower channel spacings were studied because it was desired to take data that would relate to the results from the two-sensor "X" configuration probe, which was restricted to relatively wide channel spacings. Data were taken at three heat flux levels ranging from 9,300 to 12,300 BTU/hr-ft^2. This range was expected to produce turbulent convection.

The local Nusselt and modified Grashof numbers have been calculated for the three individual channel spacings using the computer program TURBHTX 1, listed in the Appendix, and are plotted in

Figure IV. 3. As with the single plate data, these data are very linear on the log-log scale and can be regressed using the SIPS linear regression program. The resulting heat transfer correlations are

$$Nu_x = .248(Gr_x^*)^{.178} \text{ for } w/L = .67 \qquad \text{(IV.23a)}$$

$$Nu_x = .244(Gr_x^*)^{.179} \text{ for } w/L = .50 \qquad \text{(IV.23b)}$$

$$Nu_x = .264(Gr_x^*)^{.176} \text{ for } w/L = .25. \qquad \text{(IV.23c)}$$

These three expressions appear nearly equal for all practical purposes. They have been graphed for comparison on Figure IV. 4. Also on Figure IV. 4 is Colwell1s (5) correlation for his vertical channel with side plates for a channel spacing of $w/L = .50$,

$$Nu_x = .238(Gr_x^*)^{.179} \text{ for } w/L = .50, \qquad \text{(IV.24)}$$

Colwell's data were taken for Grashof numbers less than 10^9 whereas the present work covered the range from 10^8 to 10^{11}. In view of this difference and the fact that Colwell's side plates did not completely enclose the channel for $w/L = .50$, the agreement is very good.

As already mentioned, from a practical standpoint, the three correlations given in equation (IV. 23) are almost equal. It is here that both statistical and practical significance of the data can be considered as discussed in "Introduction". From a practical standpoint, the most that the results ever differ is about 5%. Due to the uncertainty inherent in the results and the uncertainty in the values of

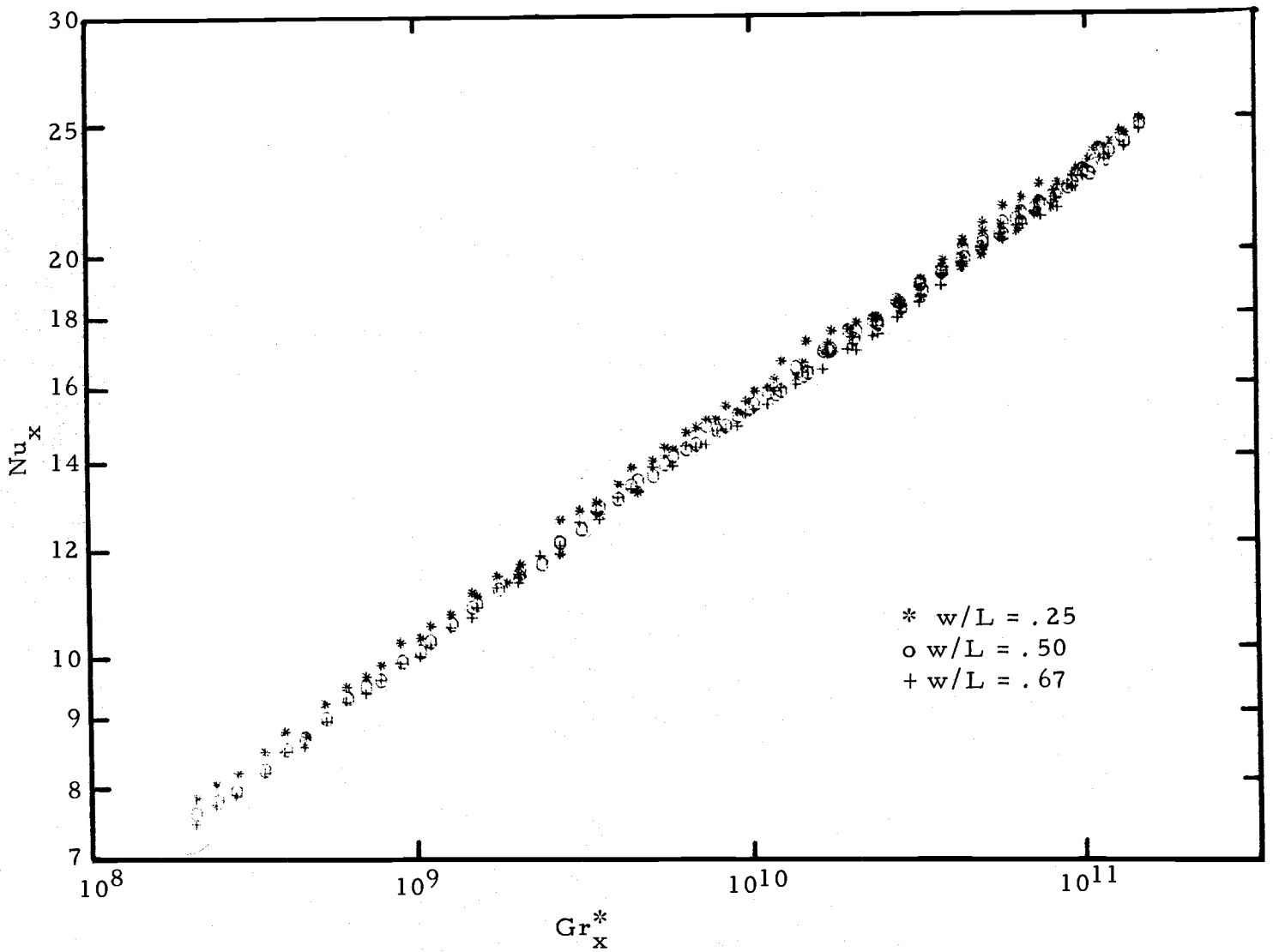

Figure IV. 3. Local heat transfer data for uniformly heated vertical channel.

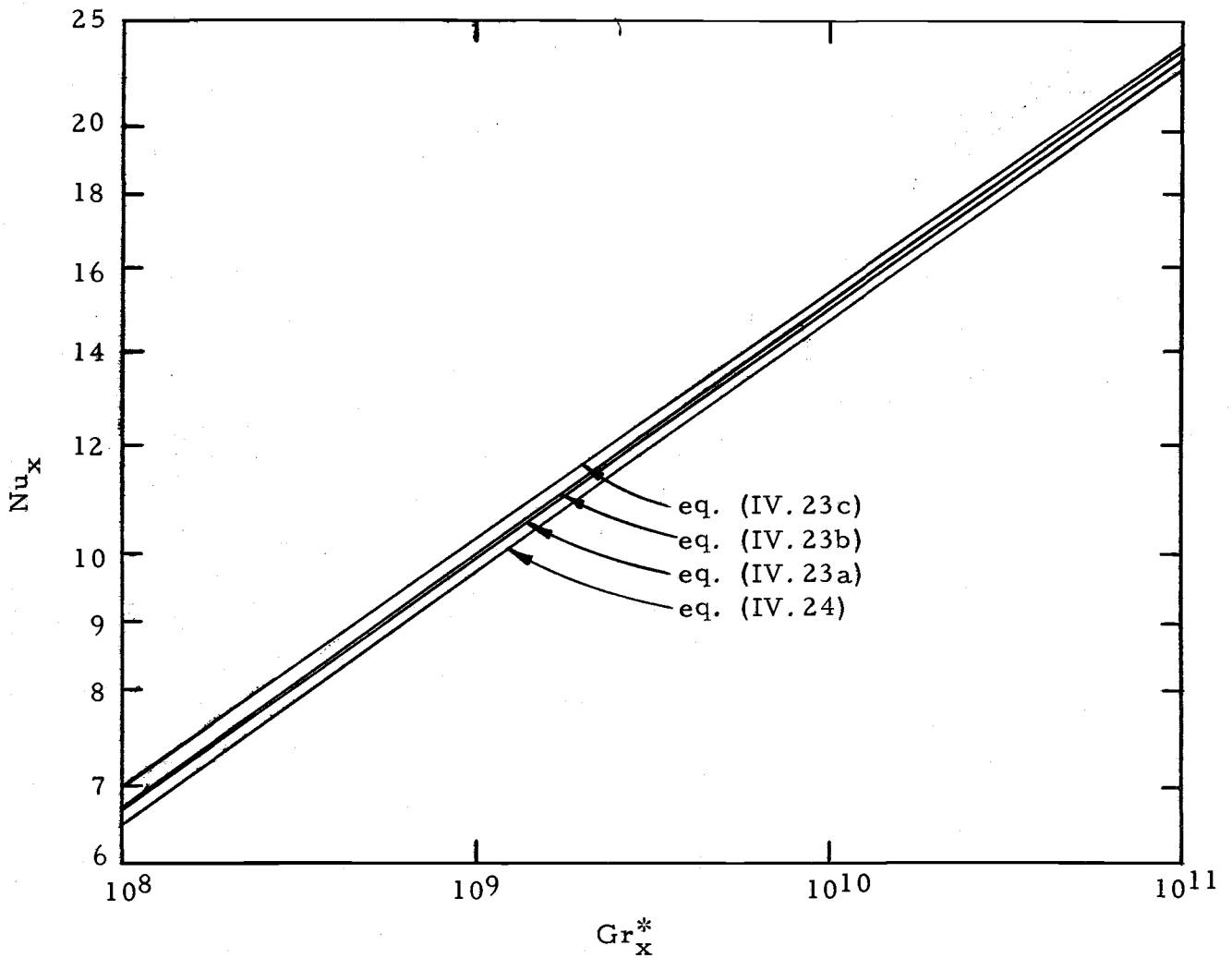

Figure IV. 4. Local heat transfer correlations for uniformly heated vertical channel.

Grashof number that an engineer would be using, three correlations that are that nearly equal are of no practical value. For this reason, all the channel data were regressed together, yielding the correlation

$$Nu_x = .252(Gr_x^*)^{.178} \quad .25 < w/L < .67,$$
$$10^8 < Gr_x^* < 10^{11} \qquad \text{(IV. 25)}$$

The average correlation, which is more likely to be used in a design situation, is

$$Nu_L = .354(Gr_x^*)^{.178}, \quad .25 < w/L < .67,$$
$$10^8 < Gr_L^* < 10^{11} \qquad \text{(IV. 26)}$$

Considering the three individual regression lines given by equations (IV. 23) from a statistical point of view, the three lines are significantly different. The statistical analysis of the significance of these lines is included in the Appendix, but the method used will be described briefly here. An assumption, called the null hypothesis, was made that the single regression line, equation (IV. 25), would fit the data just as well as the three separate lines, equations (IV. 23). If this null hypothesis were true, then an F-statistic, which indicates how much the residual sum of squares (what the regression lines can't account for) is reduced by using three lines instead of one, would be small. The F-statistic calculated for this situation was so large, however, that if the null hypothesis were still true, the chances of

getting an F-statistic that large would be much less than 0.1%. This is very strong evidence for rejection of the null hypothesis, which indicates the three separate lines to be statistically significant.

Since the three individual lines are statistically significant, observations can be made about trends between the lines. Note that the Nusselt number consistently increases as the channel spacing is decreased. This is consistent with the results reported by Colwell (5). Contrary to results found for other fluids, Colwell found that for mercury the wall temperature of the constant heat flux plate decreased as the channel width decreased. This effect became more pronounced as the channel spacing parameter decreased from 0.1 to 0.05. Somewhere in the vicinity of $w/L = .05$, the viscous effects of the two plates began to limit the fluid flow so that plate temperature then increased as the channel width was further decreased. It is significant that even at these wide channel spacings but at a higher Grashof number range than Colwell, this same effect was observed. Colwell was also concerned that the correlation lines would intersect around a modified Grashof number of 10^{11}, indicating a reversal in this trend. There is no evidence for the range of data taken here that this will occur.

So that these results might be compared with results of other studies, several other forms of the regression will be given. The average Nusselt number correlations for the three individual channel

spacings are, for $10^8 < Gr_L^* < 10^{11}$

$$Nu_L = .348(Gr_L^*)^{.178} \text{ for } w/L = .67 \qquad \text{(IV. 27a)}$$

$$Nu_L = .341(Gr_L^*)^{.179} \text{ for } w/L = .50 \qquad \text{(IV. 27b)}$$

$$Nu_L = .375(Gr_L^*)^{.176} \text{ for } w/L = .25. \qquad \text{(IV. 27c)}$$

Colwell found a convenient way to include channel spacing in the heat transfer correlation, to be

$$Nu_x(w/L) = K(Gr_x^*(w/L)^5)^n \qquad \text{(IV. 28)}$$

For the limited effect of the channel spacing in this work, a correlation of this form gives poorer results than equation (IV. 25) which simply ignores the effect. For purposes of comparison, however, the data were regressed in this form, and are plotted in Figure IV. 5. The resulting correlation for $10^5 < Gr_x^*(w/L)^5 < 10^{11}$ is

$$Nu_x(w/L) = .190(Gr_x^*(w/L)^5)^{.188} \qquad \text{(IV. 29)}$$

This is compared to Colwell's resulting correlation for $10^3 < Gr_x^*(w/L)^5 < 10^9$

$$Nu_x(w/L) = .268(Gr_x^*(w/L)^5)^{.165} \qquad \text{(IV. 30)}$$

Equations (IV. 29) and (IV. 30) are also graphed on Figure IV. 5.

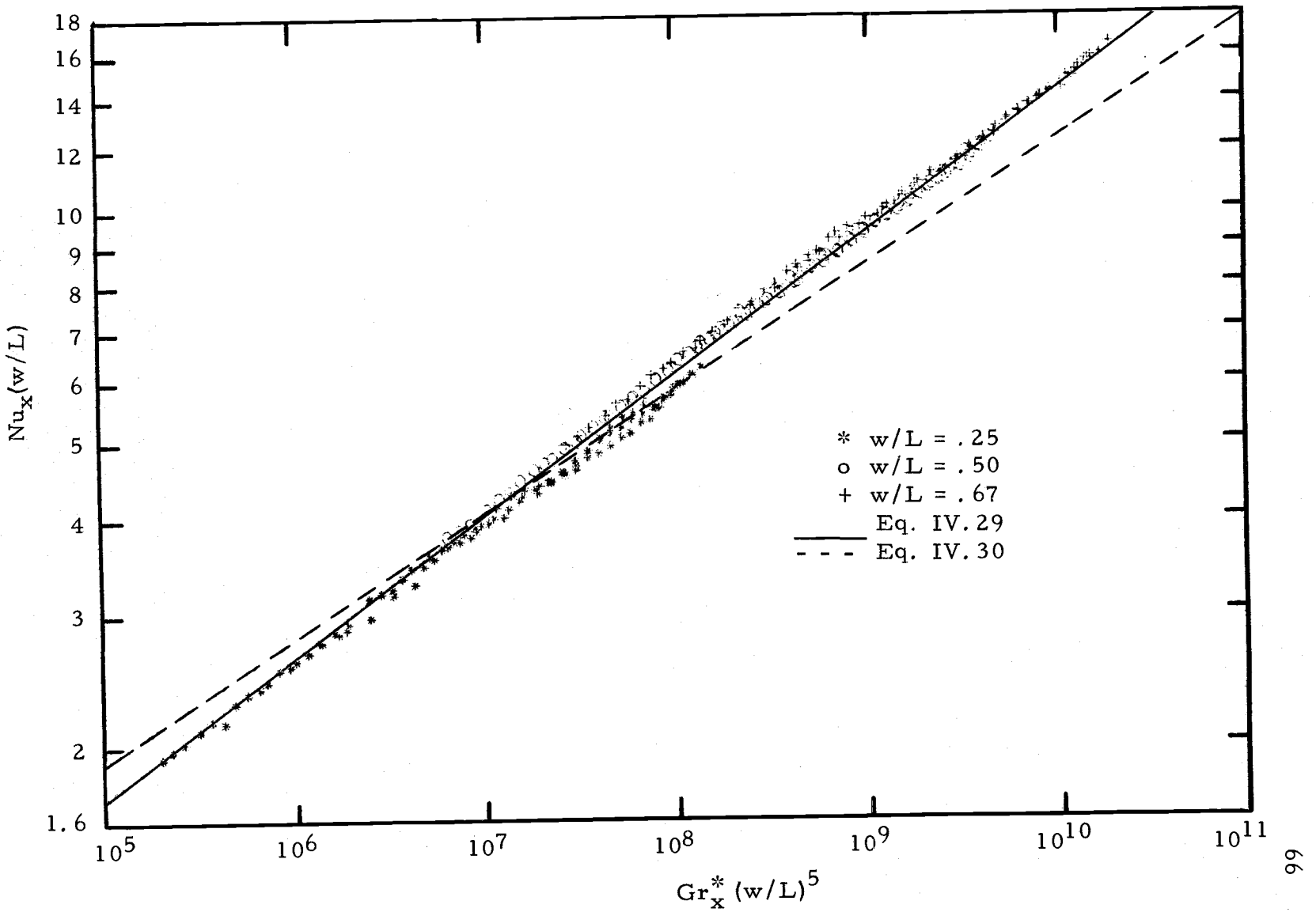

Figure IV.5. Channel heat transfer correlations with w/L in correlation.

In conclusion, as with the single vertical plate, no drastic change in the slope of the regression line was observed for the uniformly heated channel within the range of Grashof numbers considered here that would indicate a change from laminar to turbulent natural convection. It is the purpose of Chapter V to investigate the characteristics of the flow within this range.

V. CHARACTERISTICS OF THE VELOCITY AND TEMPERATURE BOUNDARY LAYERS

Introduction

In Chapter IV, the heat transfer correlations were presented which give a rather precise, quantitative summary of the heat transfer characteristics, but say very little about what is actually happening in the channel and inside the boundary layer. It is the purpose of this chapter to describe the convection in a more qualitative manner, and to describe what the data indicate about the characteristics of the flow.

The information to be considered in this chapter consists first of mean temperature and velocity profiles. Consideration is then given to the fluctuating velocity using instantaneous anemometer outputs and measuring the characteristic amplitudes and frequencies. The mean profiles are common to nearly all flow situations and will be treated first. Consideration of the amplitudes of the instantaneous velocity readings seems to give the most intuitive description of the type of flow. Finally, to conclude the chapter, measurements of the frequencies will be presented which give quantitative information about the type of convection.

Velocity and temperature profiles were taken for the single heated plate and the three spacings of the uniformly-heated channel for vertical positions of 1, 2, 3, and 4 inches from the leading edge.

With a constant heat flux of 11, 500 BTU/hr-ft^2 and very little property variation between configurations at the same vertical position, the four vertical positions corresponded to local modified Grashof numbers of 2.5×10^8, 4.0×10^9, 2.0×10^{10}, and 6.5×10^{10}, respectively.

For each profile a horizontal traverse was made; readings were taken of mean temperatures and recordings made of instantaneous anemometer output. Data were taken at intervals of 0. 005 inch until well past the velocity peak, then at increasing intervals as the velocity and temperature gradients became less steep. While it was possible to read the wall temperature with the thermocouple protruding past the hot film sensor, the closest velocity readings were made at 0. 013 inch from the plate.

The stainless steel plate was a better conductor than the mercury, thus as the operating hot film anemometer was brought into the proximity of the unheated plate in a quiet pool of mercury, the anemometer reading increased from its rest voltage reading due to the additional heat conducted up the plate since more voltage was required to maintain the constant overheat. With the plate heated in a natural convection field, the data seemed to indicate that this effect was giving an erroneously high velocity measurement near the plate. To correct for this effect, an empirical equation was fit to the measurements taken for the unheated plate. This equation was then used to calculate a voltage correction factor in the reduction program for the

data points closest to the plate. Since this effect was only felt within 0.034 inch of the plate, the value of the velocity peak was not affected. This correction produced profiles with a reasonable velocity gradient at the wall.

Two final general considerations are uniformity of the channel and repeatability of the data. Temperature profiles were taken and compared for several configurations and at several vertical locations from both walls. There was no appreciable difference in the profiles from opposite plates. This indicated that the two plates were heating uniformly. Velocity and temperature profiles for several cases were retaken three and four weeks after the original profiles had been taken. The difference in the results was between 0 and 5% with no noticeable trend to the deviations. This indicated the velocity data to be very repeatable.

Mean Velocity and Temperature Profiles

Mean velocity and temperature profiles provide quantitative indications of the magnitude of flow and amount of temperature difference, and a qualitative indication of the change in shape and relative sizes of the boundary layers. Figure V.1 presents mean dimensional velocity profiles for the single plate and three channel configurations. Note first that the highest velocity peaks occur for the single plate, with little difference in the peaks for the wider channels w/L = .67 and

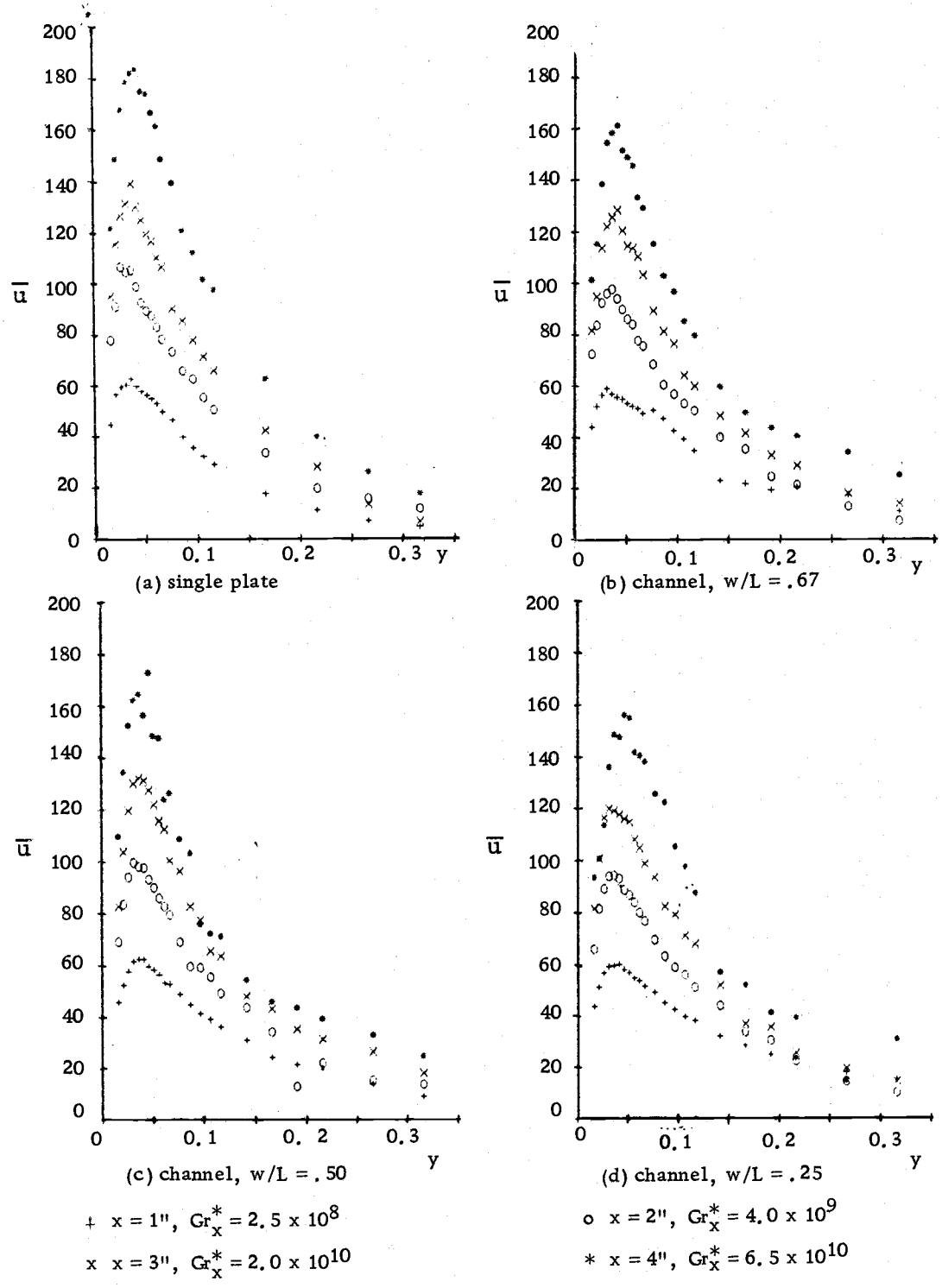

Figure V.1. Velocity profiles, $\bar{u}$ (in./min) vs. y (in.)

w/L = .50, but that the peaks are somewhat lower for the narrowest channel spacing, w/L = .25. Just the reverse of this trend, however, may be observed in that the velocities drop off toward zero one-half inch from the single plate but that, as the channel spacing decreases, the velocity level outside the peak seems to increase. This would be expected -- a channel flow situation should develop as the spacing decreases.

Also, in Figure V.1, there are some small changes in the position of the velocity peak. Two trends can be noticed. First, as is to be expected, in every case the peaks are located further away from the plate as the vertical position increases, which is indicative of the increasing thickness of the boundary layer. Also, for a given vertical location, particularly at 4 inches, the velocity peak moves further away from the plate as the channel spacing decreases. This seems to indicate a thicker boundary layer for narrower channel spacings and might explain why the Nusselt number tended to increase as the spacing decreased.

Another matter of interest is the relation between the thermal and momentum boundary layers. This is shown in Figure V.2 for the intermediate channel spacing, w/L = .50, for vertical positions of 1 and 4 inches. Here the horizontal position, y, is non-dimensionalized with the channel width, w, and the curve carried out to the middle of the channel, y/w = .50. Velocities are scaled with the peak

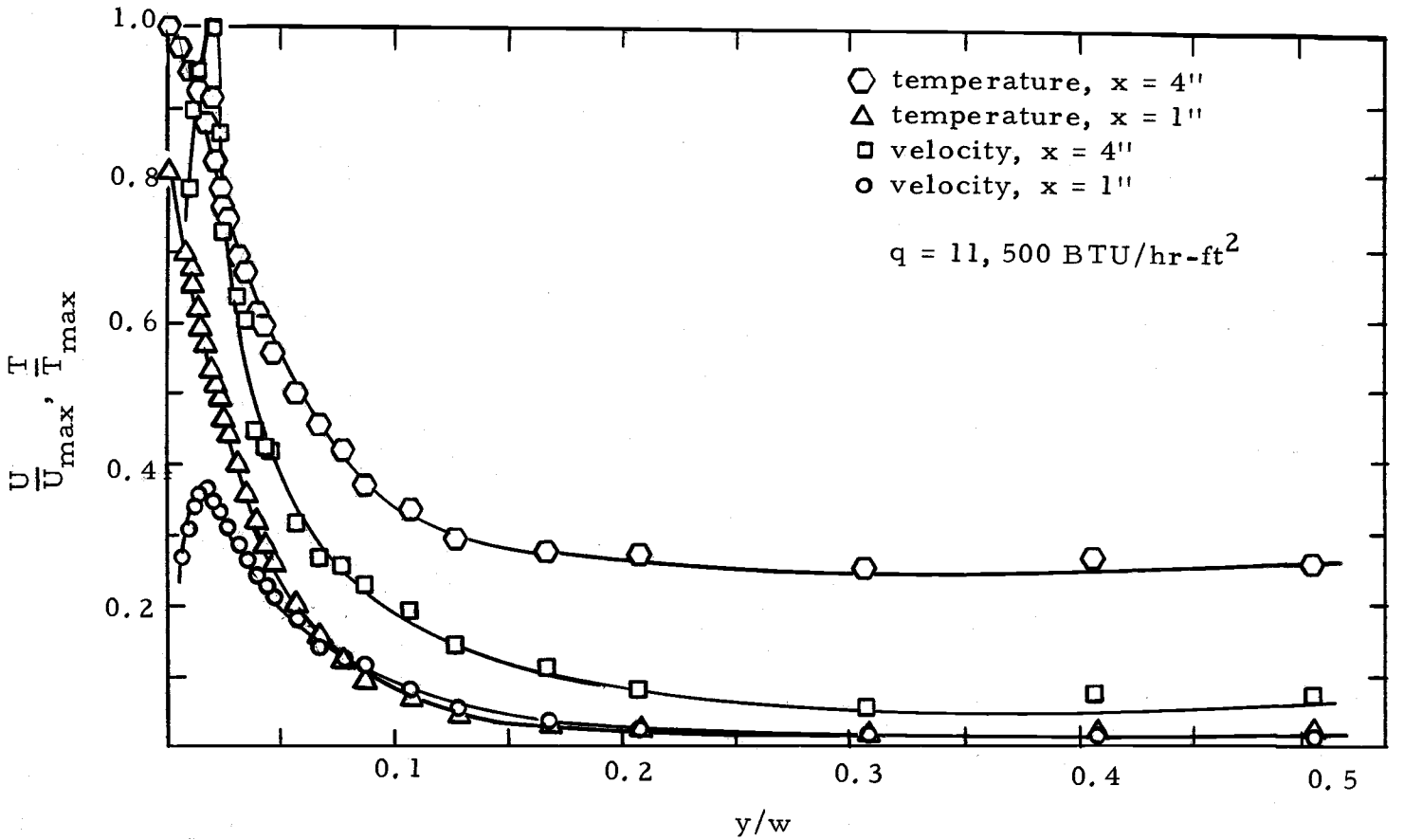

Figure V.2. Comparison of the velocity and temperature boundary layers.

velocity at 4 inches and the temperatures are scaled with the wall temperature at 4 inches. Note at the 1 inch position the velocity has reached zero near $y/w = .3$ and the temperature shows very little stratification (above the ambient temperature). On the other hand, at 4 inches, there appears to be a finite velocity all the way to mid-channel, and there is considerable indication of temperature stratification. The change between 1 and 4 inches is once again an indication of the growth of the boundary layer. It is difficult to draw any conclusions about the relative thickness of the thermal and momentum boundary layers, because they are so difficult to define. The large degree of stratification in the middle of the channel is an indication, however, of the tendency for a low Prandtl number fluid to form a thermal boundary layer that is much thicker than the momentum boundary layer.

For purposes of comparison with analytical results, the mean velocity and temperature profiles have been expressed in terms of the dimensionless similarity parameters defined by Sparrow and Gregg (36):

$$\eta = y/x(Gr_x^*)^{.2} \text{ (dimensionless position)} \qquad (V.1)$$

$$f' = Ux/[5\sqrt{}(Gr_x^*/5)^{.4}] \text{ dimensionless velocity)} \qquad (V.2)$$

$$\theta = (Gr_x^*/5)^{.2}k(T - T_a)/(xq) \text{ (dimensionless temperature)} \qquad (V.3)$$

Figure V. 3 shows the dimensionless velocity for the single plate and three channel spacings. Considering first Figure V. 3a for the single heated plate we observe the trends to be the same as predicted by Chang, Akins, Burris, and Bankoff (4). Note that the velocity peaks increase as x is increased, but outside the velocity peak the profile lines cross each other so that the lowest value of F' occurs for the highest x location. Chang et al. only made these predictions for a single vertical plate, but observation of Figures V. 3b through V. 3d shows this same trend to be present and much more exaggerated for the channel configurations.

Figure V. 4 presents the dimensionless temperature profiles for the four situations. Once again the results for the single plate in Figure V. 4a follow the predictions of Chang et al. In this case, the temperature increases slightly with vertical location, but the temperature profiles do not intersect. Figures V. 4b through V. 4d demonstrate a similar but much more exaggerated trend due to stratification of the temperature in the channel. The results for the single plate appear to agree very well with the similarity perturbation analysis, and serve as a good standard of comparison for the uniformly heated channel results.

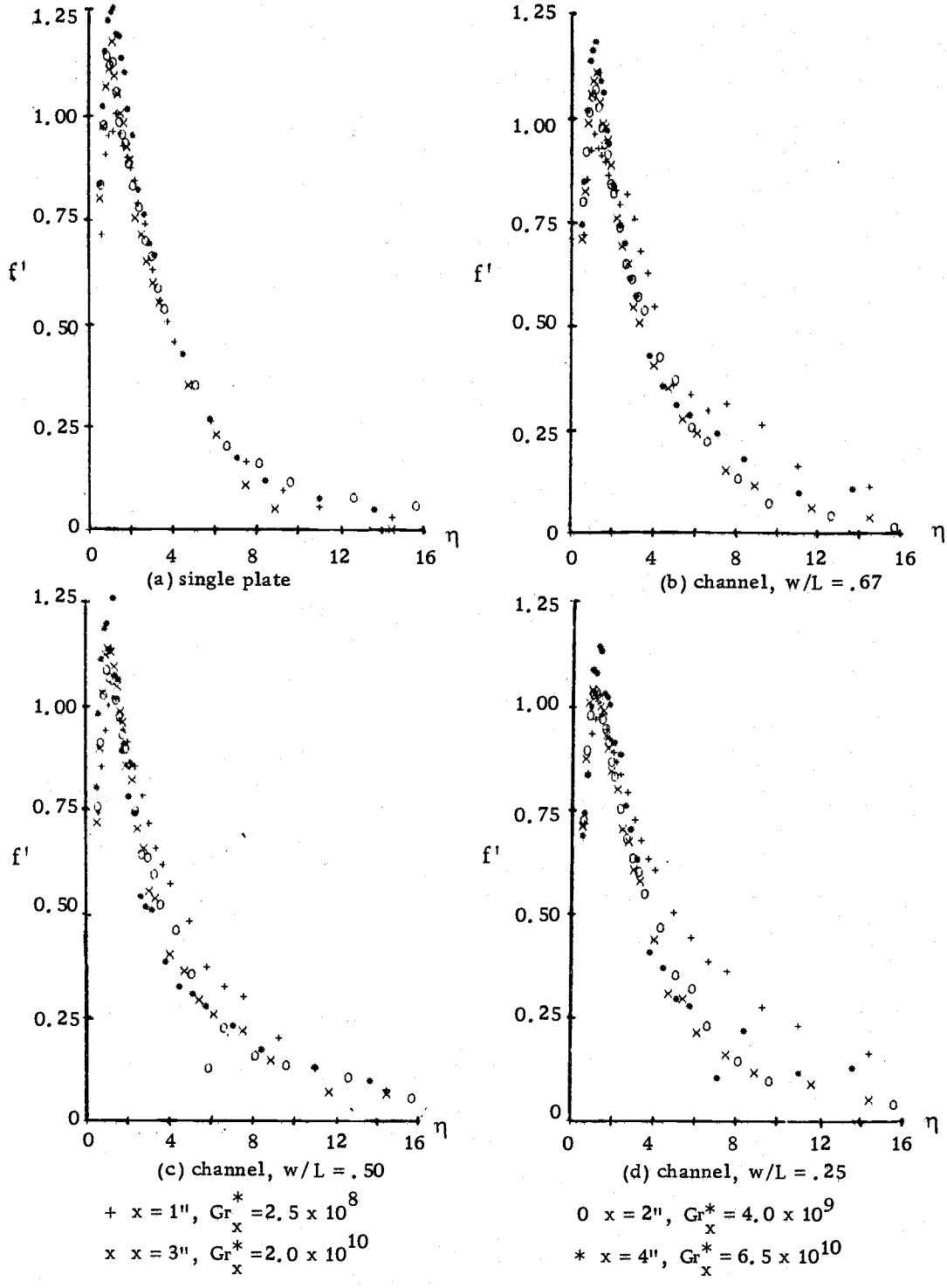

Figure V.3. Dimensionless velocity profiles.

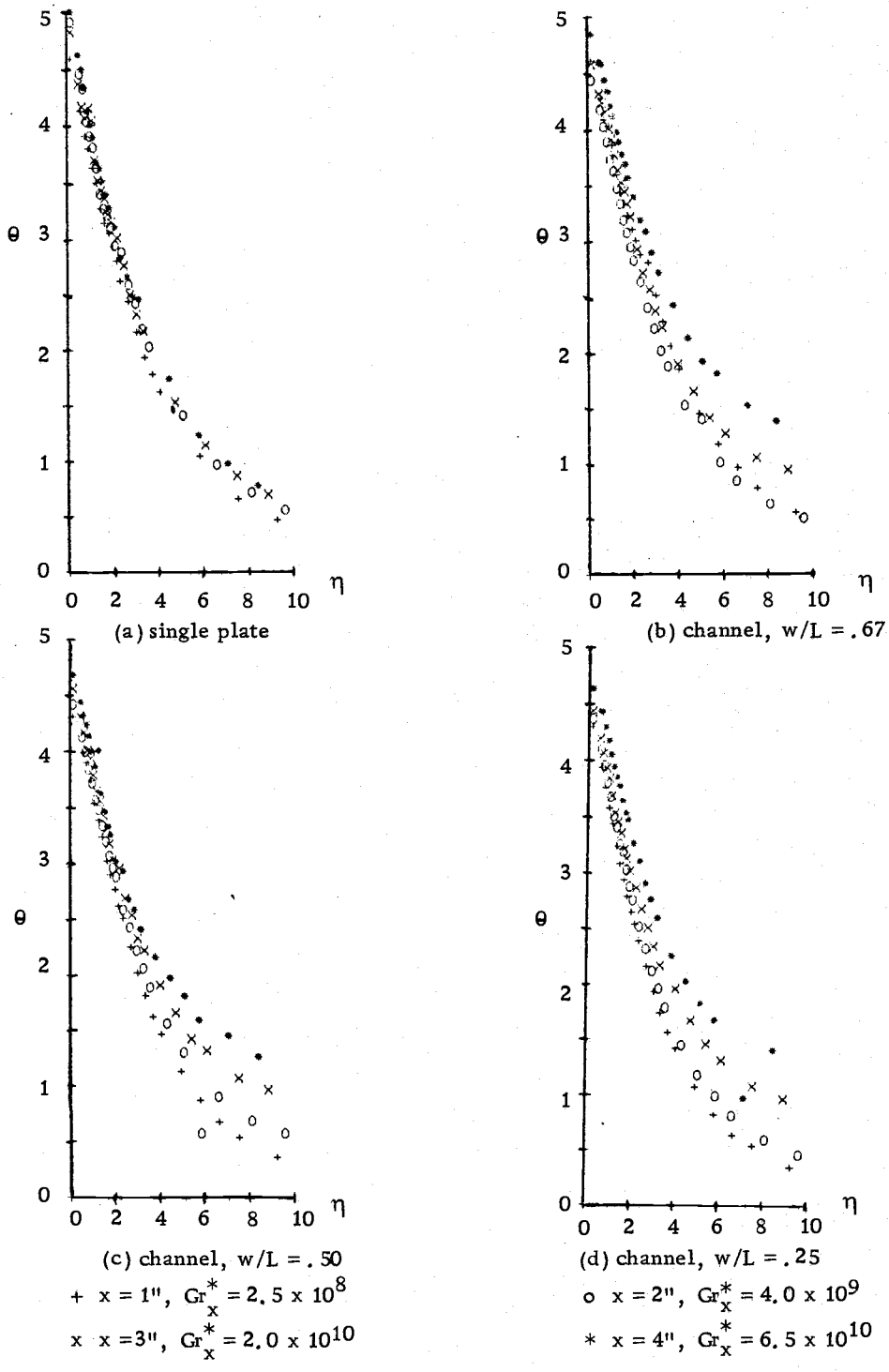

Figure V. 4. Dimensionless temperature profiles.

Amplitude of the Instantaneous Velocity Disturbance

One disadvantage in studying convection in mercury as opposed to studying convection in a transparent fluid is that no flow visualization techniques can be implemented. Any mental visualization of the flow situation must be deduced from instantaneous electronic signals measuring the velocity or temperature. For this experiment two- to three-minute plots of the instantaneous anemometer output were kept for every velocity data point taken, from which mean values and amplitude and frequency of the fluctuations were taken. In this section several samples of this multitude of plots are presented to demonstrate trends observed consistently from all plots.

Figure V. 5 demonstrates the typical instantaneous velocity as the probe was moved away from the plate at a constant vertical position. This set of plots corresponds to the narrowest channel spacing, $w/L = .25$, at 4 inches up the plate, a local modified Grashof number of 6.5×10^{10}. The scales of each plot are indicated. Each plot represents a time period of one minute. Plots are shown for six horizontal distances away from the plate, 0.025, 0.050, 0.075, 0.100, 0.150, and 0.200 inch. This plot corresponds to the same situation as Figure V. 1d, from which it is again observed that the velocity peak occurred at approximately 0.050 inch from the plate with a peak velocity of 160 inches per minute; outside the peak the velocity

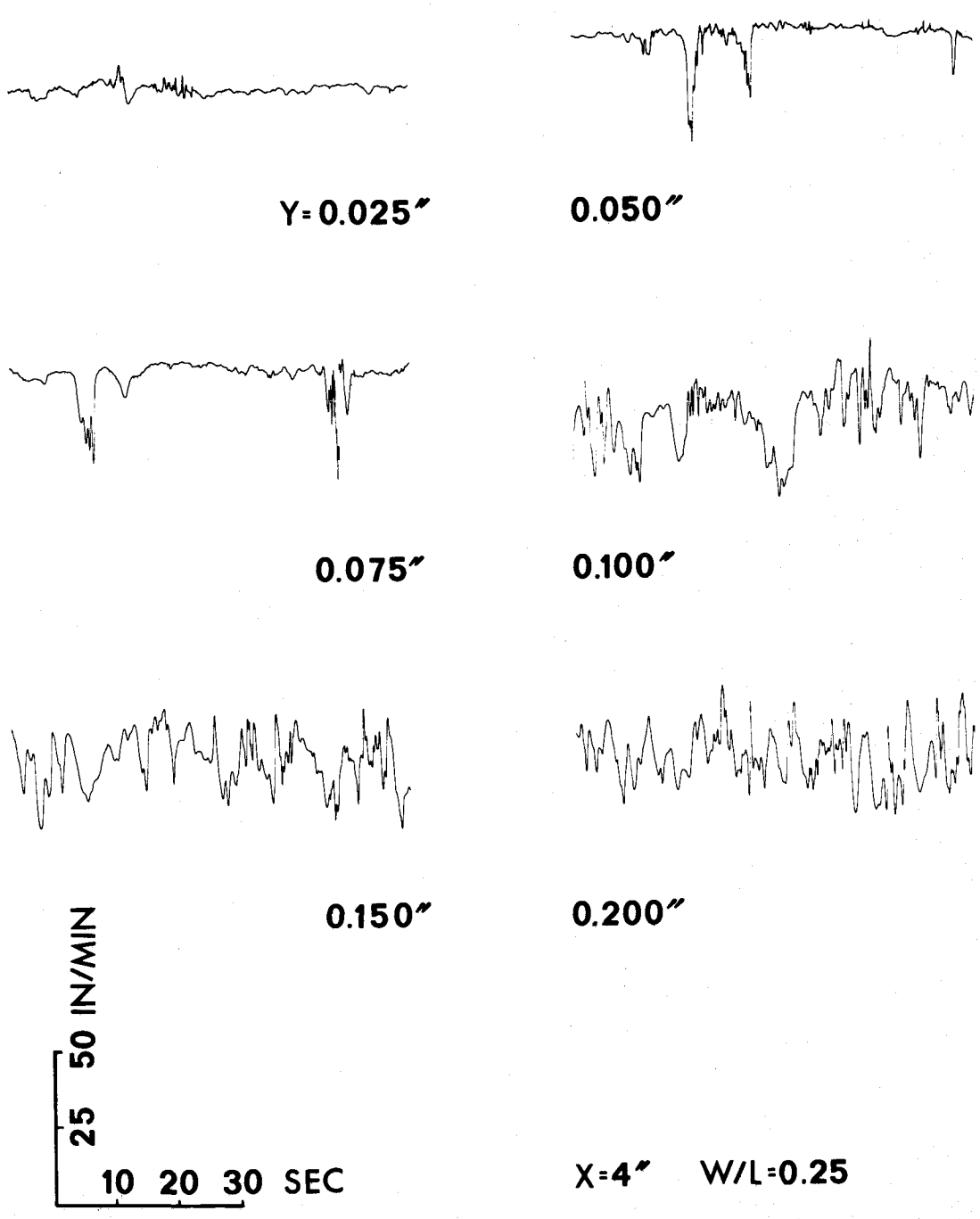

V.5. Instantaneous velocity variation with y at constant x.

decreased from about 100 inches per minute at 0.100 inch to 50 inches per minute at 0.200 inch.

Note that the velocity has a small amplitude fluctuation at the 0.025-inch position. As the probe moves out to 0.050 inch, corresponding to the velocity peak, these small amplitude fluctuations actually get smaller, but occasionally a large magnitude fluctuation is seen. These large amplitude fluctuations are always downward peaks, corresponding to a packet of fluid moving much slower than the mean flow. At 0.075 inch the small amplitude fluctuations begin increasing in amplitude and the large negative fluctuations become more frequent. Finally at 0.100 inch the large amplitude fluctuations are occurring continually, and do not change appreciably in characteristic as the probe is moved to 0.150 inch and 0.200 inch.

This same trend was observed at corresponding positions for the other two channel configurations. This effect was never observed for the single plate, however. Whereas on the single plate, fluctuations were observed of nearly the same amplitude as the small amplitudes observed near the velocity peak, no large negative fluctuations developing into a large amplitude fluctuating flow were seen. Figure V.6 shows a comparison of the fluctuations at a constant horizontal position away from the plate, for the four vertical positions and the three channel configurations. These plots were taken in the region of large fluctuation, $y = 0.150$ inch, where there is little change in

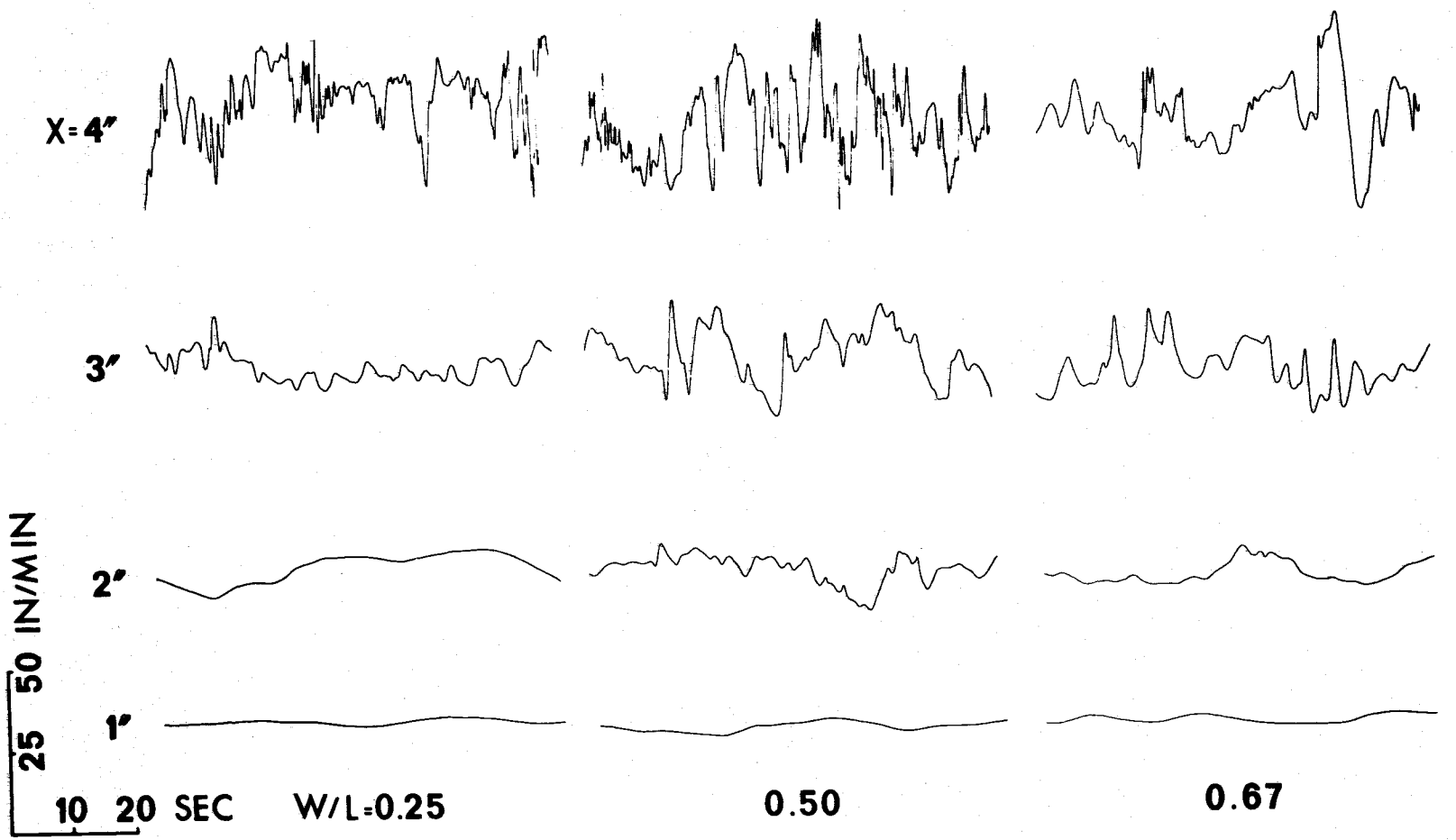

V.6. Instantaneous velocity variation with x and w/L at constant y.

characteristics over a considerable horizontal distance. As would be expected, the amplitude of fluctuations increases as the distance from the leading edge increases.

Comparison of the plots at the 4 inch vertical position shows that the amplitudes of fluctuation are larger for the intermediate spacing, but that the frequencies appear to increase as the channel width decreases. Frequencies are the subject of "Characteristic Frequencies of Velocity Disturbances". A more complete, quantitative comparison of Figures V. 5 and V. 6 is presented in Figure V. 7 . This shows the amplitudes of the velocity fluctuations at the 4 inch position for the three channel spacings, as a function of η, the dimensionless distance from the plate. The amplitudes of the fluctuations were the peak to peak values which appeared to be the most representative of that situation. There is some potential error in judgement here as to the "most representative" and this must be considered with the results, but this method proved to be much more practical than the use of an RMS meter for the low frequencies encountered. The velocity fluctuations are scaled against the maximum fluctuation, which in each case was approximately 25 inches per minute. The large disturbances were observed first at the intermediate spacing, which might indicate that this spacing is more favorable for the development of large eddies. While the data are not conclusive here, this agrees with trends reported by Colwell (5).

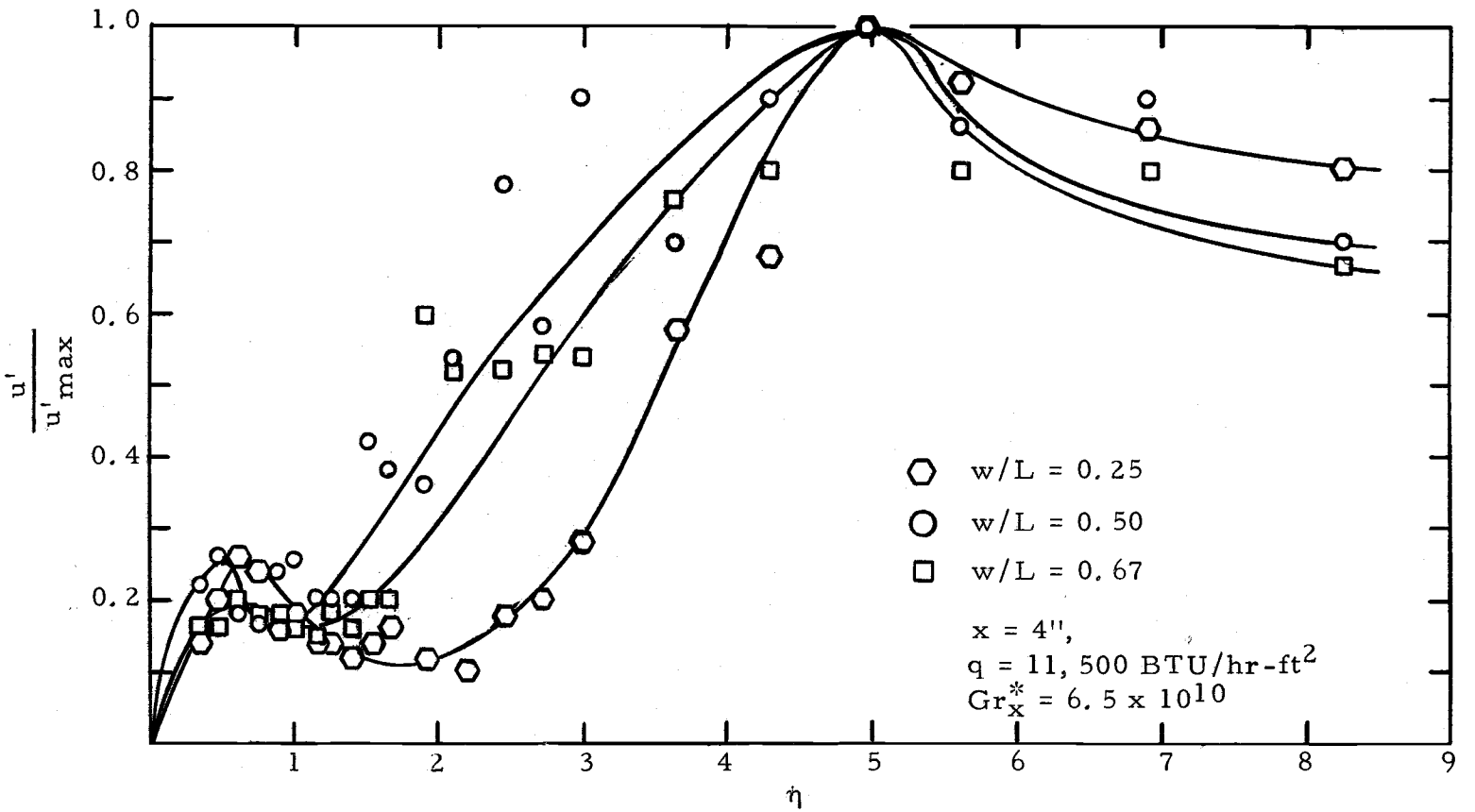

Figure V.7. Amplitude of the velocity disturbance.

To conclude this section, a description of the phenomena described above is proposed. While more data, particularly information from an "X" configuration probe and instantaneous temperature data, will be needed to complete the description, this will offer a plausible explanation of the observations made thus far. For the region between the wall and the velocity peak, the positive velocity gradient would tend to cause counter-clockwise vortices superposed on the mean flow as shown in Figure V. 8. The largest of these eddies is constrained by the distance between the peak and the wall, about 0. 045 to 0. 050 inch. These eddies therefore remain small and are dissipated by wall shear as they approach it. For the region between the velocity peak and the middle of the channel, the negative velocity gradient would tend to cause clockwise vortices, also shown in Figure V. 8. Since a symmetrical effect would be expected from the opposite wall, the size of these eddies would be limited by the distance between the velocity peak and the middle of the channel, which varies from 0. 75 to 1. 50 inches. These eddies would be much larger, therefore, than the eddies on the inside of the velocity peak and would tend to have a much larger peak-to-peak fluctuation, as mixing of fluid over a much greater distance occurs.

One would expect that occasionally these eddies would pass to the opposite side of the velocity peak. While a small eddy passing from the inside of the velocity peak to the outside would be barely

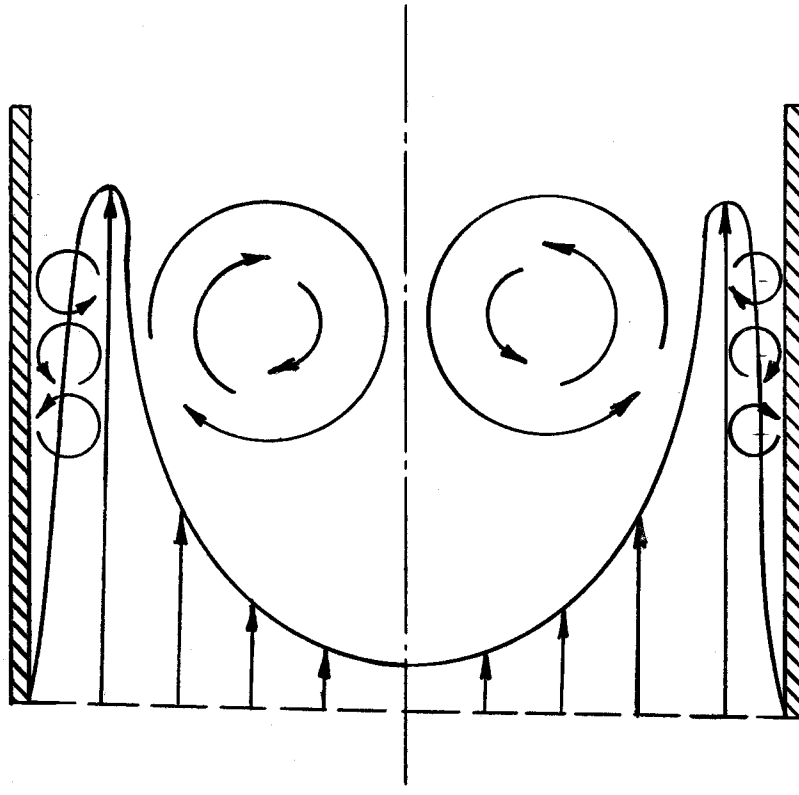

Between the wall and the mean velocity peak, the positive velocity gradient causes eddies that roll towards the plate. Since their size is governed by the distance between the wall and the peak, they remain small. The negative velocity gradient outside the peak causes eddies that roll away from the plate. Their size is governed by the half-width of the channel and thus are much larger.

Figure V. 8. Hypothesized formation of eddies.

noticeable, a large eddy passing to the inside of the velocity peak would likely be carrying some rather cool fluid from the middle of the channel with a relatively low mean velocity. Such a packet of fluid would cause a noticeable velocity deficit inside the peak and would account for the large negative bursts observed in the anemometer output. Finally, the formation of large eddies in the channel must accompany the low level of velocity all the way across the channel and the considerable temperature stratification up the channel, otherwise similar large eddies would have been observed for the single plate profiles, which was not the case.

Characteristic Frequencies of Velocity Disturbances

Laminar instability theory has demonstrated that natural convection acts as a frequency filter, selectively amplifying only a narrow bandwidth of disturbance frequencies. Instability theory predicts when, in terms of the parameters of natural convection, a disturbance at any given frequency will tend to become unstable. A disturbance is unstable when it extracts energy from the mean flow so that it can amplify and grow as it proceeds downstream. Large scale amplification of these disturbances occurs only over a narrow bandwidth of frequencies. Disturbances within this bandwidth will be amplified considerably whereas those outside this bandwidth will tend to go unnoticed in contrast to the highly amplified ones. Observed

fluctuations in velocity and temperature will tend, therefore, to have frequencies distributed about this characteristic, most highly amplified, frequency. It is important to remember that the flow as described thus far is still laminar, even though the velocity and temperature fields are fluctuating.

The behavior described above is best expressed quantitatively in terms of a stability plane as shown in Figure V. 9. This figure is taken from the analytical work of Hieber and Gebhart (18) for natural convection from a constant-heat-flux vertical plate for a Prandtl number of 0. 025. The frequency, f, is included in the non-dimensional frequency parameter, β^*, where β^* is defined as

$$\beta^* = \frac{25x^2}{\nu G^{*3}} 2\pi f \qquad (V.4)$$

β^* is plotted as a function of G^*, which is related to the fifth root of the local modified Grashof number as

$$G^* = 5\left(\frac{Gr_x^*}{5}\right)^{.2} \qquad (V.5)$$

The solid contour lines are lines of constant amplification rates, the outside line represents zero amplification or neutral stability, and the inner contours represent increasing degrees of amplification. The dashed lines represent lines of constant frequency.

Since the conditions of Figure V. 9 correspond to those of the single vertical plate data in the present work (the Prandtl number is

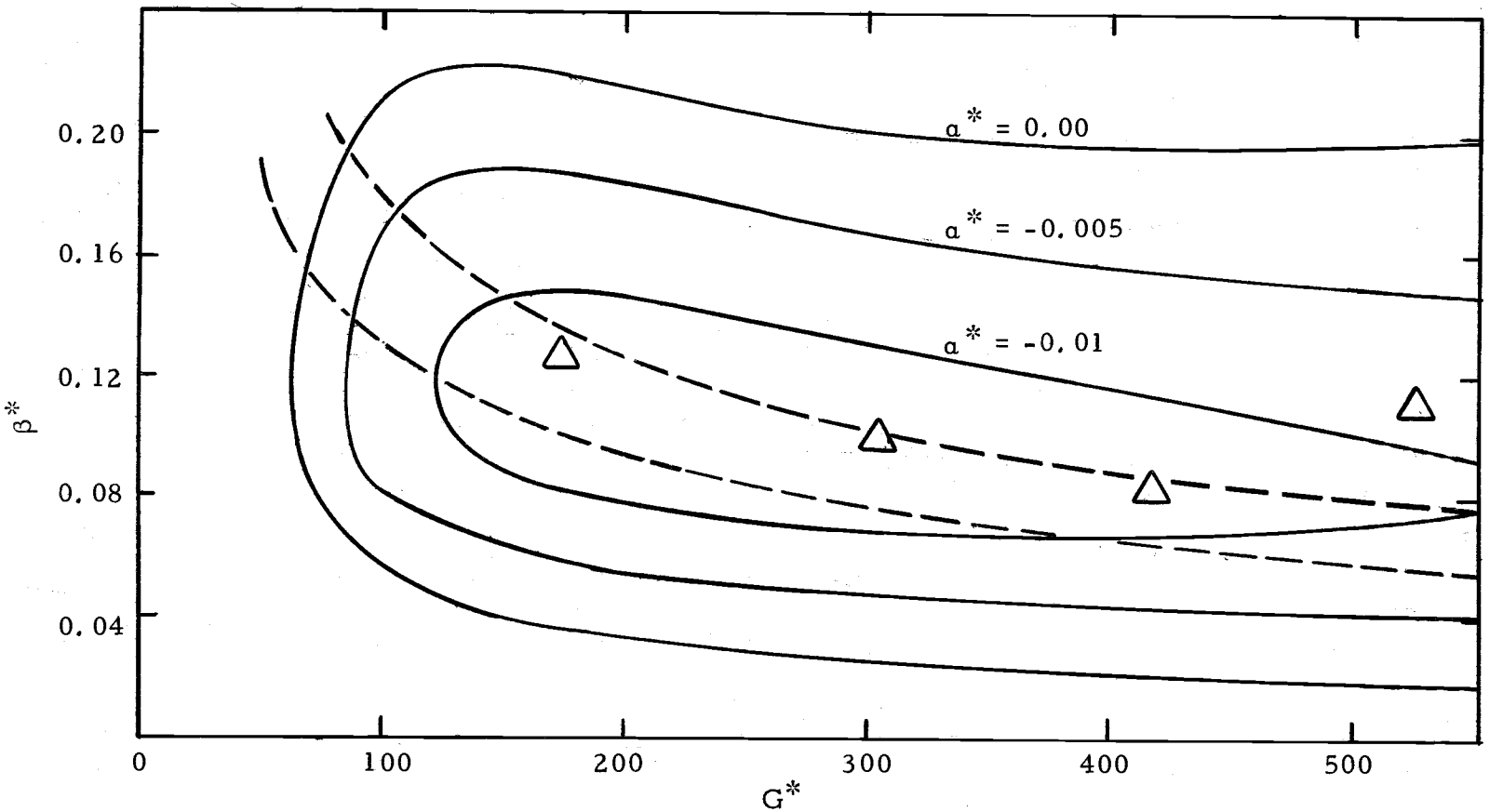

Figure V.9. Stability plane from Hieber (18) showing present results.

actually 0.023), frequencies obtained at four vertical positions adjacent to the single vertical plate are plotted on Figure V.9. These frequencies were taken from plots of instantaneous anemometer output by counting the number of peaks in the sinusoidal fluctuations within a 30-second period. Such counts were made for several different horizontal locations and averaged to provide a single value for each vertical position or corresponding value of G^*. While there was some deviation in these counts for different y-positions, these deviations were no greater than those found by counting over a different 30-second interval at the same y-position. Note how closely the first three data points fall to the frequency line of maximum amplification. This is very reassuring since these are the first data to verify this instability solution for a low Prandtl number fluid. This result further indicates that the flow at these three points is still laminar even though it is unstable. The fourth point does not lie near the line of maximum amplification, and its significance will be discussed shortly.

Jaluria and Gebhart (21) have done extensive work on transition mechanisms in vertical natural convection flow using water as a test fluid. They found very good agreement between the laminar principal frequency and the linear stability theory predictions. They have observed, however, that "the predominant frequency, in periods of turbulence, is seen to be progressively greater than the corresponding laminar value." It appears that the characteristic frequency for

turbulent flow is considerably higher than for laminar flow under the same conditions. During transition, where the flow is intermittent with a combination of periods of this faster frequency and periods of the characteristic laminar frequency, the frequency determined by counting the number of peaks within a given time period should yield values lying between the laminar and turbulent frequencies, but will be markedly higher than that predicted by laminar stability. The uncertainty in this estimated frequency increases, also, as the instantaneous output becomes more irregular and peaks become more difficult to define.

It appears that the reason that the fourth point plotted at a G^* value of 527 in Figure V.9 is considerably higher than the other three points which lie on the frequency line of maximum amplification is because of the phenomena described above. That is to say, it appears that, at the 4-inch vertical position where G^* is 527, the flow has undergone transition and therefore has a characteristic frequency noticeably higher than that predicted by laminar stability theory. This trend is seen even more graphically in Figure V.10. Here the dimensional frequency is plotted against $G^*x^{-1/2}$. Note that the first three points for the single plate data lie very nearly on a straight line which would correspond to the line predicted by stability theory, but that the frequency at a $G^*x^{-1/2}$ value of 912 is about 60% higher than this. Jaluria and Gebhart (21) have reported similar results for their

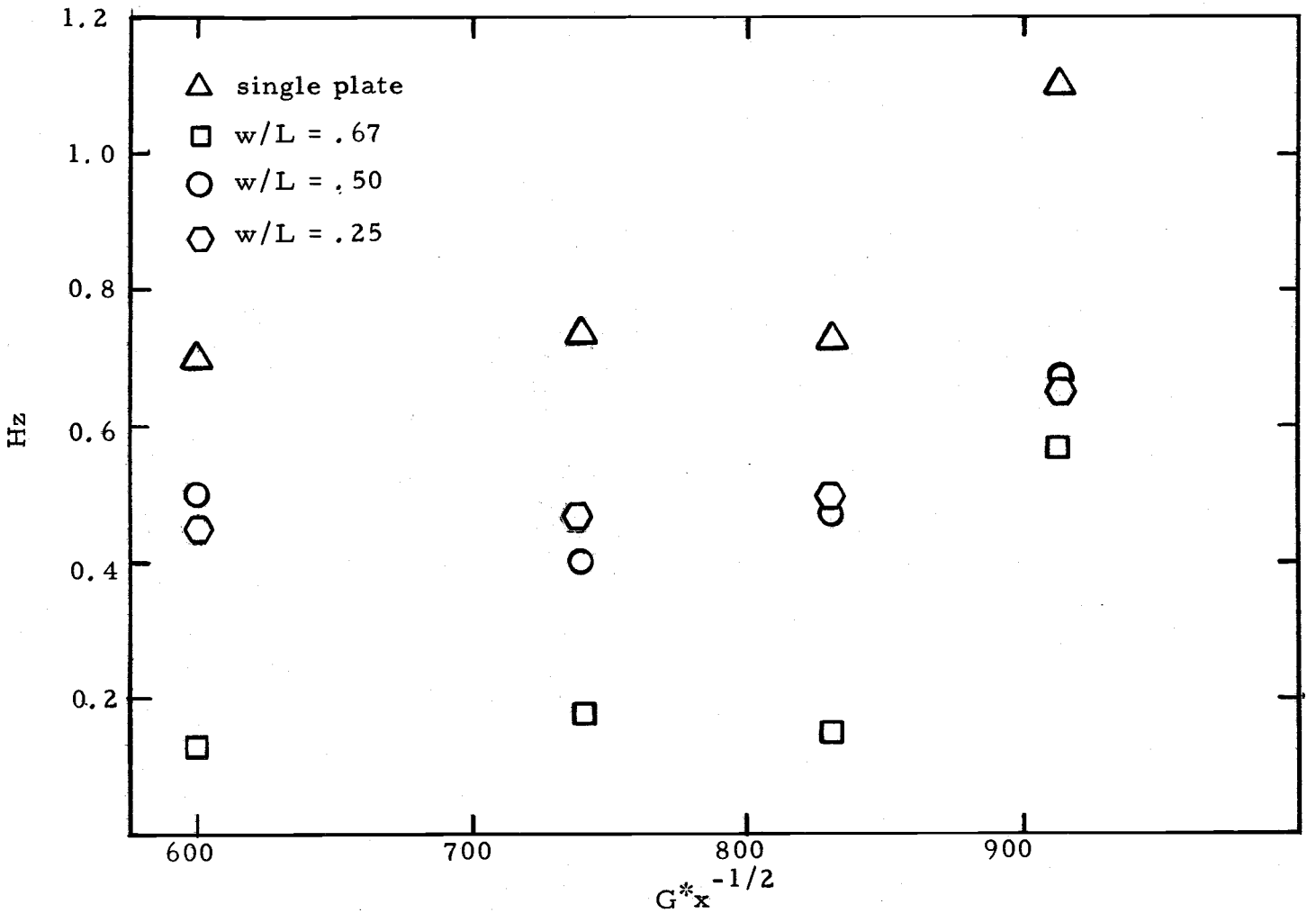

Figure V.10. Characteristic frequencies of the velocity disturbance.

studies in water, noting that the increase in the frequency was very dependent on heat flux level.

Figure V. 10 also presents similar frequency data taken from the anemometer outputs for the three channel spacings. There is more scatter in the data for the channel than that for the single plate, probably due to the much larger disturbance occurring at mid-channel. Nevertheless, for each case, the frequency appears to be constant for the first three points up to $G^*x^{-1/2}=830$ and then increases considerably for $G^*x^{-1/2}=912$. There are no laminar stability planes that have been analyzed for this channel flow situation, however, by analogy with similar results obtained for the single vertical plate which are in good agreement with the stability predictions, it seems reasonable to conclude that in all four situations the velocity regime has changed from unstable laminar to transition. This change in regime appears to have occurred for values of $G^*x^{-1/2}$ somewhere between 825 and 925, corresponding to modified Grashof numbers between 2×10^{10} and 6.5×10^{10}.

Jaluria and Gebhart (21) have also stated that the modified Grashof number is not a very satisfactory parameter for predicting the onset of transition. From their work, they propose the following parameter as being the proper criterion for transition.

$$E = G^*\left(\frac{\nu^2}{gx^3}\right)^{2/15} \qquad (V.6)$$

For their work in water they found the onset of velocity transition to occur at an E value of 13.6. When this E parameter was calculated for the fourth set of data points corresponding to $G^*x^{-1/2}=912$, E was found to be 13.42. This result is very pleasing as it lends more support both for the predictions of Jaluria and Gebhart and for the conclusion that the flow is undergoing transition. It should be noted that this experiment was not conducted for the purpose of determining the best value of E for the onset of transition. The data only indicate that transition begins somewhere between $G^*x^{-1/2}$ values of 830 and 912, corresponding to E values between 11.9 and 13.4. More work should be done to define this E value precisely.

In closing, several final observations will be made concerning Figure V.10, though there are insufficient data to make any definite conclusions. Note first that the predominant frequencies are much lower for the channel data than the single plate, and that the lowest frequency corresponds to the widest channel spacing. Thus the frequency does not simply decrease as a second plate is brought in from infinity, the single plate case, to some finite distance, the channel case, as one might expect. Rather, it appears that there is a different phenomenon occurring in the channel than with the single plate. The characteristic frequency, which seems to be nearly constant both inside and outside the velocity peak, is apparently controlled by disturbances in mid-channel. Since the frequency is proportional to

u'/w, and u' at mid-channel seems to decrease as the channel width w increases (see Figure V. 7), it is reasonable to find a decrease in the frequency as the channel width increases, as long as a channel flow effect is still present. Once again, this is a proposed explanation for the phenomena observed; more data are needed before any definite conclusions can be drawn in this regard.

VI. THE TWO-SENSOR "X" CONFIGURATION PROBE

Introduction

The results using a single sensor anemometer were presented in Chapter V. The single sensor is ideal for one-dimensional flow as it provides information at a very well defined location in the x-y plane, and can measure mean velocities as well as the magnitudes and frequencies of fluctuations, as already presented. The disadvantage of the single sensor is that it cannot discern a difference in the direction of two velocity vectors as long as both vectors are perpendicular to the axis of the sensor. With respect to Figure VI. 1, there will be no difference in the anemometer output for a velocity component along the x or y axes, and there is no way to know if flow

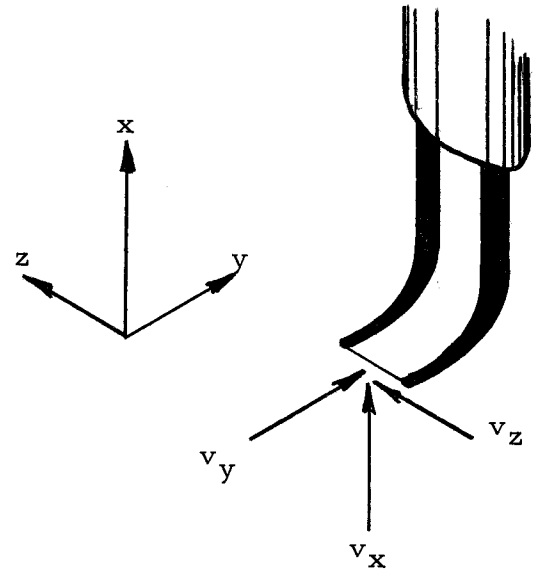

Figure VI. 1. Velocity components relative to a single sensor.

is in the positive or negative y direction. For the study of turbulence, the magnitudes and correlation between the fluctuating velocity components and the development of secondary flow become important. By placing two or more mutually perpendicular sensors on the same velocity probe, the ambiguities of the single sensor are eliminated.

Work on this thesis included the use of a two-sensor "X" configuration probe, already described in Chapter III. While this probe can help answer some questions the single sensor could not, some ambiguities still remain. Also, whereas the single sensor took essentially a "point" reading in the x-y plane and could approach within 0.013" of the wall, the "X" configuration sensor takes an average reading over a region approximately 0.030" on each side, and can only come within about 0.050" of the wall without considerable danger of damaging the probe. Since the velocity peaks discussed in Chapter V occurred between 0.040" and 0.050" from the wall, there are some serious limitations to the applicability of the "X" configuration probe for boundary layer studies. As might be expected with more sophisticated equipment, there were new problems to be overcome not encountered with the single sensor probe.

The work that has been accomplished to date with the "X" configuration probe on this project has been mostly in the area of technique development. While some data were taken for the widest channel spacing, an electrical short which developed between the mercury and

the plate destroyed both the plate and the probe, precluding the completion of a meaningful set of data. Three "X"-configuration probes were purchased for this initial study. The first, which is pictured in Chapter III, developed a short with the mercury after being submerged for approximately 24 hours. It was a practice not to operate any sensor until it had been submerged for two days, so this probe was never operated in the mercury as this would have caused immediate failure. The sensors on the two remaining probes failed to be perpendicular by as much as 20 degrees, which led to the considerations which will be discussed next. Of these two probes, one was destroyed in the plate failure and one has not been used. The remainder of this chapter will be devoted to the theoretical considerations and operation of the "X" configuration probe.

Theoretical Considerations

The main advantage of the "X" configuration sensor is its ability to break a two dimensional velocity vector down into its components. How this is accomplished will now be explained. In this development the angles are defined in a manner that can be physically measured. Also to be discussed is the cost of inaccurate angles due to assembly. In this analysis two assumptions are made which are standard for this type of treatment, neither of which is completely true. The first assumption is that the sensor output is linearized. This is essential

so that a given voltage fluctuation will always be associated with the same magnitude of velocity fluctuation, regardless of its location on the calibration curve. Though the non-linearized output was used for this work, the calibration for the velocity range of interest was nearly linear and did not cause a major problem. The linearized output also equates zero velocity with zero voltage. This is not the case for a normal bridge output which has a non-zero rest voltage as shown in Figure VI. 2. The rest voltage term, a_o, will be retained in the analysis.

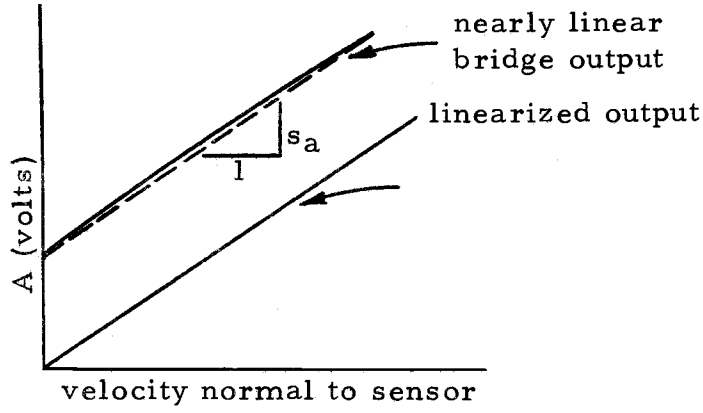

Figure VI. 2. Linearized anemometer output.

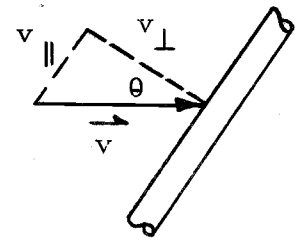

Figure VI. 3. Parallel and perpendicular velocity components.

The second assumption is that there is no cooling effect on the sensor due to flow parallel to the sensor axis, as shown in Figure VI. 3. Champagne, Sleicher and Wehrman (3) have shown that this is not

completely true, that the effective cooling velocity is actually

$$U^2(\theta) = U^2(\cos^2\theta + P^2 \sin^2\theta) \qquad \text{(VI. 1)}$$

They found the value of P for a platinum hot wire to vary from 0.2 with an active length to diameter ratio, $l/d = 200$, to 0 at $l/d = 600$. They present no results for hot film sensors, but since l/d is about 20, P is probably not negligible. The inclusion of P in the analysis at this point makes consideration of angular deviations impossible; therefore, P will be taken to be 0, and equation (VI. 1) reduces to the cosine cooling law,

$$U(\theta) = U \cos \theta. \qquad \text{(VI. 2)}$$

Figure VI. 4 shows the "X" configuration sensor as it was used against the vertical heated wall, in terms of the coordinate system used in this thesis. The angles α and β are the angles sensors "A" and "B" make with the normal to the heated wall. In terms of the geometry of Figure VI. 4 and using equation (VI. 2), the anemometer outputs for sensors "A" and "B" are

$$A - a_0 = s_a(u \cos \alpha + v \sin \alpha) = us_a \cos \alpha + vs_a \sin \alpha \qquad \text{(VI. 3)}$$

$$B - b_0 = s_b(u \cos \beta - v \sin \beta) = us_b \cos \beta - vs_b \sin \beta \qquad \text{(VI. 4)}$$

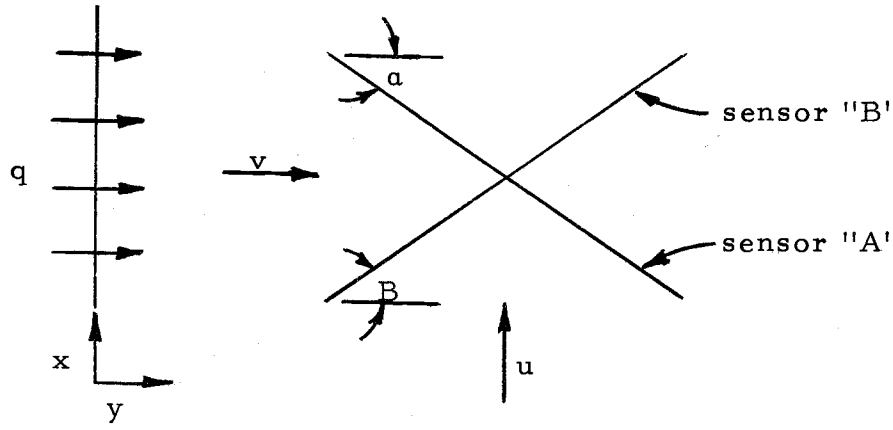

Figure VI. 4. Coordinate system relative to "X" configuration sensors.

Here, s_a and s_b are the slopes of the calibration curves of the anemometer voltage versus the velocity normal to the sensors "A" and "B". It is the presence of the plus sign in equation (VI. 3) and the minus sign in equation (VI. 4) that makes the "X" configuration probe work. Whereas on the one sensor the components perpendicular to it are additive, on the other sensor these components subtract from each other. Multiplying equation (VI. 4) by $\frac{s_a \sin \alpha}{s_b \sin \beta}$ and adding this result to equation (VI. 3) gives

$$\left[(A-a_o)+\left(\frac{s_a \sin \alpha}{s_b \sin \beta}\right)(B-b_o)\right] = \tag{VI. 5}$$

$$u\left[s_a \cos \alpha + \left(\frac{s_b \cos \beta}{s_b \sin \beta}\right) s_a \sin \alpha\right]$$

Solving for u,

$$u = \frac{[(A-a_o) + (\frac{s_a \sin \alpha}{s_b \sin \beta})(B-b_o)]}{s_a[\cos \alpha + \cot \beta \sin \alpha]} \qquad \text{(VI. 6)}$$

In a similar manner, by multiplying equation (VI. 4) by $\frac{s_a \cos \alpha}{s_b \cos \beta}$, subtracting this from equation (VI. 3), and solving for v,

$$v = \frac{[(A-a_o) - (\frac{s_a \cos \alpha}{s_b \cos \beta})(B-b_o)]}{s_a[\sin \alpha + \tan \beta \cos \alpha]} \qquad \text{(VI. 7)}$$

For a properly constructed probe, $\alpha = \beta = 45^o$, and with a linearized output, $a_o = b_o = 0$. Furthermore, the correlator has an amplifier on each input channel so that the effective sensitivities, s_a and s_b, can be made equal. This can best be accomplished by calculating the ratio s_a/s_b from the calibration curves as shown in Figure VI. 5, then setting the variable gain on channel B to this value by using a constant dc source and a digital voltmeter. Under these

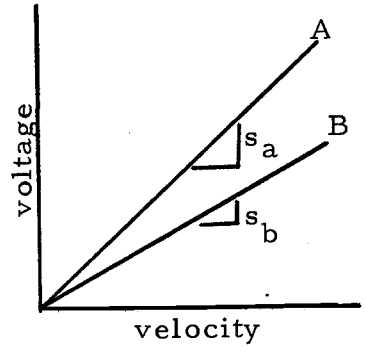

Figure VI. 5. Linear calibration curves.

circumstances, equations (VI. 6) and (VI. 7) reduce to

$$u = (\sqrt{2}/2s_a)(A+B) \tag{VI. 8}$$

$$v = (\sqrt{2}/2s_b)(A-B). \tag{VI. 9}$$

Both the velocity components and the anemometer outputs can be broken down into mean values (shown with a bar) and fluctuating components (shown with a prime):

$$\begin{aligned} u &= \bar{u} + u' \\ v &= \bar{v} + v' \\ A &= \bar{A} + A' \\ B &= \bar{B} + B'. \end{aligned} \tag{VI. 10}$$

Using the conventional averaging process, the mean velocity components are found to be

$$\bar{u} = (\sqrt{2}/2s_a)\overline{(A+B)} = (\sqrt{2}/2s_a)(\bar{A}+\bar{B}) \tag{VI. 11}$$

$$\bar{v} = (\sqrt{2}/2s_a)\overline{(A-B)} = (\sqrt{2}/2s_a)(\bar{A}-\bar{B}) \tag{VI. 12}$$

The mean velocities therefore can be determined by adding or subtracting the average values taken from the individual anemometer versus time plots from sensors "A" and "B".

If there is secondary flow, $\bar{u}$ and $\bar{v}$ both nonzero, then the direction of $\bar{u}$ and $\bar{v}$ are of interest. Referring back to equations (VI. 3) and (VI. 4), as long as α and β are approximately 45^{o} and it is known

that $\bar{u}$ is in the positive x direction (mean flow is up), then A will be greater than B if v is in the positive y direction, and B will be greater than A if v is in the negative y direction. Note that there is no such thing as "negative cooling" on the sensors, so A and B will always be positive, but A-B can be positive or negative. Therefore, if the direction of $\bar{u}$ is known, the direction of $\bar{v}$ can be determined. If $\bar{u}$ and $\bar{v}$ both point in their respective negative directions, this will be indistinguishable from the case where $\bar{u}$ and $\bar{v}$ are both positive. The direction of one of the two mean components must be known.

To determine the RMS values of the fluctuating velocity components, the true RMS voltmeter is used. In analog circuitry, the mean component is determined and subtracted from the signal before it is squared, so that by inputting A+B or A-B, the resulting outputs are

$$\sqrt{\overline{u'^2}} = (\sqrt{2}/2s_a)\sqrt{[(\bar{A} + A' + \bar{B} + B') - (\bar{A} + \bar{B})]^2} = \\ = (\sqrt{2}/2s_a)\sqrt{(A' + B')^2} \qquad \text{(VI. 13)}$$

$$\sqrt{\overline{v'^2}} = (\sqrt{2}/2s_a)\sqrt{(A'-B')^2} \qquad \text{(VI. 14)}$$

In a similar manner, the correlation $\overline{u'v'}$ can be determined from the A and B signals which are again corrected for their mean

$$\overline{u'v'} = (1/2s_a^2)\overline{(A' + B')(A' - B')} = (1/2s_a^2)(\overline{A'^2} - \overline{B'^2}) \qquad \text{(VI. 15)}$$

The correlator also has the capability to normalize the inputs so that the normalized correlation coefficient is obtained

$$C = \frac{\overline{u'v'}}{\sqrt{\overline{u'^2}}\sqrt{\overline{v'^2}}} \qquad \text{(VI. 16)}$$

Operation of the "X" Configuration Probe

In closing, several of the practical aspects and problems associated with the use of the "X" configuration probe are presented in this section. Values for s_a and s_b can be determined using the same calibration apparatus described in "Velocity Measuring System", which was developed for the single sensor, if the angles α and β are known. Since during calibration the y component of velocity, v is zero, equation (VI. 3) indicates that the slope of the velocity calibration curve is $s_a \cos \alpha$. Determination of s_a is then quite simple. Likewise, determination of s_b follows from the slope of the calibration curve for sensor "B", $s_b \cos \beta$.

To operate a constant temperature sensor, the proper overheat ratio must be set, based on a probe resistance versus temperature curve. For the "X" configuration probe a separate curve must be obtained for each sensor and then each channel resistance set separately. Since each sensor will increase the effective fluid temperature

near the sensor slightly, the temperature should be measured with both sensors off but each probe resistance should be measured while the other sensor is operating at the intended overheat ratio.

Two basic problems were encountered with the use of the "X" configuration sensor, (1) use of the RMS voltmeter, and (2) considerable deviation from perpendicularity of the two sensors in the probes that were purchased. Difficulty with the RMS voltmeter has already been mentioned. The magnitudes and frequencies of the fluctuations were such that the most sensitive scales and longest time constants were required. Often after a period of 15 to 20 minutes, using a time constant of 100 seconds, a stable reading could not be obtained. It appears that the experimental conditions are pushing the limit of the analog equipment. The basic solution seems to be the selection of a minimum number of data points so that 30 minutes or more can be devoted to taking each reading, and so that these readings can be checked for repeatability. An alternate solution would be to use a digital recorder and computer to determine the RMS values numerically.

For the probe that was used to take data, α and β were not 45^{o} but were each about 55^{o}. The sine and cosine functions vary about 10 to 20% for this deviation, and could tend to introduce significant error if the angles were each assumed to be 45^{o}. While this complicates the situation, the problem can be handled if P (the sensitivity to

cooling velocity along the sensor axis) is still assumed to be zero. Looking again at equations (VI. 6) and (VI. 7), α and β are geometric properties of the probe, and a_o, b_o, s_a and s_b are known from the anemometer calibrations. The parameters n_1, n_2, m_1 and m_2 defined as

$$\begin{aligned} n_1 &= s_a[\cos\alpha + \cot\beta \sin\alpha] \\ n_2 &= s_a[\sin\alpha + \tan\beta \cos\alpha] \\ m_1 &= s_a \sin\alpha / s_b \sin\beta \\ m_2 &= s_a \cos\alpha / s_b \cos\beta \end{aligned} \qquad \text{(VI. 17)}$$

are therefore just constants for a given probe. In terms of these parameters, u and v are

$$u = 1/n_1[(A-a_o) + m_1(B-b_o)] \qquad \text{(VI. 18)}$$

$$v = 1/n_2[(A-a_o) - m_2(B-b_o)] \qquad \text{(VI. 19)}$$

The mean velocity components are determined as before from the voltage versus time plots for each sensor, according to equations (VI. 18) and (VI. 19). To measure the fluctuating components u' and v', recall that it was necessary for the amplifier on channel B to be set such that the constant preceding the $B-b_o$ term was unity. This is accomplished by amplifying channel B by m_1 to measure u', and by amplifying channel B by m_2 to measure v'. Note that, since m_1 does not equal m_2, the amplifier must be changed each time to read u' and

v', and also that there is no way to input A and B properly so as to get $\overline{u'v'}$. For the probe used to take data, however, although α and β were not 45^{o}, they were still nearly equal in which case both m_1 and m_2, and n_1 and n_2 were equal; thus, u', v', and $\overline{u'v'}$ could be determined with a single amplifier setting. Therefore, even if α and β do deviate from 45^{o}, the problem is not greatly complicated if $\alpha = \beta$.

VII. CONCLUSIONS AND RECOMMENDATIONS

The purpose of this thesis was the study of natural convection in the turbulent regime. While turbulent flow was only partially realized, experimental heat transfer results were extended by two orders of magnitude beyond previous experiments, and some new light has been shed on the onset of transition and the flow mechanism involved for channel flow. The basic conclusions reached in this thesis were

1. Heat transfer results were presented for the single plate for $10^5 < Gr_x^* < 10^{11}$, and for channel spacings, w/L, of .25, .50, and .67 for $10^8 < Gr_x^* < 10^{11}$. These results are for higher Grashof numbers than for other results to which they are compared, but still are in good agreement with earlier analytical and experimental results.
2. Although, for the range of channel spacings studied, there was no practical difference in heat transfer between the three spacings, statistically there was a definite increase in heat transfer as the channel spacing was decreased, consistent with the trend reported by Colwell (6).
3. The maximum peak velocities were observed adjacent to the single plate with minimum peak velocities occurring for the narrowest channel spacing. Mid-channel, the velocity was the largest,

however, for the narrowest spacing and decreased as the channel width increased.

4. Trends in the dimensionless velocity and temperature profiles were in agreement with analytical predictions.

5. Instability occurs first and the disturbances are amplified most for the intermediate channel spacing, $w/L = 0.50$. This is consistent with the observations of Colwell (6).

6. It appears that disturbances have a single characteristic frequency for any x position and channel spacing, but the amplitude of the fluctuations outside the velocity peak is much larger than the amplitude of those inside the velocity peak. It is suggested that this is because the size of the outer eddies is governed by the width of the channel while the inner eddies are governed by the distance between the velocity peak and the wall. In the same way, the wide channel spacings appear to impose a lower characteristic frequency on the boundary layer.

7. Characteristic frequencies from the single plate data are in good agreement with the linear stability predictions of Hieber and Gebhart (18) for $Pr = 0.025$.

8. Transition appears to occur between 3 and 4 inches from the bottom for a heat flux of 11,500 BTU/hr-ft^2 for both the single plate and channel. This corresponds to an E factor, proposed by Jaluria and Gebhart (21) for predicting transition, of between 11.9 and

13.4. This is in good agreement with their results.

This thesis has by no means completely covered the subject of turbulent natural convection in a uniformly heated vertical channel. More documentation of the characteristic frequencies and the onset of transition should certainly be conducted. The following are some recommendations for further work which would help complete the picture.

1. Heat transfer data and mean profiles should be taken for the narrower spacings even though the two-sensor "X" configuration probe cannot be used there. This information is very important for a continued study of the optimum plate spacing problem.
2. Instantaneous plots of the temperature disturbances should be recorded for comparison with the velocity fluctuations and for predicting thermal transition.
3. Strip charts of the velocity and temperature should be taken for a considerable period of time to determine the intermittency, the amount of time the flow is turbulent, for use in determining the end of transition.
4. Determine a more precise value for the transition predictor, E, by selecting an x position and slowly increasing the heat flux until the first turbulent bursts appear.
5. Use the "X" configuration probe to check for secondary mean flow and to find the magnitudes of the instantaneous velocity components,

and the value of the uv correlation coefficient.

6. This brings up the problem of obtaining analog equipment capable of handling these small low frequency signals. It appears that the state of the art lies in digital recording equipment and statistical analysis. Acquisition of this type of equipment seems to be the best solution to the problem.

7. Finally, to obtain higher Grashof numbers and more turbulent flow, longer plates would be desirable. The heater elements are already being used well above their maximum power level. Also, both the Grashof number and E are more dependent on x than they are on the heat flux, q.

NOMENCLATURE

a, b, a_1, b_1	arbitrary constants
A_1, A_2	relative amplitudes of a disturbance
A, a_o, B, b_o	run and rest voltages from sensors "A" and "B"
A_s	total heat flux area
c	specific heat
C	non-dimensional correlation coefficient of $\overline{u'v'}$
d	diameter of hot film sensor
E	parameter for prediction of turbulence, Jaluria (21)
f	physical frequency
g	acceleration due to gravity
h	coefficient of convection
k	thermal conductivity
K	arbitrary constant
l	sensor length or significant dimension in Q^*
L	channel height
m, n	arbitrary exponents
m_1, m_2, n_1, n_2	parameters defined for use of "X" configuration sensor
P	sensor sensitivity, Champagne (3)
q	heat flux
Q	total heat

Q^*	relative thermal capacity, Knowles (23)
R	electrical resistance
R_1, R_2	thermal resistance
s_a, s_b	slopes of anemometer calibration curve
T	general temperature
T_a	ambient temperature
T_e	reference temperature
T_f	heater foil temperature
T_r	reference temperature, Sparrow and Gregg (37)
T_s	plate surface temperature
u, v	instantaneous velocity components
u', v'	fluctuating components of velocity
$\bar{u}$, $\bar{v}$	average (with time) velocity components
U	velocity of mean flow
v_x, v_y, v_z, $v_\parallel$, $v_\perp$	velocity components in x, y, z, parallel and perpendicular directions
w	width of channel
x, y, z	cartesian coordinates
α	thermal diffusivity
α	angle (context obvious)
α^*	rate of amplification
β	coefficient of thermal expansion
β	angle (context obvious)

β^*	dimensionless frequency
μ	viscosity
ν	kinematic viscosity
ρ	density
θ	angle

Significant Parameters

$Gr_x,\ Gr_L = \frac{\beta g L^3 (T_o - T_a)}{\nu^2}$	local, average Grashof number
$Gr_x^*,\ Gr_L^* = \frac{\beta g L^4 q}{k \nu^2}$	local, average modified Grashof number
$G^* = 5(Gr_x^*/5)^{1/5}$	local vigor
$Nu_x,\ Nu_L = \frac{hL}{k}$	local, average Nusselt number
$Pr = \frac{\nu}{a}$	Prandtl number

BIBLIOGRAPHY

1. Bodoia, J. R. and J. F. Osterle. The Development of Free Convection Between Heated Vertical Plates, Trans. ASME, Ser. C, J. Heat Transfer, 84, 40-44 (1962).

2. Brindley, J. An Approximation Technique for Natural Convection in a Boundary Layer, Int. J. Heat Mass Transfer, 6, 1035-1048 (1963).

3. Champagne, F. H., C. A. Sleicher and O. H. Wehrmann. Turbulence Measurements with Inclined Hot-Wires, J. Fluid Mechanics, 28, 174 (1967).

4. Chang, K. S., R. G. Akins, L. Burris, Jr., and S. G. Bankoff. Free Convection of a Low Prandtl Number Fluid in Contact with a Uniformly Heated Vertical Plate, AEC Research and Development Report ANL-6835, Argonne National Laboratory (1964).

5. Colwell, R. G. Experimental Investigation of Natural Convection of Mercury in an Open, Uniformly Heated, Vertical Channel, Ph.D. Thesis, Oregon State University (1974).

6. Colwell, R. G. and J. R. Welty. An Experimental Study of Natural Convection with Low Prandtl Number Fluids in a Vertical Channel with Uniform Wall Heat Flux, ASME Paper 73-HT-52 (1973).

7. Coutanceau, J. Convection Naturelle Turbulente Sur Une Plaque Verticale Isotherme, Transition, Echange De Chaleur et Frottement Parietal, Lois de Repartition De Vitesse et de Temperature, Int. J. Heat & Mass Transfer, 12, 753-769 (1969).

8. Cygan, D. A. and P. D. Richardson. A Transcendental Approximation for Natural Convection at Small Prandtl Numbers, The Canadian Journal of Chemical Engineering, 46, 321-324 (1968).

9. Dring, R. P. and B. Gebhart. A Theoretical Investigation of Disturbance Amplification in External Laminar Natural Convection, J. of Fluid Mech., 34, 551-564 (1968).

10. Eckert, E. R. G. and T. W. Jackson, Analytic Investigation of Flow and Heat Transfer in Coolant Passages of Free Convection Liquid-Cooled Turbines. NACA RFM 50 D25 (1950).

11. Gebhart, B. Transient Natural Convection from Vertical Elements - Appreciable Thermal Capacity, Trans. ASME, J. of Heat Transfer, Ser. C, 85, No. 1, 10-14 (1963).

12. _____ Natural Convection Flow, Instability and Transition, Trans. ASME, J. of Heat Transfer, 91, 293-309 (1969).

13. _____ Heat Transfer, Second edition, McGraw-Hill Book Company, New York (1971).

14. _____ Instability, Transition and Turbulence in Buoyancy Induced Flows, Ann. Rev. of Fluid Mech. 5, 213 (1973).

15. Godaux, F. and B. Gebhart. An Experimental Study of the Transition of Natural Convection Flow Adjacent to a Vertical Surface, Int. J. Heat Mass Transfer, 17, 93-107 (1974).

16. Gosse, J., R. Schiestel and M. G. Robin. A New Model of Turbulence Applied to Prediction of Liquid Metal Heat Transfer, ASME Paper 73-HT-55 (1973).

17. Griffiths, E. and A. H. Davis. The Transmission of Heat by Radiation and Convection, Brit. Food Invest. Board Spec. Rep. 9, DSIR, London (1922).

18. Hieber, C. A. and B. Gebhart. Stability of Natural Convection Boundary Layers: Some Numerical Solutions, J. of Fluid Mech., 48, 625-646 (1971).

19. Hinze, J. O. Turbulence: An Introduction to Its Mechanism and Theory. McGraw-Hill Book Company, New York (1959).

20. Hurt, J. C. and J. R. Welty. The Use of a Hot Film Anemometer to Measure Velocities Below 10 FPM in Mercury, ASME Paper 72-HT-3 (1972).

21. Jaluria, Y. and B. Gebhart. On Transition Mechanisms in Vertical Natural Convection Flow, to be published in the Journal of Fluid Mechanics.

22. Julian, D. V. and R. G. Akins. Experimental Investigation of Natural Convection Heat Transfer to Mercury, I. and E. C. Fundamentals, 8, No. 4, 641-646 (1969).

23. Knowles, C. P. and B. Gebhart. The Stability of the Laminar Natural Convection Boundary Layer, J. of Fluid Mech., 34, 657-686 (1968).

24. Kuiken, H. K. Free Convection at Low Prandtl Numbers, J. Fluid Mech., 37, Part 4, 785-798 (1969).

25. Kurtz, E. F. and S. H. Crandall. Computer-Aided Analysis of Hydrodynamic Stability, J. of Math and Physics, 41, No. 4, 264-279 (1962).

26. Kutateladze, S. S., A. G. Kirdysahkin and V. P. Ivakin. Turbulent Natural Convection on a Vertical Plate and in a Vertical Layer, Int. J. Heat Mass Transfer, 15, 193-202 (1972).

27. Levy, E. K. Optimum Plate Spacings for Laminar Natural Convection Heat Transfer from Parallel Vertical Isothermal Flat Plates, ASME Trans., J. Heat Transfer, 93, 462-465. (1971).

28. Lorenz, L. Uber das Leitungsvermogen der Metalle fur Warme und Electricitat, Ann. Phys. Chem., 13, 582-591 (1881).

29. Lyon, R. N. (ed.). Liquid Metals Handbook, second edition, Washington, D. C., U. S. Government Printing Office, 269 p. (1952).

30. Mollendorf, J. C. and B. Gebhart. An Experimental Study of Vigorous Transient Natural Convection, Trans. ASME, J. of Heat Transfer, Ser. C, 92, 628-634 (1970).

31. Ostrach, Simon. An analysis of Laminar Free-Convection Flow and Heat Transfer About a Flat Plate Parallel to the Direction of the Generating Body Force. NACA Report 111 (1953).

32. Plapp, J. E. The Analytic Study of Laminar Boundary Stability in Free Convection, J. of Aeronautical Science, 24, 318 (1957).

33. Quintiere, J. and W. K. Mueller. An Analysis of Laminar Free and Forced Convection Between Finite Vertical Parallel Plates, ASME Paper 72-WA/Ht-3 (1972).

34. Schmidt, E. and W. Beckmann. Das Temperatur und Geschwindigkeitsfeld vor einer Warmeabgenbenden senkrechten Platte bei naturlicher Konvection, Technische Mechanik und Thermodynamik, 1, 341-349 and 391-406 (1930).

35. Sparrow, E. M. Laminar Free Convection on a Vertical Plate with Prescribed Non-uniform Wall Heat Flux or Prescribed Non-uniform Wall Temperature. NACA TN 3508 (1956).

36. Sparrow, E. M. and J. L. Gregg. Laminar Free Convection from a Vertical Plate with Uniform Surface Heat Flux. Trans ASME, 78, 435-440 (1956).

37. _____ The Variable Fluid Property Problem in Free Convection, Trans. ASME, 80, 879-886 (1958).

38. _____ Details of Exact Low Prandtl Number Boundary-Layer Solutions for Forced and Free Convection, NACA Memo 2-27-59 E (1959).

39. Sparrow, E. M. and L. Guinle. Deviations from Classical Free Convection Boundary-Layer Theory at Low Prandtl Numbers, Int. J. Heat Mass Transfer, Vol. 11, 1403-1406 (1968).

40. Szewcyzk, A. A. Stability and Transition of the Free Convection Layer along a Vertical Flat Plate, Int. J. Heat Mass Transfer, 5, 903-914 (1962).

41. Tennekes, H. and J. L. Lumley. A First Course in Turbulence, The MIT Press, Cambridge (1972).

42. Thermo-Systems, Inc. Hot Film and Hot Wire Anemometry, Theory and Application, Bulletin TB5, St. Paul, Minn.

43. _____ Temperature Compensation of Thermal Sensors, Anemometry News, 2, No. 1, 3-8, St. Paul, Minn.

44. Welty, J. R., C. E. Wicks, and R. E. Wilson. Fundamentals of Momentum, Heat and Mass Transfer, John Wiley & Sons, Inc., New York (1969).

45. Welty, J. R. and D. H. White. Experimental Study of Natural Convection Heat Transfer from Vertical Flat Plates in Mercury, Proc. of Third Canadian Congress of Applied Mechanics (CANCAM), Calgary, Alberta (1971).

46. White, D. H., J. R. Welty, and J. C. Hurt. Experimental Study of Natural Convection Heat Transfer from Vertical Flat Plates in Mercury, Heat Transfer in Liquid Metals Conference, Trogir, Yugoslavia (1971).

47. White, D. H. An Experimental Investigation of Natural Convection Heat Transfer from Vertical Flat Plates in Mercury, Ph. D. Thesis, Oregon State University (1971).

48. Wiles, L. E. An Experimental Investigation of Laminar Natural Convection with a Uniformly Heated Vertical Cylinder in Mercury, M. S. Thesis, Oregon State University (1974).

APPENDICES

APPENDIX A

Computer Program for Reduction of Velocity Data

```
      PROGRAM TURBVEL
C
      X=TTYIN(2HX=)
      X=X/12.
      VOLT=TTYIN(4HVOLT,1H=)
      AMP=TTYIN(4HAMP=)
      Q=AMP*VOLT*3.4129/0.1535
      T=TTYIN(4HTINF,1H=)
      TINF=30.822+35.33*T
      TC=TTYIN(4HTVAL,2HL=)
      TEMP=30.822+35.33*TC
      TP=0.7*TEMP+0.3*T
      TCOND=.000438*(TP+686.03)
      VISC=.001167-.00000192*TP
      DENS=850.3-.0805*TP
      BETA=.00101
      GRX=BETA*32.174*DENS**2*X**4*Q/(TCOND*VISC**2)
      GX=(GRX*.2)**.2
      TDIF=TEMP-TINF
      THETA=GX*TCOND*TDIF/(X*Q)
      WRITE(61,60)THETA
   60 FORMAT(1X,9HTHETA(0)=,F6.3)
      WRITE(61,61)GRX
   61 FORMAT(1X,4HGRX=,E12.3)
      VP=TTYIN(4HVPRES,2HT=)
      PP=TTYIN(4HPPRES,2HT=)
      PPREST=0.0061+.32933*T
      PPCOR=PPREST-PP
      VPREST=VP+9.65*PPCOR
   21 READ(10,10)Y,TC,P,VRUN
   10 FORMAT(F5.3,F6.3,F5.2,F6.3)
      IF (EOF(10)) STOP
C     CORRECTION FOR EFFECT OF METAL PLATE
      YACT=Y+0.013
      IF(YACT.GE..032) GO TO 20
      DELV=.069207-.0057827/YACT+.000141551/YACT**2
     1-.000000079467/YACT**3
      VRUN=VRUN-DELV
   20 PPUN=0.0061+.32933*TC
      PCOP=PPUN-P
      VPUN=VPUN+9.65*PCOP
      V=VPUN-VPREST
      VEL=.98564+53.217*V-12.018*V**2+6.0935*V**3
      TEMP=30.822+35.33*TC
      TCOND=.000438*(TEMP+686.03)
      VISC=.001167-.00000192*TEMP
      DENS=850.3-.0805*TEMP
      VELNEW=VEL/720.
      YFT=YACT/12.
      ETA=YFT*GX/X
      TDIF=TEMP-TINF
      THETA=GX*TCOND*TDIF/(X*Q)
      FPRIME=.2*VELNEW*X*DENS/(VISC*GX**2)
C
      WRITE(11,11)YACT,TEMP,VEL,ETA,THETA,FPRIME
   11 FORMAT(F6.3,2F7.2,3F7.3)
      GO TO 21
      END
```

Computer Programs for Reduction of Heat Transfer Data for (a) Channel Configuration and (b) Single Plate

(a)

```
      PROGRAM TURBHTX1
C
      C1=4.47924
      C2=8.30958E-03
      C3=-3.80163E-06
      C4=4.34620
      C5=-9.91162E-03
      C6=1.79060E-05
      C7=-1.27524E-08
      C8=851.514
      C9=-8.64880E-02
      C10=9.86194E-06
      C11=-5.92566E-09
      AMP1=TTYIN(4HAMP1,1H=)
      AMP2=TTYIN(4HAMP2,1H=)
      VOLT1=TTYIN(4HVOLT,2H1=)
      VOLT2=TTYIN(4HVOLT,2H2=)
      Q=(AMP1*VOLT1+AMP2*VOLT2)*3.4129/0.15502/2.
      AR=TTYIN(3HAR=)
      AR5=AR**5
      BETA=.000101
    1 READ(10,10)X,TWALL,TINF
   10 FORMAT(F5.3,2F6.3)
      TINF=30.84+35.30*TINF
      IF (EOF(10)) STOP
      X=X/12.
      TWALL=30.84+35.30*TWALL
      T=0.7*TWALL+0.3*TINF
      TCOND=C1+C2*T+C3*T**2
      VISC=(C4+C5*T+C6*T**2+C7*T**3)/3600.
      DENS=C8+C9*T+C10*T**2+C11*T**3
      TDIF=TWALL-TINF
      GRX=BETA*32.174*(DENS**2)*X**4*Q/(TCOND*VISC**2)
      XNUX=Q*X/(TCOND*TDIF)
      A=ALOG10(GRX)
      B=ALOG10(XNUX)
      C=ALOG10(GRX/AR5)
      D=ALOG10(XNUX/AR)
      WRITE(11,11)A,B,C,D
   11 FORMAT(1X,4F7.4)
      GO TO 1
      END
```

(b)

```
      PROGRAM TURBHTX2
C
      C1=4.47924
      C2=8.30958E-03
      C3=-3.80163E-06
      C4=4.34620
      C5=-9.91162E-03
      C6=1.79060E-05
      C7=-1.27524E-08
      C8=851.514
      C9=-8.64880E-02
      C10=9.86194E-06
      C11=-5.92566E-09
      AMP=TTYIN(4HAMP=)
      VOLT=TTYIN(4HVOLT,1H=)
      Q=AMP*VOLT*3.4129/0.15502
      TINF=TTYIN(4HTINF,1H=)
      TINF=30.84+35.30*TINF
      BETA=.000101
    1 READ(10,10)X,TWALL
   10 FORMAT(F5.3,F6.3)
      IF (EOF(10)) STOP
      X=X/12.
      TWALL=30.84+35.30*TWALL
      T=0.7*TWALL+0.3*TINF
      TCOND=C1+C2*T+C3*T**2
      VISC=(C4+C5*T+C6*T**2+C7*T**3)/3600.
      DENS=C8+C9*T+C10*T**2+C11*T**3
      TDIF=TWALL-TINF
      GRX=BETA*32.174*(DENS**2)*X**4*Q/(TCOND*VISC**2)
      XNUX=Q*X/(TCOND*TDIF)
      A=ALOG10(GRX)
      B=ALOG10(XNUX)
      WRITE(11,11)A,B
   11 FORMAT(1X,2F9.4)
      GO TO 1
      END
```

APPENDIX B

Determining the Optimum Location for a Breakpoint in a Regression of Two Linear Functions Constrained to Meet at the Breakpoint

A simple linear regression of a set of data, (x, y) has the form

$$f = a\,x + b \tag{B.1}$$

In this expression, f is an estimate of y based on a and b, which are estimators of the values of the intercept and slope of the true linear relation between x and y. For this model there will be an error between the predicted y value and the observed y value because (1) the true relation between x and y is probably not exactly linear, (2) a and b are only estimates of the true intercept and slope, and (3) any set of observations x and y will have some random variation from the true relation due to measurement errors and factors not accounted for in the model.

For the present situation we assume that the data is linear in two segments but has a definite change in slope, so that it is well represented by two lines

$$f_1 = a_1 + b_1 (x - \bar{x}_1) \qquad x < \alpha \tag{B.2}$$

$$f_2 = a_2 + b_2 (x - \bar{x}_2) \qquad x > \alpha \tag{B.3}$$

It is also desirable that f_1 and f_2 be equal at $x = \alpha$. Adding this constraint means that only one intercept, a, needs to be specified.

The resulting expressions are

$$f_1 = a + b_1 (x - \bar{x}_1) \qquad x \leq a \qquad \text{(B. 4)}$$

$$f_2 = a + b_1 (a - \bar{x}_1) + b_2 (x - a) \qquad x \geq a \qquad \text{(B. 5)}$$

The objective now is to determine the best estimates of a, b_1, b_2, and a. The data is assumed to be distributed normally about $f(x; a, b_1, b_2, a)$, where f is defined by equations (B. 4) and (B. 5), with a variance, due to the sources of error mentioned, of σ^2. Then the likelihood function of the parameters a, b_1, b_2, a and σ^2, given the data with n observations, is defined as

$$L(a, b_1, b_2, a, \sigma^2; x, y) \sim \frac{1}{\sigma^n} e^{(-1/2\sigma) \sum_{i=1}^{n} [y_i - f(x_i; a, b_1, b_2, a)]^2} \qquad \text{(B. 6)}$$

The likelihood function, evaluated for a particular set of parameters, expresses the probability that the observed data, (x, y), would have been observed if that particular set of parameters were indeed the true set of parameters. The likelihood function, therefore, provides a means of evaluating any set of estimated parameters relative to any other set of estimated parameters.

By maximizing the likelihood function defined above for the parameters a, b_1, b_2, and σ^2, a pseudo-likelihood function of only a and the data can be defined which isolates the effect of the selection

of α. The likelihood function is maximized, and the appropriate estimators for a, b_1 and b_2 obtained, by differentiating equation (B.6) by each of the parameters and simultaneously equating the three derivatives to zero. The result, which is the solution of the normal equations for the restricted model is

$$\begin{bmatrix} a \\ b_1 \\ b_2 \end{bmatrix} = [A]^{-1} \cdot [B] \tag{B.7}$$

where

$$A = \begin{bmatrix} n & (n-k)(\alpha - \bar{x}_1) & (n-k)(\bar{x}_2 - \alpha) \\ (n-k)(\alpha - \bar{x}_1) & \sum_{i=1}^{k} (x_i - \bar{x}_1)^2 + (n-k)(\alpha - \bar{x}_1)^2 & (n-k)(\alpha - \bar{x}_1)(\bar{x}_2 - \alpha) \\ (n-k)(\bar{x}_2 - \alpha) & (n-k)(\bar{x}_2 - \alpha)(\alpha - \bar{x}_1) & \sum_{i=k+1}^{n} (x_1 - \alpha)^2 \end{bmatrix} \tag{B.8}$$

$$B = \begin{bmatrix} \sum_{i=1}^{k} y_i + \sum_{i=k+1}^{n} y_i \\ \sum_{i=1}^{k} y_i(x_1 - \bar{x}_1) + (\alpha - \bar{x}_1) \sum_{i=k+1}^{A} y_i \\ \sum_{i=k+1}^{n} y_i(x_1 - \alpha) \end{bmatrix} \tag{B.9}$$

there are k values of $x \leq \alpha$ and n-k values of $x > \alpha$. The 3 x 3 matrix is easily inverted in a computer program using Cramer's rule.

Maximization of equation (B. 6) with respect to σ^2 yields the residual sum of squares divided by the number of observations as the proper estimator for σ^2.

$$\text{est}(\sigma^2) = \frac{1}{n} \sum_{i=1}^{n} [y_i - f(x_i; a, b_1, b_2, \alpha)]^2 = \frac{RSS}{n} \qquad (B.10)$$

The resulting pseudo-likelihood function is

$$L^*(\alpha; x, y) \sim (n/RSS)^{n/2} e^{-n/2} \sim (RSS/n)^{-n/2} \qquad (B.11)$$

The optimum location of the breakpoint, α, can now be obtained by a trial and error scheme to find the value of α that produces a minimum value of RSS, hence a maximum value for L^*. Since values of any likelihood function are usually small, in practice an estimate of the maximum value is made and a likelihood ratio is expressed relative to this.

For this project a computer program, LIKLEHUD, was developed to calculate the likelihood ratio for L^* and the corresponding regression equations for any selected value of α. It was written to make use of operator-computer interaction on a teletype. To use LIKLEHUD, which is listed on the following page, the operator selects an estimated value for L^*_{max} and selects a starting value for α. He then

continues to search for the optimum α by typing "1" in reply to the "GO?" command and selecting another value of α until he has found the location of the maximum L^* to his own degree of satisfaction. To terminate execution, a "0" is typed in reply to "GO?". The results using the single heated plate data and LIKLEHUD, which led to the breakpoint regression presented in Chapter IV, are shown graphically below.

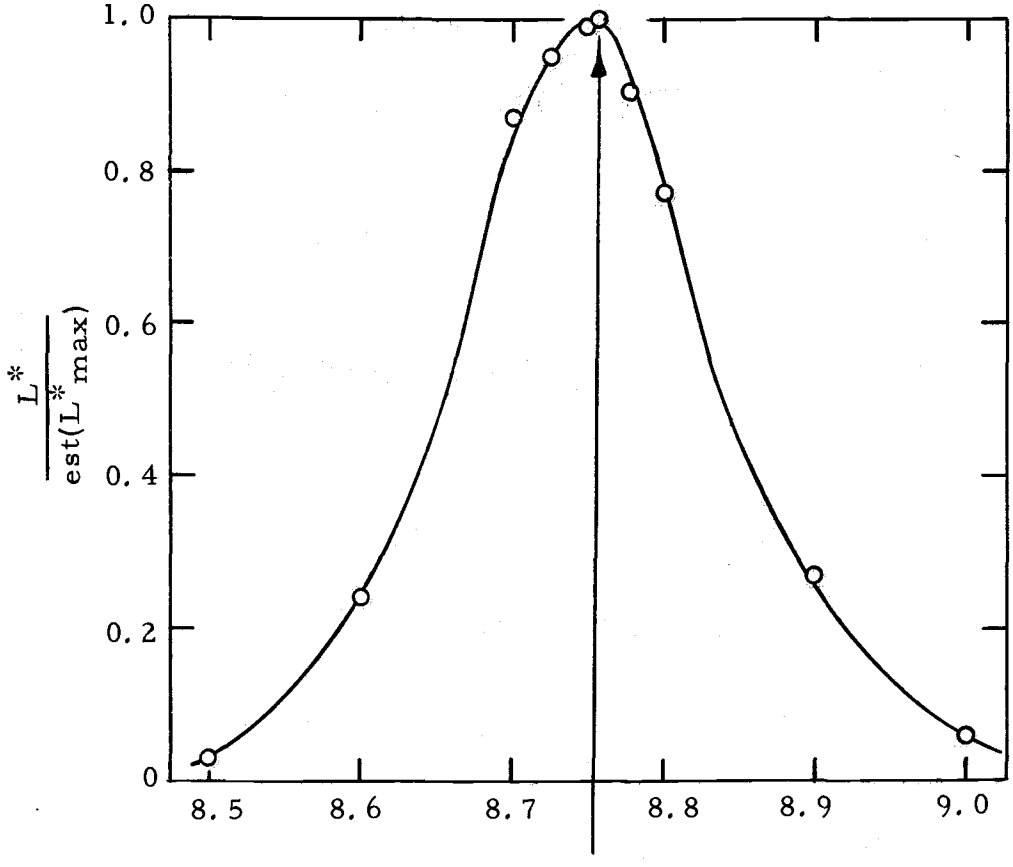

```
      PROGRAM LIKLEHUD
      DIMENSION X(500),Y(500),XL(500),YL(500),XH(500),YH(500)
C
      STARTMAX=TTYIN(4HLIMA,2HX=)
C
      K=1
    9 READ(10,10)X(K),Y(K)
   10 FORMAT(1X,2F9.4)
      IF(EOF(10))GO TO 20
      K=K+1
      GO TO 9
C
   20 K=K-1
      XK=K
C
   21 ALPHA=TTYIN(4HALPH,2HA=)
C
      SUMX1=SUMX2=SUMY1=SUMY2=0.
      SUMXSQ1=SUMXSQ2=SUMYSQ1=SUMYSQ2=0.
      K1=K2=0
C
      DO 30 I=1,K
      IF(X(I).GE.ALPHA)GO TO 31
      K1=K1+1
      SUMX1=SUMX1+X(I)
      SUMY1=SUMY1+Y(I)
      XL(K1)=X(I)
      YL(K1)=Y(I)
      GO TO 30
   31 K2=K2+1
      SUMX2=SUMX2+X(I)
      SUMY2=SUMY2+Y(I)
      XH(K2)=X(I)
      YH(K2)=Y(I)
   30 CONTINUE
C
      X1=K1
      X2=K2
      X1BAR=SUMX1/X1
      X2BAR=SUMX2/X2
      AMX1=ALPHA-X1BAR
      AMX2=X2BAR-ALPHA
C
      DO 40 I=1,K1
      SUMXSQ1=SUMXSQ1+(XL(I)-X1BAR)**2
      SUMYSQ1=SUMYSQ1+YL(I)*(XL(I)-X1BAR)
   40 CONTINUE
C
      DO 50 I=1,K2
      SUMXSQ2=SUMXSQ2+(XH(I)-ALPHA)**2
      SUMYSQ2=SUMYSQ2+YH(I)*(XH(I)-ALPHA)
   50 CONTINUE
C
C  DEFINITION OF MATRICES AND USE OF CRAMER'S RULE
C
      A11=XK
      A12=X2*AMX1
      A21=A12
      A13=X2*AMX2
      A31=A13
      A22=X2*AMX1**2+SUMXSQ1
      A23=X2*AMX1*AMX2
      A32=A23
      A33=SUMXSQ2
C
      C1=SUMY1+SUMY2
      C2=SUMYSQ1+AMX1*SUMY2
      C3=SUMYSQ2
C
      DENOM=A11*(A22*A33-A32*A23)+A12*(A31*A23-A21*A33)
     1+A13*(A21*A32-A22*A31)
      ANUM=C1*(A22*A33-A32*A23)+A12*(C3*A23-C2*A33)+A13*(C2*A32
     1-C3*A22)
      B1NUM=A11*(C2*A33-C3*A23)+C1*(A31*A23-A21*A33)+A13*
     1(A21*C3-C2*A31)
      B2NUM=A11*(A22*C3-A32*C2)+A12*(A31*C2-A21*C3)+C1*
     1(A21*A32-A31*A22)
C
      A=ANUM/DENOM
      B1=B1NUM/DENOM
      B2=B2NUM/DENOM
      A1=A-B1*X1BAR
      A2=A+B1*AMX1-B2*ALPHA
C
      RSS=0.
      DO 60 I=1,K1
      RSS=RSS+(YL(I)-A1-B1*XL(I))**2
   60 CONTINUE
      DO 70 I=1,K2
      RSS=RSS+(YH(I)-A2-B2*XH(I))**2
   70 CONTINUE
C
      EX=XK/2.
      STARL1=(1./RSS)**EX/STARTMAX
      WRITE(61,61)A1,A2,B1,B2,RSS,STARL1
   61 FORMAT(1X,3HA1=,E12.4/1X,3HA2=,E12.4/1X,3HB1=,E12.4/
     11X,3HB2=,E12.4/1X,4HRSS=,E12.4/1X,3HL1=,E12.4////)
C
      GO=TTYIN(3HGO?)
      IF(GO.EQ.1.)GO TO 21
      STOP
      END
```

Listing of computer program LIKLEHUD (continued in column 2).

APPENDIX C

Determining the Statistical Significance of a Parameter in a Regression Model

The F test is probably the most useful tool in analyzing the significance of parameters in a model. A null hypothesis is formulated based on the premise that the parameters of concern are not significant. The difference in the residual sums of squares for the regression of the full model and for the regression of the model under the null hypothesis indicates the importance of the parameters. The F statistic provides a means by which to make this comparison.

The question of interest in Chapter IV was whether the three lines for the three channel spacings,

$$\begin{aligned} f_1 &= a_1 + b_1 x \\ f_2 &= a_2 + b_2 x \\ f_3 &= a_3 + b_3 x, \end{aligned} \tag{C.1}$$

actually represented different lines. To test this, the null hypothesis was assumed,

$$\begin{aligned} a_1 &= a_2 = a_3 = a_o \\ b_1 &= b_2 = b_3 = b_o \\ f_o &= a_o + b_o x. \end{aligned} \tag{C.2}$$

For any linear model like those above, the residual sum of squares is defined as the sum over all n observations of the square of the

difference between the observed value, y_i, and the value of y predicted from the model, f_i.

$$RSS = \sum_{i=1}^{n} (y_i - f_i)^2 \qquad (C.3)$$

The residual sum of squares is a measure of how well a model represents a set of data, a smaller value indicating a better fit.

For the full model represented by equation (C. 1), the residual sum of squares is just the sum of the RSS from each regression line,

$$RSS_{full} = RSS_1 + RSS_2 + RSS_3. \qquad (C.4)$$

The F statistic provides a means to compare the difference between RSS_{full} and the residual sum of squares under the null hypothesis, RSS_o, with a tabulated probability distribution, the F distribution. If the F statistic is greater than the relevant tabulated F value for a confidence level, $1-\alpha$, then the null hypothesis can be rejected realizing that the probability of making an error in this rejection is less than α. If there is sufficient cause to reject the null hypothesis, then the parameters of concern are significant.

The F statistic test is defined as follows: if the null hypothesis is true, then

$$\frac{(RSS_o - RSS_{full})/q}{(RSS_{full})/m} < F_{q,m}^{1-\alpha}. \qquad (C.5)$$

In this expression, m is the number of degrees of freedom in the full model and q is the difference in the number of degrees of freedom between the full model and the reduced model under the null hypothesis. For each linear regression, one degree of freedom is lost from the total number of observations for the mean value of y and one degree of freedom is lost for the slope of the line. Thus for the full model the number of degrees of freedom for each line was n_1-2, n_2-2, and n_3-2. The total degrees of freedom was then $n_1 + n_2 + n_3 - 6$. Under the null hypothesis there was only one line, the degree of freedom was $n_1 + n_2 + n_3 - 2$, and q was 4.

From the actual regressions for the data

$$
\begin{aligned}
RSS_1 &= 2.21236394 \times 10^{-3} \qquad n_1 = 91 \\
RSS_2 &= 1.47174491 \times 10^{-3} \qquad n_2 = 93 \\
RSS_3 &= 4.48207892 \times 10^{-3} \qquad n_3 = 93 \\
RSS_o &= 1.34081551 \times 10^{-2} \qquad n_o = 277 \\
RSS_{full} &= 8.16618777 \times 10^{-3} \qquad \text{by equation (C. 4)} \\
m &= 91 + 93 + 93 - 6 = 271
\end{aligned}
\tag{C. 6}
$$

The F statistic becomes

$$
\frac{(13.4081551 \times 10^{-3} - 8.16618777 \times 10^{-3})/4}{(8.16618777 \times 10^{-3})/271} = 43.489 \tag{C. 7}
$$

The value for $F_{4,271}$ with $\alpha = 0.001$ is somewhere between 4.62 and 4.95. Since the F statistic was so very much larger than this, the null hypothesis was rejected and it was concluded that all the parameters of the full model were significant, hence the lines were indeed different lines.

One final remark must be made about analyzing the significance of these lines. The probability of correctly rejecting the null hypothesis is called the power of the test. For the data just considered, the power of the test was found to be negligibly different from 1. This means that if there is any variation between runs of data, and there must be at least some random variation, the probability of detecting this variation and calling it significant is very high, almost inevitable. It is therefore not surprising that these lines were found to be significant, but one should be dubious about what conclusions can be drawn from the F test under this situation. Unfortunately, a complete set of data of the same size was never repeated on a different occasion to check the relative significance of this random variation.

The conclusion in Chapter IV was that there was no practical significance of the three different lines, but since there was a consistent trend in the data in agreement with a previously reported trend, this gives more reason to believe that the differences in the lines were a significant result of the change in channel spacing, and not merely random variation. A similar test was performed for a set

of data for a single channel spacing but for the different heat flux levels within that spacing. The separate regressions were found to be significant, but at the 0.01 to 0.05 level, which is much less significant than the channel spacing effect where the α was much less than 0.001.